Acoustic Analysis of Rock Cutting Process for Impregnated Diamond Drilling

by

Santiago Pérez Ospina

A thesis submitted for the degree of

Doctor of Philosophy

School of Civil, Environmental and Mining Engineering

Faculty of Engineering, Computer and Mathematical Sciences

The University of Adelaide

February 2016

To my beloved parents, Jose Gregorio and Adriana Patricia, for their endless support

Contents

List of figures

List of tables

Abstract

The rock cutting industry has experienced important changes with the introduction of diamond-based drilling tools in the last few decades. Impregnated diamond (ID) bits are part of that introduction and their main use is to drill hard and abrasive rock formations. ID core drilling has emerged as the most commonly used technology employed in the advanced stages of mineral exploration. Through this technology, existing resources - mineral and energy - are expanded and greenfield exploration is carried out. As near-surface deposits are depleted, there is a global trend towards targeting deeper for exploration. Currently, in near-surface drilling, bit wear condition is determined by the experience of drilling operators –trial and error–. Although it makes the evaluation very subjective and prone to errors, it is an accepted practice. Conversely, in deep drilling, direct assessment of the bit wear condition is difficult and time consuming. Therefore, alternative techniques must be developed in order to evaluate, in real time, the wear condition of the bit and properties of the drilling medium. In this thesis, Acoustic Emission (AE) along with Measuring While Drilling (MWD) parameters are considered as an alternative technique to remotely monitor the ID bit wear condition (sharp and blunt) and rock properties (abrasivity). A series of rigorous and specialized drilling and abrasivity tests are utilised to generate the acoustic signatures with (topologically variant) and without (topologically invariant) changes in the topology of the tool cutting face.

Main findings of this work are as follows: firstly, based on the step test results, linear relationships were developed that make it possible to estimate the depth of cut, weight on the bit (WOB) and torque on the bit (TOB) by simply using the time domain parameters of the AE signals. Wear tests also showed that AE amplitudes start to trend down as wear begins to accelerate. Secondly, acceptable pattern recognition rates are obtained for the majority of tool condition monitoring systems developed for predicting sharpness or bluntness of ID bits. In particular, the system

composed by AE_{rms} and TOB excels due to the high classification performance rates and the fewer input variables compared to other tool condition monitoring systems.

Lastly, AE parameters, such as total number of events and root mean square of AE, in addition to testing parameters are found to accurately predict rock abrasivity measured via Cerchar Abrasivity Index (CAI). The importance of this index lies on: (i) the fact that ID drilling is commonly used in abrasive rock formations, and (ii) the way CAI has been defined (length of wear flat exerted on a steel pin after being scratched on one centimetre of rock surface), which intrinsically relates it to wear condition of the tool. The insights presented in this thesis open up a new promising field of study, impregnated diamond drilling using AE as an indirect technique to evaluate tool condition.

Statement of Originality

I, Santiago Perez Ospina, hereby certify that this work contains no material which has been accepted for the award of any other degree or diploma in my name, in any university or other tertiary institution and, to the best of my knowledge and belief, contains no material previously published or written by another person, except where due reference has been made in the text. In addition, I certify that no part of this work will, in the future, be used in a submission in my name, for any other degree or diploma in any university or other tertiary institution without the prior approval of the University of Adelaide and where applicable, any partner institution responsible for the joint-award of this degree.

I give consent to this copy of my thesis when deposited in the University Library, being made available for loan and photocopying, subject to the provisions of the Copyright Act 1968. The author acknowledges that copyright of published works contained within this thesis resides with the copyright holder(s) of those works.

I also give permission for the digital version of my thesis to be made available on the web, via the University's digital research repository, the Library Search and through web search engines, unless permission has been granted by the University to restrict access for a period of time.

Signature: _____ Date: _____

Acknowledgments

This thesis marks an important moment on my personal life and academic formation. This is made possible thanks to the collaboration and support of many people, to whom I would like to express my gratitude.

First, I would like to sincerely thank my supervisor, Dr. Murat Karakus, who gave me advice during research and helped me to embark in this research journey. Without his support and encouragement, this thesis would not have been possible to complete. I appreciate his contribution, continuous guidance and unconditional and persistent support throughout my PhD candidature. My gratitude also goes to my co-supervisor Associate Professor Chaoshui Xu.

I would also like to acknowledge Dr Luiz Franca from CSIRO Earth Science and Resource Engineering, who helped along with his team in my testing program and invaluable discussions.

To my friends in Adelaide, who helped me during my stay with all the everyday aspects of life. Special thanks to the friends I made in the office, Mr. Exequiel Sepulveda, Mr. Henry Munoz, Mr. Javier Buitrago, Mr. Adam Schwartzkopff and Mr. Arash Mirahmadizoghi, just to name a few.

Thanks to my parents - Jose Gregorio and Adriana - and my sister - Natalia - for their support and love, which I feel even from the distance.

Finally, I would like to acknowledge The University of Adelaide, specially Prof. Mark Jaksa, and Deep Exploration Technologies Cooperative Research Centre (DET CRC) for providing financial support through my Postgraduate Research Scholarship. This is DET CRC document 2016/795.

Abbreviations and Symbols

AE	Acoustic Emission
AI	Artificial Intelligence
ANN	Artificial Neural Network
ASTM	American Society for Testing and Materials
BSE	Back-Scattered Electrons
BT	Boosted Trees
CAI	Cerchar Abrasivity Index
CSIRO	The Commonwealth Scientific and Industrial Research Organisation
C_{qtz}	Quartz Content
D	Depth of cut
DAQ	Data Acquisition Card
DET CRC	Deep Exploration Technologies Cooperative Research Centre
E_{tan}	Young's Modulus
FN	False Negative
FP	False Positive
FFT	Fast Fourier Transform

GMDH	Group Method Data Handling
h_p	Pin Hardness
HRC	Rockwell Hardness C
ID	Impregnated Diamond
IEEE	Institute of Electrical and Electronics Engineering
ISRM	International Society of Rock Mechanics
KNN	K-Nearest Neighbours
LCPC	Laboratoire des Ponts et Chaussées
MAE	Mean Absolute Error
MLP	Multi Layered Perceptron
MWD	Measuring While Drilling
NTNU	Norwegian University of Science and Technology
PDC	Polycrystalline Diamond Compact
QCAT	Queensland Centre for Advanced Technologies
RPM	Revolutions Per Minute
SE	Specific Energy
SEl	Secondary Electrons
SEM	Scanning Electron Microscopy
ST	Simple Trees
SVM	Support Vector Machines
TCM	Tool Condition Monitoring
TN	True Negative

TOB	Torque On Bit
TP	True Positive
UCS (σ_c)	Uniaxial Compressive Strength
ROP (V)	Rate of Penetration
VAF	Variance Account For
WOB	Weight On Bit
Ω	Rotary Speed

Chapter 1

Introduction

1.1 Background

Exploration industry of mineral (coal, iron, potash, limestone, etc.) and energy (uranium, geothermal, fossil fuels, etc.) resources is a crucial industry for the lifestyle of the modern society. In Australia, for example, total mineral exploration expenditure decreased from roughly $1 billion in September of 2011 to $400 million in September 2015 [1], this generates the need of improved and cheaper techniques for the industry. Existing mineral and energy resources are expanded and new resources are discovered through mainly mechanical drilling. This, in turn, may be classified into two categories: rotary and percussive drilling [2].

Impregnated diamond (ID) core drilling is a key rotary drilling technology employed in the advanced stages of mineral and energy resources exploration. Currently diamond drilling relies on the drillers expertise to assess and adjust drilling parameters. Operators use operational parameters, such as weight-on-bit (WOB) and cutting speed (RPM), to control the performance, measured by torque-on-bit (TOB) and rate of penetration (ROP). The process is subjective and prone to errors. Both disadvantages are susceptible to escalate during deep exploration, which is significantly increasing as near surface deposits are being depleted at higher rates than new mineral deposits are being discovered.

Since direct measurement and visualization of the ID bit/rock interface is extremely difficult and time consuming in deep exploration drilling, indirect techniques have to be sought in order to remotely assess the interaction of ID drill bit and rock, including the diamond bit wear state.

Given the importance of mineral and energy resources industries in today's international market, overall growth and modern lifestyle, it is imperative that improvements be made to current drilling practices. Therefore, in this thesis acoustic emission (AE) is employed as alternative technique to remotely study ID drilling and closely related rock properties. Although AE monitoring has been used extensively to monitor different aspects of drilling across different manufacturing processes, and to better understand the mechanisms behind the drilling process, it has not yet been applied to impregnated diamond drilling in order to remotely assess drilling conditions.

1.2 Literature review

An overview of the literature covering Acoustic Emission (AE) on rock drilling and rock properties is presented in this section. However, more comprehensible and detailed information pertaining each topic is given in respective chapters.

1.2.1 Acoustic emission

AE signals are transient elastic stress waves generated as a result of the rapid release of strain during transformation, plastic deformation and changes in the internal structure of a material [3]. AE signals are dependent on the basic deformation mechanism. They are dislocation motion, grain boundary sliding which is defined as the process in which grains slide past each other along or in a zone immediately adjacent to their common boundary [4], twinning which occurs when two crystals share lattice points in a symmetrical manner and vacancy coalescence which takes place when two or more vacancies, point defects that arise when an atom is 'missing' from the ideal crystal structure, merge [5]. All of these mechanisms occur during ID drilling.

Frequency ranges of the emitted waves range from as low as the audible frequency range up to megahertz frequencies [6]. Amongst the large number of

materials from which AE can be detected is rock. Characteristics of the AE signals produced ultimately depend on the material properties and the source of generation [7]. AE signals are unique therefore cannot be reproduced. Thus, statistical analysis is to be applied to measure signals. The stochastic nature of the signals is generated by factors affecting the signal generation, transmission and detection [8].

Acoustic emissions can produce two types of signals, burst (discrete) emissions or continuous emissions (see Figure 1-1); the **continuous signals** are of lower amplitude and of high frequency (minimal separation of occurrence). They are associated erosion processes in brittle materials [7]. These types of signals are appropriate for controlling the operation of machines [9]. In cutting processes, burst signals appear to be continuous signals as there is always present a cutting force, which emits burst signals so close in time [3]. In contrast, the **burst signal** consists of pulses with amplitudes substantially larger than the background noise and well separated in time of occurrence that are generated by spontaneous release of energy [6, 10]. The energy of the elastic wave generated in burst signals may exceed several orders of magnitude to that of elastic waves in continuous emission. These emissions are characterized by an increase in amplitude of acoustic pulses and is therefore registered as a discrete (or burst) AE [11].

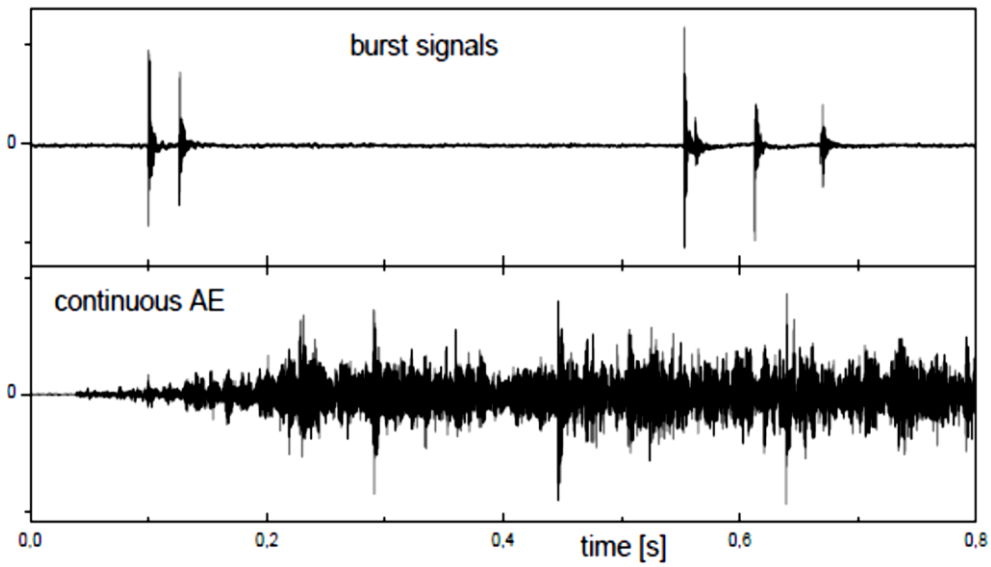

Figure 1-1. Burst and continuous acoustic signals [9].

Baranov, *et al.* [11] explain that the sources of AE can be from several different nature: elastic deformation, changes in stress-strain state of a local volume of solid surface layer, plastic deformation, energy liberation at repeated deformation phase hardening-weakening and damage on surface layer, changes in friction surface structure, formation of microcracks, appearance of wear debris or surface spalling.

AE has been utilized to monitor not only tool condition but also tool breakage in single-contact turning operation at laboratory scale for approximately 20 years in different manufacturing processes. [12]. Sudev and Ravindra [13] studied the correlation between drill bit wear and measured AE parameters using empirical methods including multiple regression and Group Method Data Handling (GMDH). The AE parameters were measured during drilling of cast iron with a high-speed steel drill bit. From their investigation, it was concluded that AE parameters provided sufficient warning of the resulting changes in tool wear and tool breakage. The models developed provided numerical estimates of tool wear and correlated well with the measured values [13]. Gómez, *et al.* [14] investigated possible relationships between AE, torque and drill bit wear using steel samples. The drill bits were modified with artificial and real failures in order to simulate different degrees of wear

AE parameters

AE parameters are used to extract information from the detected AE signals in order to infer physical phenomena such as tool wear and material fracture. Commonly used signal parameters are defined as follows (Figure 1-2):

Frequency (Hz) is defined as the number of times an event (waveform) occurs over a one second interval.

Sampling frequency (Hz) is defined as $1/\delta t$, where δt is the regular time interval of which the samples are recorded. Sampling Frequency is measured in cycles per second or Hertz (Hz).

Sampling interval is defined as the time-domain between two sampling points. The time between successive points is generally equal.

Frequency Domain is obtained using a mathematical transformation known as the Discrete Fourier Transform (DFT). This is a very important domain over which signal information is interpreted. Understanding the distribution of signal strength or power over different frequency components is fundamental in signal analysis. The frequency spectrum provides information regarding the nature of the AE source.

Threshold is a specific voltage level above which AE response will be detected and will convert the AE signal to a pulse format. [13, 15]

Amplitude is defined as the peak voltage of the signal waveform. It simply provides information regarding the energy of the AE source. The peak amplitude is the maximum amplitude reached by a signal during an event. Magnitude of source event and amplitude have a strong connection [16].

AE events count is defined as the number of times the threshold value is exceeded (waveform). The AE events count rate provides information regarding the rate of defect growth [11]. However, Hardy [15] states that for continuous type signals AE_{rms} value is more practicable than AE count. Other name for this parameter are: number of events [16].

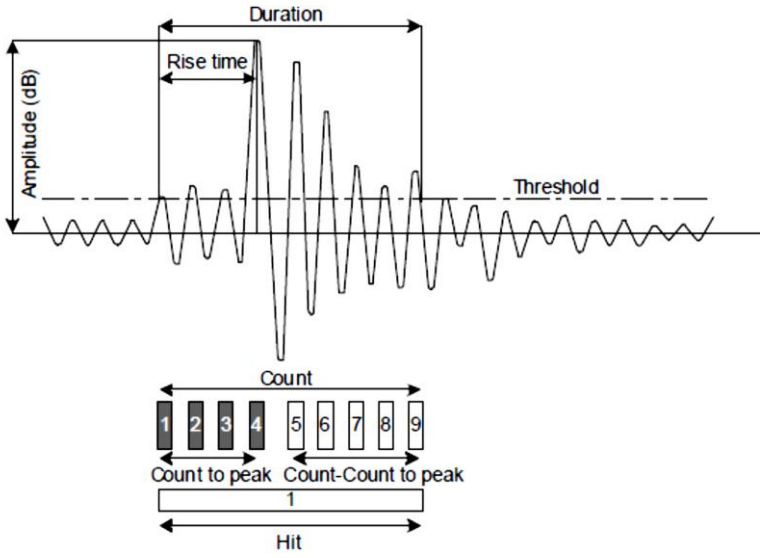

Figure 1-2. AE signal parameters [16]

Factors influencing the AE and its sources

Acoustic emissions generated during the ID drilling are very complex due to rock fracture, chip formation, wear and friction. As it will be discussed later (Section 1.2.2), ID drilling is a friction intensive process whereby diamonds set in the matrix dislodge rock crystals by forces exceeding their cohesive strength. ID drilling is a thermodynamically interchangeable process whereby energy is interchanged with the environment in the form of a number of sources including acoustic energy, which is the focus of this research. *The characteristics of the AE signals produced in drilling are still largely unknown and there is* ***no*** *literature available which directly addresses AE sources from ID drilling and drilling-associated rock properties.*

The AE generated by frictional processes occur mainly due to the same phenomena as the mechanical loading and failure of material. The main distinction between the frictional process of ID drilling and mechanical loading is the presence of additional AE sources resulting from frictional process. These processes include elastic interaction of surface asperities, chemical processes including corrosion which accompany friction in many cases, and the formation and rupture of adhesion joints. It is difficult to provide experimental conditions isolating one of these forms of AE from the other and it is therefore impossible to study a single source of exact AE during friction [11]. One of the dominate sources of AE signals during diamond drilling results from the IDs having to overcoming both surface interaction forces and mechanical resistance related to surface deformation. The identification of discrete AE sources is a future research topic as the current research is to investigate the feasibility of identifying overall signal characteristics associated with IDD.

The presence of drilling fluids on the surface of the rock weakens its surface bonds and affects the overall characteristics of the AE generated. The influence of drilling fluids may be more pronounced if lubricants other than water are used. For instance, monomolecular layers of fatty acids or soaps in the lubricant form a film on the surface, encouraging sliding and hence reducing friction and affecting the resulting AE [11]. Reducing the friction between surfaces influences the characteristics of the AE emissions. Drilling fluids also fill and expand

discontinuities in the rock, leading to additional fracturing which also affect AE signals.

Rapid temperature increases (flashes) occur at frictional contact spots, such as the area of immediate contact of the diamond and rock. The presence of these temperature flashes coupled with heavy contact dynamic loads and high energy absorption also cause a range of emission processes, including AE [11].

The wear stages a diamond drill bit experiences also affects AE. Higher wear-rates at the initial running in stages of drilling results in higher amplitude AE as a result of the initial frictional relief, bit matrix decay and the exposure of fresh diamonds. As the wear-rate stabilises the AE signals reduce their amplitude and become more continuous, with minimal occurrence of burst signals. During the catastrophic stage of wear, the increase in frictional wear characteristics leads to the generation of higher frequency and higher amplitude AE signals. The AE signals may exhibit burst behaviour due to the higher wear-rates and the increased friction. In this wear state, the diamond bit is likely to experience catastrophic wear such as segment failure or complete erosion of the crown. Such failures increase drilling pressures and forces, which translates to pronounced burst signals and higher amplitudes.

Acoustic emissions in friction are commonly attributed to changes in the stress-strain state of contact spots and to the appearance of wear debris due to surface damage [11]. The wear modes contributing to frictional surface damage include adhesion, abrasion, fatigue, corrosion and erosion may contribute to the AE. The surface damage is a combined effect of several elementary processes including micro-cutting, plastic deformation, delaminating, bulking and pit tearing; one of which may dominate. The dominant form of damage is likely to have the greatest influence on the AE characteristics. The deformation occurring at the diamond drilling interface is still not well understood [17]. The AE emissions at any time come from one dominant source or from a combination of them. Some of the sources expected to emit during ID drilling are [3]:

- Friction between tool and rock interfaces

- The interaction between the rock and loose cutting
- Rock fracturing
- Tool chipping and fracturing
- Shear and plastic deformation of the rock
- Collision between drill bits and rock face
- Entrapment of drill cuttings between drill flue and cylindrical wall.

The amplitude is the most informative AE characteristic generated during IDD and it depends on properties of the mating materials, load, frictional conditions (wear state of the bit), surface roughness, temperature and other factors.The wear mode of the bit influences AE characteristics. In comparison to adhesive and fatigue wear, abrasive wear is synonymous with higher intensity AE. Generally, materials damaged by adhesion and fatigue produce continuous signals with small amplitudes while materials damaged by adhesion with seizure produce burst type signals. Abrasive wear can increase the amplitude signals 2-3 times in size when it dominates the frictional process [11].

The AE sources, listed in Table 1-1, may apply to ID drilling given the signals from drilling tend to be continuous in nature. However as there is no literature addressing AE monitoring of ID drilling the AE sources inherent in this process are still largely unknown.

Sensors and preamplifiers

AE sensors detect the stress induced elastic waves propagating through the rock and convert them into electrical signal. Transducer elements which are contained inside the sensor are classified as either resonant or broadband and are selected based on the desired operating frequency and environmental characteristics. Piezoelectric crystals are most commonly used as transducer elements in AE sensors. Piezoelectric (PZT) sensors operate in resonance and typically transform elastic motions of 1 Pico meter into electrical signals of 1μV voltage. In contrast, broadband sensors are operated outside their resonant frequencies [9].

Table 1-1 AE Sources Generated by Frictional Process [11]

Factors increasing amplitude	**Factors decreasing amplitude**
Rough relief	Smooth relief
High hardness	Low Hardness
Surface anisotropy	Surface isotropy
Inhomogeneity in surface properties	Homogeneity of surface properties
Coarse grains	Fine grains
Absence of texture	Presence of texture
Low toughness	High toughness
Defects in surface layers	Absence of defects in surface layers
Low temperature	Elevated temperature
High sliding velocity	Slow sliding velocity
Heavy load	Light load
Non-stationary friction conditions	Stationary friction conditions
Abrasive wear	Adhesive wear
Failure due to micro-cutting	Failure due to plastic deformation
Dry Friction	Presence of a lubricant
Boundary friction with a liquid lubricant	Boundary friction with solid lubricants
Presence of surfactants	Absence of surfactants
Presence of corrosive environment	Absence of corrosive environment

In order to maximise the preservation of signal characteristics, sensors with a frequency range of 100-900 kHz are required to detect the AE signals generated during the rock drilling process. This range would be suitable for sampling properly the emitted signals, as demonstrated by [18] who used SE375-MI AE sensors with a smaller frequency range of 50-500 KHz in a similar rock drilling experiment. A minimum preamplifier gain of 40 dB was also determined to be necessary. To minimise the loss of signal energy, sensors need to be firmly attached to the test material. Crosland, *et al.* [19] investigated options to attach the sensor using both bees-wax and superglue. However better signal resolutions were achieved using superglue as a result of less attenuation in comparison to bees-wax. Other couplants commonly used include vacuum greases, water soluble glycols, solvent-soluble resins and proprietary ultrasonic couplants [9].

Crosland, *et al.* [19] also found that the sensor locations influence the signal strength due to the attenuation properties of the rock mass, and suggested sensors should be located on the test material so that they provide good signal coverage.

Pre-amplifiers are employed in the AE testing circuit to magnify AE signals. In order to reduce the amount of electronic noise, pre-amplifiers with modern transistors should be used [9]. Preamplifiers can either be integrated or non-integrated. Integrated pre-amplifiers are located within the sensor and as a result are advantageous as they simplify the AE circuit setup. In [19], pre-amplifiers with three selectable gain settings (20 dB, 40 dB and 60 dB) were used. Different researchers [6, 13, 14, 20] have used preamplifiers with a 40 dB gain in their drilling experiments.

Signal processing

The recorded acoustic emissions signals contain large amounts of information, it is therefore important to be able to distinguish between relevant data and background noise. Signal processing is an operation, which can both extract and enhance the valuable data from a busy signal. Due to the stochastic nature of acoustic emission signals, the use of statistical methods and signal analysis tools are required [8]. There are varieties of tools and techniques that can be implemented in order to interpret signals. Amongst them, the following ones are of particular interest and will be utilised in this work.

Root Mean Square method (AE_{rms}), described in Eq. 1.1, provides a measure of magnitude of the signal, despite the shape of the waveform [21]. Chandrashekhar, *et al.* [22] successfully developed an empirical relationship to estimate the Root Mean Square (RMS) error value of an AE signal generated during the drilling of a 'Hasteloy' with tin and zircon coated drill bits. The AE_{rms} values correlated well with those values measured using a new drill bit during the experiment. However, as the drill bit wore, a significant difference between the estimated and measured AE_{rms} values was observed. A conclusion was drawn that the difference between the estimated and measured AE_{rms} values can be used to infer drill bit wear [22].

$$V_{RMS} = \sqrt{\frac{1}{T}\int_0^T V_i^2 dt} \tag{1.1}$$

where T = period of the waveform and V_i is the instantaneous voltage [21]. RMS is similar to a moving average, capable of 'smoothing' out the data, helping to make any present trends in the data more obvious. In a study by Jemielniak and Otman [23], the AE_{rms} value was considered as a useful mean of tool failure detection, although further studies revealed that this may not be the case. Kannatey-Asibu Jr and Dornfeld [8] concluded that the AE_{rms} values and associated distribution parameters can be very sensitive in regard to the degree of tool wear. Most of tool condition monitoring systems make use of AE_{rms} of the signal to detect tool wearing state or even tool breakage [12].

Fast Fourier transform (FFT) is a well-known algorithm used to compute the continuous time Fourier transform (CTFT), described in Equation 1.2, on signals [24].

$$X(f) = \int_{-\infty}^{\infty} x(t) e^{-j2\pi ft} dt \tag{1.2}$$

where f is the frequency, $x(t)$ is signal in time domain and $X(f)$ is the signal in frequency domain. Heideman, *et al.* [25] give a detail history of the FFT dating back to 1800s and especial editions with publications about FFT have also been published by the Institute of Electrical and Electronics Engineering (IEEE) [26]. This tool aids to convert a signal in the time domain, to one in the frequency domain, highlighting characteristic frequencies which would not have been clear otherwise [27].

The FFT has been extensively used by engineers across a variety of applications. Li and Li [28] performed an extensive study on AE analysis to monitor bearing conditions. They used a number of observations which were based on the characteristic frequencies related to the failure of bearings, found by using the FFT. Williams and Hagan (2002) studied the AE levels present with changes in rock cutting conditions. They found that due to their relatively low sampling rate, FFT did not produce any worthwhile results. This introduces the concept of Nyquist

theorem, which states that the maximum frequency that can be calculated from a sampling frequency is half of such a frequency [24, 26]. Although acoustic data is initially recorded as function of time, much of the analysis is performed in the frequency domain. For this reason, FFT is considered to be a key tool when it comes to signal analysis.

1.2.2 Impregnated diamond drilling

Drilling is a tribological process used to penetrate the subject mass. Three of the most common types of rock drilling include percussive, rotary crushing and roto-percussive drilling, each with vastly different applications, methods and tools [29, 30]. A similarity between the fundamental drilling processes common to most drilling methods, regardless of subject mass, is the use of a rotating tool to assist indentation. In rock drilling, this tool is referred to as the bit [31]. Applications of ID drilling include exploration drilling, precision machining and manufacturing.

Impregnated diamond (ID) drilling refers to drilling with bits that contain an arrangement of diamonds in a layer or layers of binding matrices. There are two major categories including ID bits and surface set bits. IDBs are used in medium to ultra-hard deep geological formations, whilst surface set bits are used in softer formations that are common in shallow drilling [32].

ID drilling products are becoming more specialised in order to cater for increasingly complex applications enabling a wider range of rock strata to be drilled more effectively and efficiently. This has been possible by optimising a range of critical drill bit parameter.

In order to study rock drillability, which is defined by Huang and Wang [33] as the performance prediction of a specific rig drilling on a rock mass with known properties, using IDBs, two main processes occurring at the rock/bit interface must be separately studied. Namely, bit or matrix wear and diamond wear process. Before going into the details of these two processes, a brief review on the principal drilling parameters is presented in the next section.

Drilling parameters

There are operational parameters that are controllable during drilling. The combination of correct bit properties and operational parameters for the drilling conditions will result in the optimum drilling rate and meters drilled achieved per bit. A number of authors have studied the tribological process during various types of drilling to ultimately optimise drilling performance. Many of these studies have resulted in the derivation of some mathematical relationships referred to as drillability equations [33]. While the literature has covered a range of different types of drilling, operational parameters that are similar between various types of drilling have been found to have similar effects on the respective drilling performance.

Major diamond drilling operational and performance parameters include penetration rate, rotational speed, thrust, penetration per revolution, specific energy and fluid flow volume and pressure. There are many relationships between various parameters and drilling performance published in the literature. Some better known relationships are reviewed in the following sections. Notably while these parameters are critical to drilling performance, there have been no attempts in the literature at determining these relationships in ID drilling through the measurement of acoustic emissions.

Penetration rate (V)

Penetration depth is the depth of a drill hole from the hole collar to the cutting face of the hole, while hole length is the target drilling distance. While neither of these is controlled in the drilling process, their intended values strongly influence drilling strategy. The penetration rate is the derivative of penetration depth with respect to time, or the drilled distance per unit of time. However, Tian and Tian [34] suggest that the depth of cut per revolution is the most important factor influencing impregnated diamond bit wear, as opposed to depth of cut over time.

Much of the literature has indicated that attempting to maintain a constant penetration rate leads to faster bit wear as a constant penetration rate requires adjusting other parameters to values outside their optimum range, leading to sub optimal drilling conditions. The penetration rate decreases with an increase in rock

strength, hardness and abrasivity as these conditions require greater energy for rock breakage thus causing the penetration rate to slow down [35].

Rotational speed (Ω)

The rotational speed is the quantity of revolutions of the drill string with respect to time, and is usually measured in revolutions per minute (RPM). Typical rotational speeds in diamond drilling range from 300 RPM to over 2000 RPM. Bhatnagar, et al. [36] found that in harder rock formations low rotational speeds (300 RPM) resulted in insignificant penetration rates. Additionally, Tian and Tian [34] observed that low rotational speeds (500 RPM) resulted in a faster rate of bit wear. These findings agree with the suggestion from Jones [37] that if the penetration rate is increased, rotational speed must be increased accordingly in order to avoid the occurrence of high bit wear-rate and concave face wear. Further, this suggests that penetration per revolution is a critical factor to control to achieve optimal drilling conditions.

Tian and Tian [34] also suggests that an increase in rotational speed reduces bit wear due to the faster displacement of loose cuttings at the drilling interface. Whereas at low rotational speeds, loose cuttings can act as a third body in the friction interaction, thus resulting in unnecessary drill bit wear. Contrary to this theory, Huang and Wang [33] suggests that increasing rotational speed results in excessive friction and heat which increases bit wear-rate. However both of these interactions may be taking place simultaneously.

Applied torque (TOB)

Applied torque is the rotational moment applied, in units of Nm. This can be measured using a tachometer. Rock properties determine the requirement of applied torque. Rao, *et al.* [38] could not define a definite relationship between torque and rock strength, however the author noted that in general the softer the rock, the higher the torque. Huang and Wang [33] presented this concept in more detail, suggesting that rock types with UCS <100 MPa became significantly harder to drill due to the large torque required. Above this level of UCS, torque requirements do not change significantly.

Various authors [33, 36, 38] have found that rotational speed had little effect on applied torque. The difference in magnitude of torque forces between the centre and side of a non-hollow bit is significant; however a typical coring diamond drill bit does not experience this phenomenon. Rao, *et al.* [38] determined that torque developed at the drilling interface increased linearly with bit pressure irrespective of rotational speed.

While drill bit diameter has been kept constant throughout the project, it is worthwhile mentioning that Rao, *et al.* [38] observed a general increase in measured torque with increasing bit diameter.

Axial force (WOB)

The axial force is the normal force applied in the direction of drilling. Excessive rotational speeds for the axial force being applied can lead to polishing of the cutting face and wear flat generation due to insufficient depth of cut per revolution [34, 35, 37, 38]. As axial force increases, the rate of penetration increases linearly; noting however that beyond an optimum thrust level there is no significant increase in penetration rate and the occurrence of hole deviation will increase [36].

Huang and Wang [33] investigated experimentally the effect of axial thrust on penetration rate and suggests a thrust range from 5-9kN for an optimised penetration rate. They also developed drillability equations relating penetration rate (ROP) and rotational speed (RPM), and penetration rate and axial force (WOB) where penetration rate is in m/hr, rotational speed in RPM and axial force in Newtons.

Weight on bit was found to be the most influential factor on drilling efficiency compared to rotational speed and rock type [33]. A higher bit weight also increases bit cutting efficiency up to a certain threshold force whilst a lower bit pressure decreases penetration rate [35, 38].

In line with the findings by Huang and Wang [33], Miller and Ball [39] found that the transition from wear flat dominated to micro-fracturing dominated wear type occurs at around 5-6 MPa of bit pressure. At this transition pressure, the specific energy of drilling was the minimum as this is the axial force at which the

optimum relationship between wear flat generation and micro-cracking occurs, thus maximising the cutting potential of each diamond.

In general, the literature suggests that for the subject rock mass the most critical drilling parameters influencing bit wear and rate of penetration are rotational speed and axial force, for which the depth of cut per revolution is the critical factor to control.

Fluid flow rate and pressure

The fluid flow rate and pressure are two characteristics of the flushing media applied to the drilling interface. The purposes of using a flushing media are to cool the drilling interface, remove cuttings, lubricate the drill string and also to stabilise the drill hole [35-38].

During the drilling process high temperatures can be reached at the drilling interface and along the drill string due to frictional interaction with the wall of the drill hole. Miller and Ball [35] suggests that the hardness of diamonds is significantly reduced above 700 ^{o}C, while Rao, *et al.* [38] found the binding matrix softens with temperatures in excess of 500 ^{o}C. This indicates that excessive temperatures are detrimental to drilling efficiency and bit wear. Miller and Ball [35] found a water flow rate of 350 l/hr at 200 kPa to be sufficient, while Huang (1997) used a flow rate of 340 l/hr. Water is the standard flushing media used in diamond drilling due to its low cost, although Bhatnagar, *et al.* [36] conducted laboratory experiments that confirmed an enhanced penetration rate can be achieved by adding Poly Ethylene Oxide to the water.

Micro-scale parameters

From Figure 1-3, the cutting force vectors (f_c) are directional towards velocity (V), which also applies to the rubbing forces from the matrix (f_m) and diamonds (f_d). However, the more important features are both the depth of cut (d) and diamond protrusion (Φ_p). Although these parameters are harder to measure than the penetration rate, they are the predominant factor affecting diamond drill bit wear [34]. At the moderate value of penetration per revolution, the matrix is worn down at an acceptable rate while there are sufficient forces to cause diamond

microfracturing. If the penetration per revolution is too high, excessive wear of both the matrix and the diamonds can occur, limiting the life and effectiveness of the bit. It has also been found that of all the drilling parameters, the penetration per revolution has the most effect on bit wear [34].

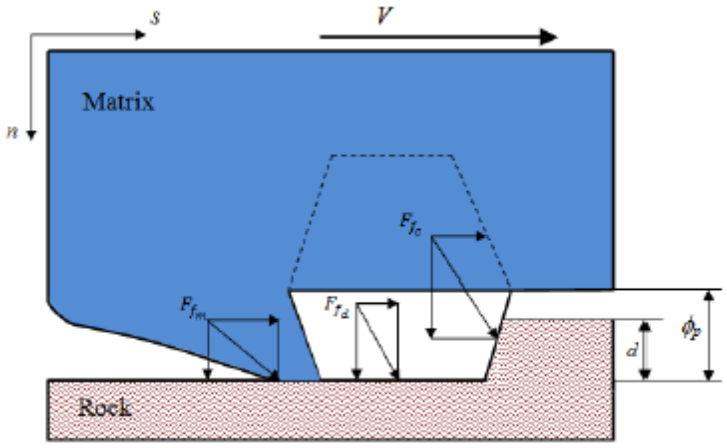

Figure 1-3 Diamond ad rock interaction (Reconstructed from [40])

Softer rock formations require lower drilling speeds for optimised drilling conditions in comparison to harder rock formations provided the bit properties are also adjusted accordingly [37].

Bit wear process

Bullen [32] describes three sequential stages in the bit wear process which typically occurs when drilling hard rocks. Firstly, active diamonds at the bit surface become worn due to interactions with hard asperities in the rock. This is then followed by a rapid stripping of blunted diamonds from the matrix structure. Finally, the matrix is worn until fresh sharp diamonds are exposed again. A steady penetration rate can be achieved so long as this wear cycle (see Figure 1-4) is sustained. Failure to replace blunted diamonds with fresh diamonds results in a smooth bit surface and, consequently, a decrease in the drilling performance. Therefore, the wear rate of the matrix structure serves an important role in maintaining the sharpness of the bit. In order to determine the most suitable wear rate for the matrix, it is vital to understand the conditions which allow for the most favourable balance of wear and performance at the diamond/rock contact.

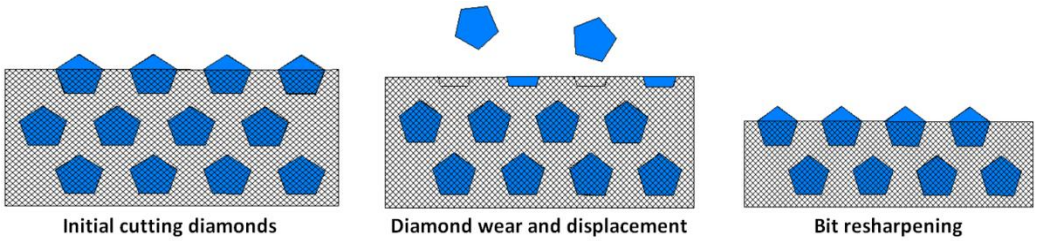

Figure 1-4. ID bits wear cycle

Diamond wear

In the current literature, the most prominent work investigating the behaviour of diamond wear in IDBs was conducted in 1990 by Miller and Ball. Using micro IDBs to drill into various types of hard rock, the diamond wear was studied by optical and SEM analyses over a range of different bit pressures (up to 12 MPa), penetration rates (up to 0.1 mm/rev) and sliding speeds (1 – 4 m/s). Set drilling conditions were repeated in a sequence of individual drill holes which were concatenated for a total drilling depth of approximately 1.5 m. For each test, tap water was used as the flushing coolant and the bits were preconditioned by drilling 0.3 to 0.5 m into abrasive sandstone to expose a fresh layer of diamonds.

At regular intervals of set incremental drilling distances, the wear of each exposed diamond was classified into four distinct wear modes. Typical SEM images of these wear modes are shown in Figure 1-5. Miller and Ball [39] found that, for all of the different rock types tested, the general nature of the diamond wear modes was the same. At low bit pressures, the depth of cut is very shallow and, therefore, less energy is transmitted into cutting. Instead, the exposed diamonds tend to slide over the rock surface producing wear flats due to cold hard mineral asperities ploughing through the heated plastically deformed diamond layers. At high velocities, it is also possible for diamonds to develop wear flats by graphitisation due to the high flash temperatures generated at the diamond surface [41].

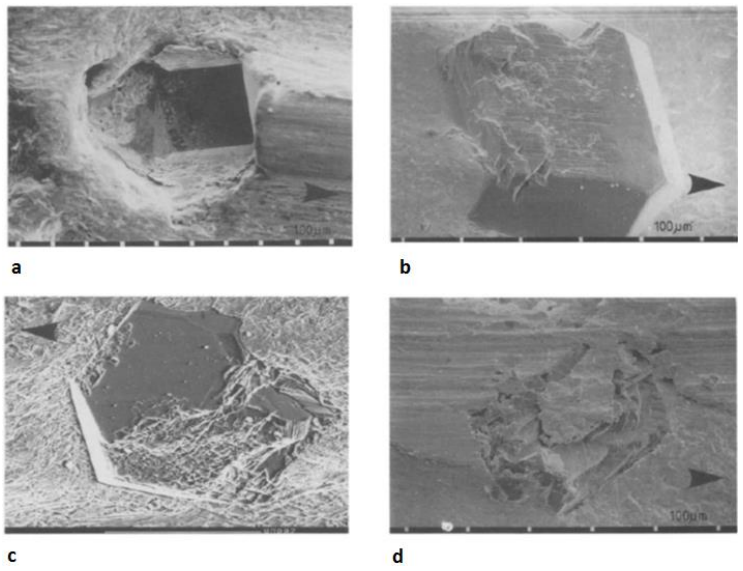

Figure 1-5. Scanning electron images of typical examples of diamond wear: (a) diamond fall-out; (b) wear flat; (c) microfracture; (d) macrofracture [35]

As bit pressure increases, a larger proportion of diamonds are able to cut the rock. This corresponds to a larger number of diamonds exhibiting microfracture whereby cyclical stresses, from the rock cutting process, build up strain and initiate cleavage microcracks which eventually lead to brittle failure. At a certain threshold pressure, the cutting work reaches an optimum level that can be provided by the exposed diamonds. Increasing the pressure above this point induces a high depth of cut and excessive forces which results in larger sized fractures, referred to as hackly macrofracture. Diamond fall-out can also occur when the depth of cut of a particular diamond is sufficiently large. The severe loss of diamonds, as a result of either macrofractures or diamond fall-outs, causes a rapid decrease in the protrusion of diamonds and, therefore, exposes more of the matrix at the bit-rock interface. This in turn reduces the cutting ability of the bit until a sufficient layer of the matrix is worn again to expose fresh sharp diamonds.

It was also observed that the drilling performance of ID microbits was related to the relative proportions of the different modes of diamond wear occurring at the bit-rock interface. For stable drilling in any given rock type a characteristic threshold pressure existed above which desirable microfracture of the exposed diamonds was

promoted over undesirable wear flat generation [35]. Furthermore, this stable drilling pressure corresponded closely with the minimum specific energy.

Based on the experimental results, Miller and Ball [39] proposed a general performance model outlining the drilling behaviour of ID bits in relation to thrust, specific energy and diamond wear. At bit pressures below the transitional phase, shallow depths of cut promote slippage and, consequently, wear flats develop. When drilling at set bit pressures, the increase of wear flat areas causes the penetration rate to continually drop and the specific energy to rise. Conversely, when drilling at a set penetration rate, the bit pressure generated will continually increase. At the transitional phase, bit pressure is sufficient for a maximal number of diamonds to sustain an optimum depth of cut. Here, microfractures become the predominant mode of wear as high rock cutting forces generate cyclical shear stresses at the diamond free-surface. Although this causes the bit wear rate to increase, it also prolongs the bit's cutting ability through a favourable balance of diamond and matrix wear. As a result, the penetration rate stabilises and the specific energy approaches a minimum. Steady drilling continues until diamonds begin to macrofracture or are prematurely removed. Such extreme pressures are considered to be inefficient as high penetration rates are coerced at the expense of a greater wear rate and specific energy. Additionally, large wear particles (or detritus), along with the diminished clearance between bit and rock, that are ineffectively flushed from the bit-rock interface can cause stalling or seizures which generate an additional reactive torque on the bit. This is often referred to as the 'cleaning problem' that is observed by drillers.

Effect of drilling parameters on diamond wear

To investigate the integrated process of diamond and matrix wear, Tian and Tian [34] conducted microbit drilling tests and measured the wear coefficients (defined as the bit mass loss over the penetration depth) against varying depths of cut and rotational speeds. Results from these tests indicate that the depth of cut plays a greater role in the wear rate of IDBs than the rotational speed. From this work, it can be concluded that the wear coefficient increased drastically when the depth of cut was increased whereas the wear coefficient only decreased slightly when the

rotational speed was increased. Tian and Tian [34] also observed a threshold depth of cut above which the drilling forces started to fluctuate significantly. From SEM analyses of the exposed diamonds, it was found that this threshold depth of cut was associated with a predominance of microfractures. For tests conducted below the threshold depth of cut, fluctuations in the drilling forces were much less pronounced and more wear flats were observed. Furthermore, when drilling at the threshold depth of cut, the drilling response appeared to be optimal. This behaviour is consistent with Miller and Ball's (1990) performance model [42].

1.2.3 Pattern recognition

Pattern recognition is part of machine learning [43] which, in turn, is a subfield of artificial intelligence (AI) [44]. The objective of machine learning is to develop algorithms that allow computers to learn from data. These algorithms are of particular importance because they are able to induce models that continually improve their performance over time as new data is available [45]. In the context of machine learning, two main classes of learning algorithms can be distinguished based upon their application and functionality:

Supervised learning: these algorithms learn from a labelled set of data. They analyse the training data and produce decision functions that are used to classify the response of new data. These sorts of algorithms are commonly used in classification and regression problems.

Unsupervised learning: those algorithms learning from non-labelled data. Their goal is to recognized different groups of data that share similar characteristics amongst themselves. These groups are the so-called clusters.

Hence, pattern recognition can be understood as the categorization of input data into identifiable classes through the extraction of significant features or attributes of the data. Formally, pattern recognition assigns new data into different discrete categories and/or classes. This is achieved by using a multidimensional input vector $X=[x_1, x_2, ..., x_n]$, where x_i are components associated to the vector X in an n-dimensional feature space, in order to calculate the optimal vector $\theta=[\theta_0, \theta_1, ..., \theta_n]$, where θ_i are the weight coefficients components of vector θ. These two vectors

constitute the so-called decision boundaries when their product equals to zero, $\theta^T X$=0. Decision boundaries can be linear or non-linear functions of the vector X [43].

Accordingly, decision boundaries can be interpreted as functions that divide the feature space into different discrete regions. Ideally, each region corresponds to one and only one of the discrete classes. Implementation of a pattern recognition system consists of two phases, training phase and classification phase. In training, the vector of weight coefficients (θ^T) of the decision boundary is obtained from the training dataset using an algorithm, which helps finding the decision boundary that minimises the classification error. Whilst in classification phase, the pattern classifier, which consists of decision boundaries, classifies incoming signal into one of the predefined classes. As the focus of this work is on the application of tool condition monitoring systems to ID drilling, more details on the theoretical background of pattern recognition and how to choose the parameters of vector θ via different algorithms can be found in [31, 32].

In this thesis, different patter recognition algorithms are used i.e. simple trees (ST), support vector machine (SVM) [46], K-nearest neighbour (KNN) with k=1 [47], boosted trees (BT) [48] and artificial neural networks (ANN) [15, 49]. A brief for these pattern recognition algorithms is given as follows since they are of particular interest on this research.

Simple trees (ST) and boosted trees (BT)

Both these algorithms are part of a bigger family of algorithms known as decision trees [44, 48, 50]. Decision trees are trees that consist of three types of nodes. Each internal node (or decision node) is initially labelled with an input feature. Then, the arcs (branches or links) coming from a decision node are branded with the possible values of the features. Finally, leaf nodes (or end nodes) of the trees are labelled with a class or a probability distribution over the classes. In this case, classes are sharp ID bit or blunt ID bit. (see Chapter 4).

Decision trees classify patterns or classes through a sequence of questions. In such a sequence, the *n* question strictly depends on the *n-1* answer. Decision trees

have the benefits of: *i)* being expressed as a logical expression, *ii)* rapid classification as a result of simple queries and *iii)* higher accuracy and speed [51].

Support vector machines (SVM)

SVMs generate one hyperplane or multiple hyperplanes in high-dimensional spaces. Such hyperplanes are then used for classifying the different classes. For instance, in a two-class classification problem using linear models of the form $y(X)=w^T\varphi(X)+b$ where $\varphi(X)$ denotes a fixed feature-space transformation and b the bias parameter. Training dataset is $X=[x_1, x_2, ..., x_n]$, and associated targets values (classes) $T=[t_1, t_2, ..., t_n]$, where t_i belongs to {-1,1}[44] and new data points X are classified by the sign of $y(X)$[50].

Assuming that the training data set is linearly separable in feature space, there exists at least one choice of the parameters w and b such that a the linear function satisfies $y(x_n)>0$ for points having $t_n=+1$ and $y(x_n)<0$ for points having $t_n=-1$, so that $t_n y(x_n)>0$ for all training data points. Certainly, there may be many solutions that separate the classes exactly, in this case, it is ideal that the solution will give the smallest generalization error.

Support vector machine approaches this problem by the concept of the margin, which is defined to be the smallest distance between the decision boundary and any of the samples [50]. In support vector machines the decision boundary is chosen to be the one for which the margin is maximized. The maximum margin solution can be found using statistical learning theory [50].

k-nearest neighbour (KNN)

KNN is a non-parametric algorithm based on the probability theory [44, 50]. For this algorithm a basic definition of local density estimation is required (Eq. 1.3). Instead of fixing V and determining the value of K from the data, KNN algorithm requires a fixed value of K and use the data to find an appropriate value for V. To do this, a small sphere is considered on the point x is at which the estimation of the density $p(x)$ is required. Next, the radius of the sphere is expanded until it contains precisely K data points. The estimate of the density p(x) is then given by (Eq. 1.3)

with *V* set to the volume of the resulting sphere. In other words, the class value of a point is determined by the average of the k-nearest neighbours.

$$P(x) = \frac{K}{NV} \tag{1.3}$$

where P(x) is probability density in D-dimension space, K is the number of points inside the selected region, N is number of observations (data points) and V is the volume of the selected region.

The particular case of K=1 is called the nearest-neighbour rule, because a test point is simply assigned to the same class as the nearest point from the training set.

Artificial neural networks (ANN)

ANNs are extensively used in different engineering applications due to their well-known capabilities of performing non-linear modelling of multiple variables. ANNs imitate the behaviour of the real neural system. The basic principle is given by the neuron activation mechanism, where a neuron is activated by an input and only responds if the input magnitude is greater than a determined threshold [52]. The type of neural network used in this study is termed Multi Layered Perception (MLP). A MLP neural network consists of an input layer, a hidden layer and an output layer. The input layer represents all selected AE features and rock properties, the hidden layer contains non-linear relationships and finally, the output layer corresponds to the prediction neurons. Each layer contains one or more processing units (neurons). Each neuron has a set of weights and an activation function in order to emulate the threshold activation that exists on real neural systems. The output of one weighted processing unit (neuron) can be calculated using Eq. (1.3).

$$\mathrm{y} = f\left(\sum_{k=1}^{n} \mathrm{w}_k x_k\right) \tag{1.4}$$

where f is the activation function, w_k is the weight for the k-input and x_k is the k-th independent variable [52]. For the most problems, sigmoid or hyperbolic tangent function can be considered a good activation function.

The weights are the interconnection between layers that contribute to the prediction and classification power of the ANN. During the learning phase, these

interconnections learn from experimental data by optimizing the quadratic error between the prediction and real value of the output variable. A widely used optimization method is the gradient descendent method. For performance assessment of the ANN model, three datasets are required: training, validation and testing datasets. The training dataset is used to find the optimal weights. Validation dataset is utilized in order to avoid overfitting, which occurs when the ANN memorizes and replicates the training dataset. For more information on ANN refer to [50].

1.2.4 Rock drilling studies and AE

Acoustic emission and ID drilling are two individually well-studied fields as evidenced above. Plenty of literature is available for individual fields; however, literature covering both fields is more limited. A review of this literature, studying the relations of AE with ID drilling and drilling-related rock properties, is given as follows.

Acoustic emission applied to rock drilling/cutting

Acoustic Emission has been successfully applied to monitor rock drilling at laboratory-scale and field-scale. Niitsuma and Chubachi [53] investigated the AE generated by a tri-cone bit in order to evaluate different rock formation and special drilling processes. In their paper, they demonstrated the feasibility of the AE monitoring in well-drilling. One of their two most outstanding findings is that the Root Mean Square signal (AE_{rms}) level was higher at welding and fractured zones, which in fact implies that AE is sensitive to different rock formations specifically its hardness [53]. Further, their other important finding is that special drilling processes, e.g. rubbing of drill collar, jarring and reaming, were clearly differentiable from the AE signature. In conclusion, well-drilling can be successfully monitored by applying AE technique [53].

Asanuma, *et al.* [54], [55] also carried out studies monitoring tri-cone bit drilling with AE technique. They also found a correlation between the mean amplitude RMS level of the signal and the hardness of the rock formation being drilled. Furthermore, homogeneity of the formation is represented by the frequency and

amplitude of peaks on the RMS signal. Rock characteristics have a direct influence on RMS level per unit of drilling advanced [56]. In addition, they also found that an increase in higher frequency emissions occurs when the drillability of rocks decreases. This occurs despite the fact that the shape of power spectrum of the AE has little variation when changing the rock types.

A landmark study is Xiaoqing Sun's work in 1999 [18], in which he made interesting conclusions from his tungsten carbide rotary drill field test, drilling in two different rock formations. Important results with regard to AE parameters and specific drilling scenario can be drawn from this research work. He concluded that AE count and AE event count linearly increase with the record time. In contrast, the rate of the AE count and AE event count remain at constant levels. Another notable conclusion is that the total AE count number is higher for drilling with a new bit compared to a worn bit. Finally, he utilised a pattern recognition analysis to demonstrate that different drilling situations may be identified by the characteristics of AE signals generated at the rock/bit interface [18].

In a similar study to that of [18], Gradl, *et al.* [57] utilise frequency-domain analysis of the sound generated by Polycrystalline Diamond Compact (PDC) bits and roller cone bits. Their principal findings are that: i) The sound generated by PDC bits shows a clear relation with their design. Such relation matches with predictions made by slip-stick process. ii) Roller cone bits do not show rotational-related peaks in their frequency spectrum. They claim that the study offers a starting point for further research using sound in order to measure bit performance or detect bit problems (wear).

Williams and Hagan [58] utilised wide tungsten carbide bits in their coal cutting experiments and found that drilling with a worn bit produced a signal with lower AE_{rms}. More recently, Klaic, *et al.* [59] create a tool condition monitoring (TCM) system to predict wear of small diameter twist drill bit. They use pattern recognition/machine learning techniques in order to infer the wear condition (sharp or worn) of the bits. As further work, they recommend drilling in different type of rocks with different drill designs at various degrees of wear.

Acoustic Emission and drilling related rock properties

In term of rock properties that have been studied using AE, there are various studies focusing on explicitly drilling-related [21] and non-explicitly drilling-related [60] properties of the rocks.

Jung, *et al.* [21] conducted indentation tests to demonstrate that AE characteristic, including AE rate, total even number, peak value of AE amplitude and total AE energy, depend to a large extent on indentation hardness. The primary aim of the study was to predict indentation hardness of rocks through AE. The study found a marked correlation between RMS of AE events with indentation hardness. As a conclusion Jung, *et al.* [21] stated that integrated RMS is the index with the highest correlation to the indentation hardness of rock. It is also suggested that peak RMS may be further employed in the prediction of rock drillability if associated with penetration rates of drilling.

In a laboratory-scale study conducted by Kumar, *et al.* [60], sound generated from carbide drill bits of multiple diameters is used to predict rock properties. Empirical relations are derived between A-weighted equivalent sound level and Uniaxial Compressive Strength, Schmidt Rebound Number and Young's Modulus while considering changes due to speed, diameter and penetration rate of the drill bit. They suggest further studies not only to cover a wider range of rock but also different rock properties.

1.3 Shortcoming of previous contributions

Based on the literature review on AE technique applied to rock drilling and drilling-related rock properties, it is evident that there is a lack of research covering both AE monitoring of Impregnated Diamond (ID) drilling and evaluation of ID drilling-related rock properties through AE.

When it comes to specifically AE monitoring of ID drilling, two important drawbacks can be identified. Firstly, the influence of ID drilling parameters, rate of penetration (v), angular velocity (Ω), weight-on-bit (WOB) and torque-on-bit (TOB), on the AE signature is unknown. Secondly, the influence of ID tool condition on the AE signature and its utility are not known.

Regarding the evaluation of ID drilling-related rock properties through AE, it is clear that the property that is believed to control the wear rate of ID tools, abrasivity [35, 61], has not yet been studied using AE.

1.4 Objectives and thesis overview

The primary objective of this thesis is to study the applicability of AE technique to ID rock drilling and drilling-related rock properties. More specifically, to address the drawbacks mentioned in Section 1.3 which can be achieved by addressing the following sub-objectives.

1. **To develop testing methodology using AE that will allow us to examine relations between AE signals and drilling parameters (TOB, WOB, v and Ω).** This objective is addressed by defining relations between TOB, WOB and depth of cut with acoustic parameters (AE_{rms}) during topologically-invariant drilling tests. See Chapter 3 for more details in regard to this objective.
2. **To define ID bits wear states in order to study the influence of the tool condition on the AE signature.** Completion of this objective is done by defining important wear states, sharp and blunt, for ID bits. Then, topologically-invariant tests are carried out at the two wear states and a series of tool condition monitoring (TCM) systems are generated. For more details see Chapter 4
3. **To identify the principal rock property directly affecting the wear rate of ID tools and study it utilising AE**. Objective 3 is addressed in Chapter 5 and Chapter 6 where abrasivity is identified as the rock property that mainly affects the wear rate of ID drilling tools. Cerchar Abrasivity Index (CAI), due to its definition, is used and studied via AE.

This document is presented in the format of combination of publications/conventional thesis. It consists of 7 chapters. Following Chapter 1, which introduces the research work, Chapter 2 provides an overview of the experimental methodology utilised in the research work. Chapters 3 to 6 present the main part of the work in which research outcomes and contributions are presented.

Lastly, conclusions of the work and recommendations for further work are presented in Chapter 7.

Chapter 2 describes the experimental methodology employed in the research work. Initially, it provides an overview on the experimental setups –drilling rig and abrasivity apparatus- and different systems –AE system and MWD system- used in the research as well as a generalisation of the procedures followed in testing, both drilling tests and abrasivity tests.

Chapter 3 is aimed at determining the relations between acoustic emission parameters and operational parameters of the drill rig taking into account the bit wear state. Echidna drill apparatus was used to monitor AE during rock–bit interaction. AE sensors are attached to both the drill and the rock under study to record acoustic signals being emitted during drilling. Two different types of tests were conducted – step tests, topologically-invariant, and wear tests, topologically-variant. Step tests included stepping down the depth of cut from 130 μm/rev to 0 μm/rev. Wear tests involved accelerating the wear rate of the drill bit by using it to cut highly abrasive rock while keeping the depth of cut constant. Based on the step test results, a series of linear relationships were developed. These relationships make it possible to estimate the depth of cut, WOB and TOB by simply using the time spectrum of the AE signals.

Chapter 4 the applicability of artificial intelligence (AI) based techniques to monitor tool condition of ID bits, sharp and/or blunt. Hence, topologically-invariant tests are performed with sharp and blunt bits while recording AE and measuring-while-drilling variables. These are then used as inputs variables to create two approaches for the prediction of bit bluntness. The first is based on the aforementioned variables and the second is by using the concept of specific energy in drilling.

Chapter 5 presents a new AI-based model to predict rock abrasiveness via CAI. It utilizes AE and "classical" rock properties as main indicators of rock abrasivity. AE sensors are attached to both the Cerchar testing apparatus and the rock in question while conducting scratch tests using hardened steel pins of 42 and 56 HRC.

Prior to the implementation of Artificial Neural Network (ANN) modelling, the selection of independent variables was carried out via Gamma test and V-ratio analyses. As a result, AE parameters, such as total number of events and root mean square of signal, in addition to testing parameters (i.e. uniaxial compressive strength, Young's Modulus, quartz content and pin hardness) are found to be the optimum model input combination needed to accurately predict CAI.

Similarly, in Chapter 6 the influence of mineral composition of granitic rocks on the AE whilst scratching rocks with a single contact tool and the feasibility of AE as a means to infer CAI are presented. Single contact tool is utilised since it allows a better understanding and identification of the mechanism generating the AE waves. A Cerchar apparatus that was modified to provide constant scratching speed is utilized to monitor AE during rock/tool interaction. HRC-56 steel pins are used for scratching the rocks. Two AE PICO sensors with an operating frequency range of 200-750 kHz were used. Continuous AE signals were recorded with 1 MHz sampling rate during scratching. Tests on the modified Cerchar apparatus are carried out under the static load of 70N and cutting speed of 1 mm/s. A Scanning Electron Microscope (SEM) is utilized to visualize the groove in the rock and to identify the mineral composition through Back-Scattered Electrons (BSE) reflected from the rock sample.

Finally, Chapter 7 summarises the main contributions and conclusions. The limitations and recommendation for further work are also discussed.

1.5 References

[1] Australian Bureau of Statistics, Mineral and Petroleum Exploration, Canberra, 2016.

[2] M. Hood, F. Roxborough, Rock breakage: mechanical, SME mining engineering handbook, Society for mining, metallurgy and exploration, inc., Littleton, CO, 1992.

[3] W.P. Dong, Y.H.J. Au, A. Mardapittas, Characteristics of acoustic emission in drilling, Tribol Int, 27 (1994) 169-170.

[4] T.G. Langdon, R.B. Vastava, An evaluation of deformation models for grain boundary sliding, in: R.W. Rohde, J.C. Swearengen (Eds.) Mechanical testing for deformation model development, American society for testing materials, Philadelphia, 1982, pp. 435-451.

[5] University of Cambridge, Dislocations in 2D, Dissemination of IT for the Promotion of Materials Science, 2008.

[6] C.E. Everson, S.H. Cheraghi, The application of acoustic emission for precision drilling process monitoring, Int J Mach Manuf, 39 (1999) 371-387.

[7] R. Kovacevic, H.S. Kwak, R.S. Mohan, Acoustic emission sensing as a tool for understanding the mechanisms of abrasive water jet drilling of difficult-to-machine materials, Proceedings of the Institution of Mechanical Engineers, Part B: Journal of Engineering Manufacture, 212 (1998) 45-58.

[8] E. Kannatey-Asibu Jr, D.A. Dornfeld, A study of tool wear using statistical analysis of metal-cutting acoustic emission, Wear, 76 (1982) 247-261.

[9] C. Grosse, M. Ohtsu, Acoustic Emission Testing: Basics for Research-Applications in Civil Engineering, Springer Berlin Heidelberg, 2008.

[10] J. Hanchi, B.E. Klamecki, Acoustic emission monitoring of the wear process, Wear, 145 (1991) 1-27.

[11] V. Baranov, E. Kudryavstev, G. Sarychev, V. Schavelin, Acoustic emission in friction, Elsevier, 2007.

[12] X. Chen, B. Li, Acoustic emission method for tool condition monitoring based on wavelet analysis, Int J Adv Manuf Technol, 33 (2007) 968-976.

[13] L.J. Sudev, H.V. Ravindra, Tool wear estimation in drilling using acoustic emission signal by multiple regression and GMDH, ASME International Mechanical Engineering Congress and Exposition (IMECE), ASME, Boston, MA, 2008, pp. 97-106.

[14] M.P. Gómez, A.M. Hey, J.E. Ruzzante, C.E. D'Attellis, Tool wear evaluation in drilling by acoustic emission, Phys Procedia, 3 (2010) 819-825.

[15] H.R. Hardy, Acoustic Emission/Microseismic Activity, Taylor & Francis, 2003.

[16] T. Shiotani, Parameter Analysis, in: C. Grosse, M. Ohtsu (Eds.) Acoustic Emission Testing: Basics for Research-Applications in Civil Engineering, Springer Berlin Heidelberg, 2008, pp. 41-51.

[17] T. Richard, CSIRO (Personal Communication), 2013.

[18] X.Q. Sun, A study of acoustic emission in drilling applications, The 37th U.S. Symposium on Rock Mechanics: Rock mechanics for industry (USRMS), A Balkema, Vail, CO, 1999, pp. 983-990.

[19] D. Crosland, R. Mitra, P. Hagan, Changes in Acosutic Emissions when cutting difference rock types, Coal 2009: Coal operators' conference, Australasian Institute of Mining and Metallurgy, University of Wollongong, 2009, pp. 329-339.

[20] A.L. Quadro, J.R.T. Branco, Analysis of the acoustic emission during drilling test, SuCT, 94–95 (1997) 691-695.

[21] S.J. Jung, K. Prisbrey, G. Wu, Prediction of rock hardness and drillability using acoustic emission signatures during indentation, Int. J. Rock Mech. Min. Sci., 31 (1994) 561-567.

[22] S. Chandrashekhar, R.H. Osuri, S. Chatterjee, Preliminary investigation into the prediction of drill wear using acoustic emission, Winter Annual Meeting of the ASME, ASME, Dallas, TX, USA, 1990, pp. 123-137.

[23] K. Jemielniak, O. Otman, Tool failure detection based on analysis of acoustic emission signals, J Mat Process Technol, 76 (1998) 192-197.

[24] R. Shiavi, Introduction to Applied Statistical Signal Analysis, 3rd ed., Academic Press, Burlington, 2007.

[25] M. Heideman, D. Johnson, C.S. Burrus, Gauss and the history of the fast Fourier transform, Arch. Hist. Exact Sci., 34 (1985) 265-277.

[26] M. Bath, Spectral Analysis in Geophysics, Elsevier Scientific Publishing Company, Amsterdam, 1974.

[27] V. Reddy, On Fast Fourier Transform-a popular tool for Spectrum Analysis, Reson, 3 (1998) 79-88.

[28] C.J. Li, S.Y. Li, Acoustic emission analysis for bearing condition monitoring, Wear, 185 (1995) 67-74.

[29] M.G. Waldenstrom, U.K.R. Fischer, L.H. Hillert, M.D. Dennis, Diamond rock tools for percussive and rotary crushing rock drilling, USA, 1992.

[30] K.U.M. Rao, B. Misra, Principles of rock drilling, A.A. Balkema, Rotterdam, 1998.

[31] S.Q. Kou, H.Y. Liu, P.A. Lindqvist, C.A. Tang, Rock fragmentation mechanisms induced by a drill bit, Int. J. Rock Mech. Min. Sci., 41, Supplement 1 (2004) 527-532.

[32] G.J. Bullen, Hard rock drilling - Some recent test results, Industrial Diamond Review, 44 (1984) 270-275.

[33] S.L. Huang, Z.W. Wang, The mechanics of diamond core drilling of rocks, Int. J. Rock Mech. Min. Sci., 34 (1997) 134.e131-134.e114.

[34] X. Tian, S. Tian, The wear mechanisms of impregnated diamond bits, Wear, 177 (1994) 81-91.

[35] D. Miller, A. Ball, The wear of diamonds in impregnated diamond bit drilling, Wear, 141 (1991) 311-320.

[36] A. Bhatnagar, M. Khandelwal, K.U.M. Rao, Enhancing diamond drilling performance by the addition of non-ionic polymer to the flushing media, Mining Science and Technology (China), 20 (2010) 400-405.

[37] L. Jones, Boart Longyear Australia PTY LTD (Personal Comunication), 2011.

[38] K.U.M. Rao, A. Bhatnagar, B. Misra, Laboratory investigations on rotary diamond drilling, Geotech Geol Eng, 20 (2002) 1-16.

[39] D. Miller, A. Ball, Rock drilling with impregnated diamond microbits—An experimental study, Int. J. Rock Mech. Min. Sci., 27 (1990) 363-371.

[40] T. Richard, L.F.P. Franca, DET-CRC confidential report - Fundamentals of rock drilling processes, Confidential report to DET CRC, CSIRO Earth science and Resource Engineering,, 2011, pp. 25.

[41] J.R. Hird, J.E. Field, A wear mechanism map for the diamond polishing process, Wear, 258 (2005) 18-25.

[42] D. Miller, A. Ball, An instrumented laboratory machine for the ecaluation of drill-bit performance, J. S. Afr. Inst. Min. Metall., 90 (1990) 283-288.

[43] X. Li, A brief review: acoustic emission method for tool wear monitoring during turning, Int J Mach Manuf, 42 (2002) 157-165.

[44] T.M. Mitchell, Machine Learning, McGraw-Hill, New York, 1997.

[45] S.J. Russell, P. Norvig, Artificial intelligence: a modern approach, 3rd ed., Prentice Hall, Sydney, 2010.

[46] C. Cortes, V. Vapnik, Support-Vector Networks, MLear, 20 (1995) 273-297.

[47] H.W. Shen, H.R. Hardy, A.W. Khair, Laboratory study of acoustic emission and particle size distribution during rotary cutting, Int. J. Rock Mech. Min. Sci., 34 (1997) 121.e121-121.e116.

[48] J.H. Friedman, Greedy Function Approximation: A Gradient Boosting Machine, The Annals of Statistics, 29 (2001) 1189-1232.

[49] S. Perez, M. Karakus, An artificial neural network approach for the prediction of abrasivity of hard rocks using acoustic emission, in: W. Schubert, A. Kluckner (Eds.) Eurock 15 & 64th Geomechanics colloquium, Salzburg, Austria, 2015, pp. 285-290.

[50] C.M. Bishop, Pattern recognition and machine learning, Springer, USA, 2007.

[51] Michigan State University, Decision trees, in: C.S.a. Engineering (Ed.), 2015.

[52] H. Vardhan, B.R. Kumar, Application of Artificial Neural Networks, Rock Engineering Design, CRC Press, 2013, pp. 105-130.

[53] H. Niitsuma, N. Chubachi, AE monitoring of well-drilling process by using a downhole AE measurement system, in: K. Yamaguchi, K. Aoki, T. Kishi (Eds.) Progress in Acoustic emission III, The Japanese Society for Non-Destructive Inspection, Tokyo, Japan, 1986, pp. 436-445.

[54] H. Asanuma, H. Niitsuma, M. Sato, N. Chubachi, Characterization of rock formation by means of AE monitorgin during well drilling, Progress in Acousti Emission III, The Japanese Society for Non-Destructive Inspection, Kobe, Japan, 1988, pp. 248-257.

[55] H. Asanuma, H. Niitsuma, N. Chubachi, Characterization of subsurface rock mass by means of pulse train analysis of AE during well drilling, JASJa, 46 (1990) 33-39.

[56] H. Asanuma, H.R. Hardy, Acoustic emission associated with rock drilling tests under laboratory conditions, in: K. Yamaguchi, H. Takahashi, H. Niitsuma (Eds.) Progress in Acoustic Emission V, The Japanese Society for Non-Destructive Inspection, Sendai, Japan, 1990, pp. 430-435.

[57] C. Gradl, A.W. Eustes, G. Thonhauser, An Analysis of Noise Characteristics of Drill Bits, Journal of Energy Resources Technology, 134 (2011) 013103-013103.

[58] E. Williams, P. Hagan, Monitoring acoustic emission levels with changes in rock cutting conditions, UNSW, Sydney, 2002.

[59] M. Klaic, T. Staroveski, T. Udiljak, Tool Wear Classification Using Decision Trees in Stone Drilling Applications: A Preliminary Study, Procedia Engineering, 69 (2014) 1326-1335.

[60] B.R. Kumar, H. Vardhan, M. Govindaraj, Sound level produced during rock drilling vis-à-vis rock properties, Eng. Geol., 123 (2011) 333-337.

[61] J. Paone, D. Madson, Drillability studies - Impregnated diamond bits, United States Department on the Interior, Washington, 1966.

Chapter 2

Experimental Methodology

This chapter describes the proposed experimental program and tools employed in the research. Initially, the experimental setup, which is composed of drilling rig, Cerchar apparatus, AE system and SEM microscope, is described. Following, a detailed description of the testing procedure employed in drilling and CAI testing is given. More details on how the drilling or CAI testing systems are integrated to the AE system as well as respective experimental procedures are given on the respective chapters.

2.1 Experimental setups

2.1.1 Echidna drilling rig

Echidna is a computer controlled laboratory drilling rig that is utilized to investigate the drilling action of ID bits. Kinematic controlled tests are exerted with this setup, that is, Ω and V are imposed via a rotary drive mechanism and an upper motor assembly respectively (Figure 4-1). Echidna rig is used to study the relations between AE signal and drilling variables in Chapter 3. Tests utilised to develop the tool condition monitoring systems, Chapter 4, also make use of Echidna rig.

A linear actuator and a geared brushless electrical servo-motor compose the upper motor assembly. This assembly has a load capacity of up to 40 kN and can provide a precise V ranging from 0.1 to 13 mm/s. Weight on bit, WOB is measured by a uniaxial force transducer placed on the end of the actuator shaft. The rotary

drive mechanism consists of an electrical brushless servo-motor, a timing belt pulley system and a torque sensor (sprocket pulley sensor). The maximum TOB capacity of this system is 94 Nm and provides rotary speed, Ω, ranging from 10 to 250 rad/s. Accurate depth of cuts from 1 to 200 μm/rev can be exerted by combining these two systems, the rotary drive system and the upper motor assembly.

2.1.2 Cerchar apparatus

A conventional West Cerchar apparatus has been used (see Figure 5-2). It has been equipped with a stepper motor. The stepper motor has been directly installed to one of the two hand cranks driving the screws in the two-axis cross table. The purpose of the modification that has been carried out is not only to match acoustic emission with the spatial location in the rock specimen but also to ensure constant velocity of scratching in the tests. 56 HRC and 42 HRC pins will be used in order to avoid discrepancies found in the literature. The adopted velocity for the current series of tests is 1 mm/s. The modified Cerchar apparatus is used for testing in Chapter 5 and Chapter 6 to evaluate abrasivity of various rock while recording AE signals.

2.1.3 AE system

The AE system used consists of a WDI-AST and PICO sensor (with pre-amplifier) sensor along with a data acquisition card (DAQ) and a LabView program developed in-house at the University of Adelaide. The WDI-AST is a wide band AE sensor with 40 dB gain integrated pre-amplifier and an operating frequency range of 200-900 kHz and the PICO AE sensors had a frequency range of 200–800 kHz and required external preamplifiers to magnify the AE signals

The DAQ is a NI PCI-61333 (16 M Samples) S Series Multifunction DAQ Device. The DAQ card has eight analogue channels each of which is able to collect up to 3 million samples per second. Sampling rate for the AE signals during drilling and scratching tests is 0.8 MHz and 1.5 MHz respectively. The WDI sensor is placed on the upper surface of the rock sample, and for safety reasons, at the furthest edge from drilling and/or scratching while the PICO sensor is place on the tool, either Echidna drill rig or Cerchar apparatus. Silicone gel is used as ultrasonic couplant between the sensors and the rock surface. The AE system is utilised in all

chapters of this thesis with only slight variations according to the experimental setup which is being used for testing.

2.2 Experimental procedure

Two experimental procedures are implemented for this research work. First, drilling tests procedure is oriented to fulfil objective 1 and 2 of this research. Secondly, the abrasivity tests procedure is applied in order to achieve objective 3 of the current work.

2.2.1 Drilling tests

Continuous topological changes take place, constantly, in the cutting face of the ID tools. These changes in the topology of the ID tools are important to define source of AE generated while drilling. Therefore, two specific responses are here considered, topologically variant (considering wear) and topologically invariant (without wear) [1].

Topologically variant

Topologically variant tests are non-stationary responses characterised by changes in the topology of the drilling face. The evidence of the changes is the variation of WOB and TOB while cutting under constant depth of cut. Non-stationary responses are conducted for determining the influence of bit wear cycle on the AE signature. These tests include weight and height losses of the bits.

Topologically invariant

For performing topologically invariant (instantaneous) tests, a rigorous test protocol proposed by Franca *et al* [1] is followed. The protocol is composed by three stages: pre-test, test, and post-test. (see Figure 2-1)

In the pre-test, tool conditioning is performed at the cutting face, sharpening or blunting, by imposing a depth of cut (kinematically controlled test) of 5 to 10 µm/rev greater than the maximum depth of cut to be applied during the testing phase.

Drilling tests (Figure 2-2) are carried out at various depths of cut with increments of 5 - 10 µm/rev for ID core bits, while the AE and drilling forces are recorded. The time interval of each depth of cut is set at about 5 s, or about 130 revolutions, which is sufficiently long to record a stationary signal while guaranteeing a topologically invariant response of the ID bit.

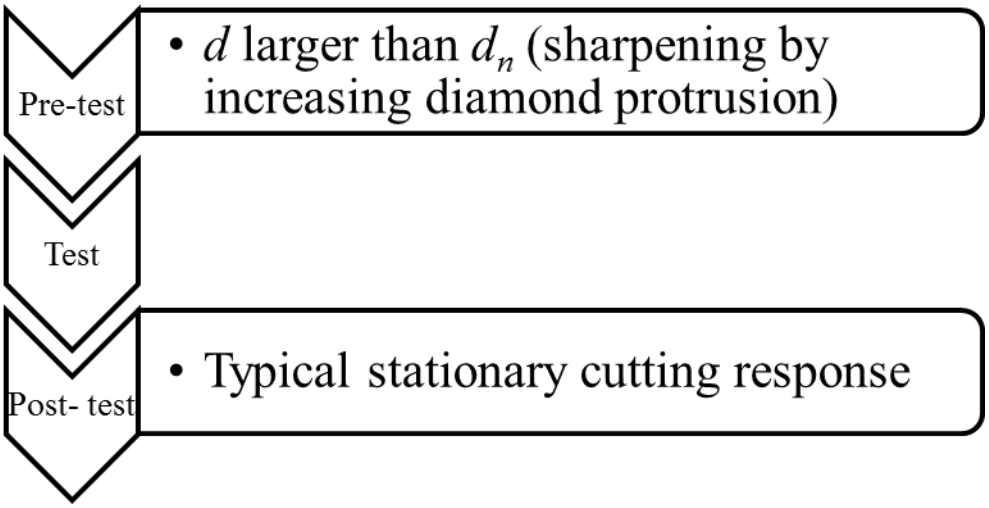

Figure 2-1. Topologically invariant testing procedure.

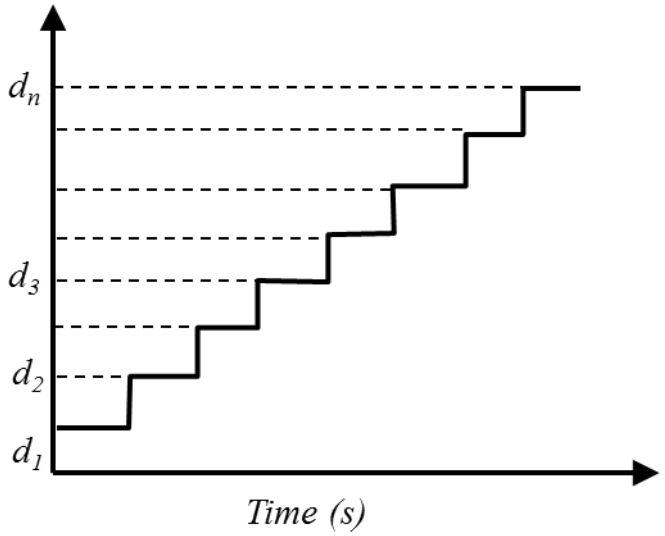

Figure 2-2. Depth of cut variation during topologically invariant testing.

2.2.2 Abrasivity tests

Abrasivity tests are performed according to ASTM [2] [63]. A conventional West Cerchar apparatus is used to scratch steel stylus with a 90° conical tip are along 10 mm of the rock surface. 42HRC and 56 HRC pin hardness are used. The surface of the rock specimens used are considered smooth as specimens were diamond sawn, according to ASTM [2]. Tests on the modified Cerchar apparatus are carried out under a static load of 70 N at a velocity of 1 mm/s. to ensure constant velocity, a stepper motor is installed in one of the two axis of the Cerchar apparatus (see Figure 2 3). One CAI is equivalent to 0.1 mm measured at the top of the conical pin. For fine-grained rocks, the reported CAI is the result of 3 individual tests are; whereas for coarse-grained rocks, 5 tests are averaged in order to obtain the reported CAI.

2.3 References

[1] L.F.P. Franca, M. Mostofi, T. Richard, Interface laws for impregnated diamond tools for a given state of wear, Int. J. Rock Mech. Min. Sci., 73 (2015) 184-193.

[2] ASTM, Standard Test Method for Laboratory Determination of Abrasiveness of Rock Using the CERCHAR Method, D7624-10, American Society for Testing and Materials, 2010.

Statement of Authorship

Title of Paper	Acoustic emission analysis for rock-bit interactions in impregnated diamond drilling
Publication Status	☑ Published ☐ Accepted for Publication ☐ Submitted for Publication ☐ Unpublished and Unsubmitted work written in manuscript style
Publication Details	Karakus, M & Perez, S, 2014. Acoustic emission analysis for rock–bit interactions in impregnated diamond core drilling, *International Journal of Rock Mechanics and Mining Sciences,* 68(0):36-43.

Principal Author

Name of Principal Author (Candidate)	Santiago Perez		
Contribution to the Paper	Data analysis, paper write-up and data collection		
Overall percentage (%)	70		
Certification:	This paper reports on original research I conducted during the period of my Higher Degree by Research candidature and is not subject to any obligations or contractual agreements with a third party that would constrain its inclusion in this thesis. I am the primary author of this paper.		
Signature		Date	

Co-Author Contributions

By signing the Statement of Authorship, each author certifies that:

i. the candidate's stated contribution to the publication is accurate (as detailed above);

ii. permission is granted for the candidate in include the publication in the thesis; and

iii. The sum of all co-author contributions is equal to 100% less the candidate's stated contribution.

Name of Co-Author	Murat Karakus		
Contribution to the Paper	Manuscript evaluation		
Signature		Date	

Chapter 3

Acoustic emission analysis for rock–bit interactions in impregnated diamond drilling

Abstract

Our goal was to determine the relationship between acoustic emission (AE) signals and diamond drill bit wear in order to gather and interpret data to allow overall improvement of drilling performance. Achieving improved performance required investigating various drilling parameters to understand the characteristics of the AE signals in terms of their interaction with the operational parameters of the drilling apparatus. Echidna drill apparatus that simulates field exploration diamond drilling on a small scale was used to monitor AEs during rock–bit interaction. AE sensors were attached to both the drill and the rock in question to record acoustic signals being emitted during the process of drilling. Two different types of tests were conducted – step tests and wear tests. Step tests on the Echidna drill included stepping down the depth of cut from 130 μm/rev to 0 μm/rev, while the cutting speed remained constant. Wear tests, again using the Echidna drill, involved accelerating the wear rate of the drill bit by using it to cut highly abrasive rock in two different ways. Based on the step test results, a series of linear relationships were developed. These relationships make it possible to estimate the depth of cut, weight on the bit (WOB) and torque on the bit (TOB) by simply using the time spectrum of the AE signals. Wear tests also showed that AE amplitudes start to trend down as wear begins to accelerate.

3.1 Introduction

Impregnated diamond core drilling is a key technology employed in the advanced stages of mineral exploration. Through this technology, existing resources are expanded and new mineral deposits are discovered. In Australia, for example, total mineral exploration expenditure increased to $790.2 million in the last quarter of 2012 from $200 million in 2003 [1]. Currently diamond drill operators use operational parameters such as weight on the bit (WOB), cutting speed (rpm), depth of cut, torque on the bit (TOB) and mud pressure to control drilling performance, and usually rely on experience to anticipate and recognise changes in drilling conditions associated with different diamond wear states and rock formations. The process is subjective and prone to error, which escalates during deep exploration, which is increasing dramatically as near surface mineral deposits are rapidly being depleted at rates significantly higher than new mineral deposits are being discovered.

Given that the direct measurement and visualization of the impregnated diamond drill bit–rock interface is extremely difficult in deep exploration drilling, AE monitoring could be a viable technique to remotely assess the interaction at the impregnated diamond drill bit–rock interface, including the diamond bit wear state. Although AE monitoring has been used extensively to monitor different aspects of drilling across different manufacturing processes, and to better understand the mechanisms behind the drilling process, it has not yet been applied to impregnated diamond drilling in order to remotely assess drilling conditions. Given the importance of mining in today's international market, overall growth and modern lifestyle, it is imperative that improvements be made to current drilling practices in order to achieve optimal performance.

Research in the laboratory has shown that the use of AE for detecting tool wear and breakage in single-contact turning operations is feasible [3]. Furthermore, the sudden release of energy that emanates from a deforming or stressed material through acoustic waves [2], i.e., AE, can also detect other aspects of rock drilling situations [4]. Therefore, the ultimate goal of the current research was to develop a drill bit–rock interface monitoring technology capable of providing the operator

with live information about the condition of the down-hole drill bit. It is anticipated that the successful implementation of this technology may lead to increased efficiency, extended drill bit life and reduced drilling costs.

3.2 Impregnated diamond core drilling

Impregnated diamond core drilling is a dynamic tribological process involving the interaction of surfaces in relative motion, which are affected by friction and wear and require lubrication [5]. Processes including indentation, cutting, scratching, grinding, ploughing, shearing and crushing are all present at the drilling interface in varying proportions depending on drilling conditions [6,7]. These interactions are accompanied by friction, which is generated by diamonds and matrix sliding along the rock surface, no matter how small the relative motion between them.

Baranov et al. [12] have stated that materials under friction conditions pass through three different stages of wear – running-in, steady state and catastrophic. The running-in stage shows changes in the friction surface and the physical–chemical characteristics of the bit and the rock. As long as external parameters remain constant, these changes will result in a decrease of the friction force, the temperature of the mating materials, and the wear rate [12]. Following the initial running-in, the steady state is characterized by constant values of the friction coefficient, wear rate, temperature and roughness. The processes of friction and wear are stationary, and the geometry of the friction surfaces is continuously reproduced [12]. During the stage of catastrophic wear, there are sharp changes in the characteristics of the friction state. The friction coefficient, wear rate and constant temperature all increase [12].

Operational variables during drilling are both dynamic and kinematic (see Figure 3-1), and are controllable. These parameters are chosen according to the drilling conditions in an attempt to optimize performance.

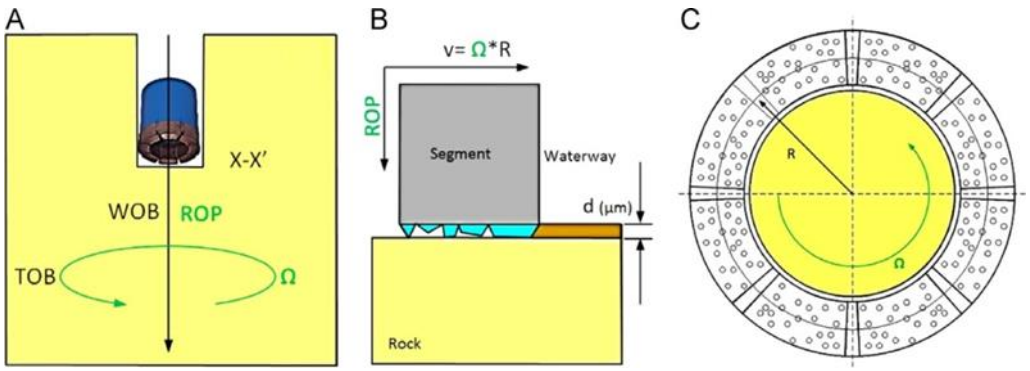

Figure 3-1. Diamond core drilling variables: (A) side view, (B) bit/rock interface view (close-up) and (C) top view (modified from [29]).

Dynamic variables include the torque-on-the-bit (TOB) and weight-on-bit (WOB). The former is the rotational moment applied to the drill bit and is conventionally stated in Newton meters (Nm), while the latter, also known as thrust, is the axial load applied in the direction of drilling. WOB is a major drilling parameter and is regarded as the most influential wear factor when compared to rotational speed and rock type [13]. WOB is responsible for maintaining rock–bit interaction.

On the other hand, kinematic variables include the rate of penetration (ROP) and angular velocity (Ω). For the current study, a unit defined as the depth of cut (d), measured in micrometres per revolution of the drill bit (μm/rev), was frequently used and gathered the kinematic variables into a single variable.

A diamond-impregnated bit is typically constructed of a steel, cylindrical body with a metal matrix attached to form a cutting tip. The matrix, commonly made from mixtures of tungsten, tungsten carbide and bronze, contains dispersed synthetic diamonds [8]. The cylindrical design of the bit allows the recovery of a solid rock core, providing information about the structural geology and mineralogical features of the formations.

Impregnated diamond drilling utilises a rotary drilling mechanism; a normal force (WOB) is applied to the bit, whilst another, torsional force (TOB), rotates the bit parallel to the rock surface.

This generates both tensile and shear stresses in the adjacent material [9]. As the bit rotates, the face of the diamonds moves along the rock surface, inducing failure in the rock through a combination of scratching, grinding, crushing and cutting [6]. Gradually the diamonds in contact with the rock surface begin to wear until the diamonds break away from the matrix and are removed by the flushing media, allowing new diamonds with fresh cutting faces to be exposed [8].

The wearing and breaking away of the diamonds occur in two different ways – through the formation of wear-flats and diamond micro fracturing [10]. Less than optimal drilling conditions may result in diamond wear-flats. Since they no longer protrude far from the matrix surface, the effectiveness of the drill bit is greatly reduced. Increase in WOB alone is not sufficient to cause rock fracturing, and only by physically breaking the diamonds or re-dressing the bit face, the bit can operate efficiently again [11].

In optimal drilling conditions, the sharp edges of the diamond are worn to transitionary wear-flats, which then begin to fracture [10]. Eventually this leads to entire failure of the diamond and its removal automatically from the surrounding matrix. The wear process of the impregnated diamond bit is, therefore, critical to its overall functioning and depends not only on the properties of the bit, but also on the operational drilling parameters [8].

3.3 Acoustic emission

Acoustic emissions are simply transient stress waves generated when the deformation state of a body changes [14]. The elastic stress waves generated as a result of the rapid release of strain energy during fracturing, plastic deformation and changes in the internal structure of a material [15] are a form of acoustic emission.

Acoustic emissions consist of two types of signals – burst (discrete) or continuous. Continuous emissions are of lower amplitude and of high frequency (minimal separation of occurrence). In this case, the energy released in a single event is small and the energy state of the solid changes insignificantly [12]. Burst emissions signals consist of pulses with amplitudes substantially larger than the background noise and well separated in time of occurrence [14]. The energy of the

elastic waves may exceed by several orders of magnitude the energy of elastic waves in continuous emission. Burst emissions are characterized by an increase in the amplitude of the acoustic pulses and are therefore registered as discrete (or burst) AEs [12].

Baranov et al. [12] explained that the sources of AE are various, and include elastic deformation; changes in the stress–strain state of a local volume of a solid surface layer; plastic deformation; energy liberation at a repeated deformation; phase hardening– weakening and damage on a surface layer; changes in friction surface structure; formation of micro cracks; appearance of wear debris or surface spalling.

AE has been used to monitor tool condition, including breakage, in single-contact drilling operations at the laboratory scale for the past two decades [20] in the manufacturing industry [3]. Sudev and Ravindra [16] studied the correlation between drill bit wear and measured AE parameters using empirical methods, including multiple regression and group method data handling (GMDH). The AE parameters were measured during drilling of cast iron with a high-speed steel drill bit. The researchers concluded that AE parameters provided sufficient warning of the resulting changes in tool wear and tool breakage. The models developed provided numerical estimates of tool wear and correlated well with the measured values [16]. Gomez et al. [17] investigated possible relations between AE, torque and drill bit wear using steel samples. The drill bits were modified with artificial and real failures in order to simulate different degrees of wear.

Sun [4] used acoustic emission to monitor bit wear during drilling using two different types of rocks and concluded that different drilling situations may be identified by the characteristics of AE signals generated at the rock/bit failure. He had extracted useful information pertaining to the degree of bit wear, impending bit failure and formation change. The experimental setup consisted of a tricone rotary drill bit in a field drilling scenario. The results showed that the AE signals collected during drilling with the worn bit were higher and rougher compared with signals from drilling with the new bit. However, research that focuses on diamond-

impregnated core drilling and its relation with AE is needed because there is no research work currently to address this specific problem.

3.3.1 Signal analysis

Acoustic emissions contain large amounts of information, and it is important to be able to distinguish between relevant data and background noise. Signal processing is an operation, which can both extract and enhance the desired data from a busy signal. Due to the stochastic nature of acoustic emission signals, the use of statistical methods and signal analysis tools is required [18], and a variety of tools and techniques have been developed in order to interpret signals. Amongst them, two of particular interests were used in the current work – the root mean square (RMS) and the fast Fourier transform (FFT).

The root mean square method (RMS), described in Eq. 3.1, provides a measure of magnitude of the signal, regardless of the shape of the waveform [19]. Chandrashekhar et al. [20] successfully developed an empirical relation to estimate the root mean square (RMS) error value of an AE signal generated during the drilling of a 'Hasteloy' with tin and zircon coated drill bits. The RMS values correlated well with those values measured using a new drill bit during the experiment. However, as the drill bit wore, a significant difference between the estimated and measured RMS values was observed. It was concluded that the difference between the values could be used to infer drill bit wear [20].

$$V_{RMS} = \sqrt{\frac{1}{T}\int_0^T {V_i}^2 \, dt} \tag{3.1}$$

where T is the period of the waveform, and Vi is the instantaneous voltage [19]. RMS is similar to a moving average, capable of 'smoothing' out the data, helping to make any present trends in the data more obvious. In a study by Jemielniak and Otman [21], the RMS value was considered to be a useful means of tool failure detection. Further studies [18], however, revealed that this might not be the case. These researchers concluded that the RMs values and associated distribution parameters could be very sensitive in terms of assessing the degree of tool wear. Nevertheless, most tool condition monitoring systems make use of the RMS of a

signal to detect the tool wear state or even tool breakage [3], although Williams and Hagan [22] found that cutting with a worn pick produced a signal with a lower RMS amplitude.

The fast Fourier transform (FFT) is a renowned algorithm used to compute the continuous time Fourier transform (CTFT) of signals [23], as follows:

$$X(f) = \int_{-\infty}^{\infty} x(t)\, e^{-j2\pi ft}\, dt \tag{3.2}$$

where f is the frequency, X (t) is the signal in time domain and X (f) is the signal in the frequency domain.

Heideman et al. [24] have provided a detailed history of FFT dating back to 1800s. Special editions with publications about FFT have also been published by the Institute of Electrical and Electronics Engineering (IEEE) [25]. The FFT can convert a signal in the time domain to one in the frequency domain, highlighting characteristic frequencies which would not have been clear otherwise [26].

The FFT has been extensively used by engineers across a variety of applications. Li and Li [27] performed an extensive study on AE analysis to monitor rolling element bearing condition, for example. They used a number of observations based on the characteristic frequencies related to the failure of bearings found by using the FFT. Williams and Hagan [22], on the other hand, studied the AE levels present as rock cutting conditions changed. They found that due to their relatively low sampling rate, FFT did not produce any worthwhile results, reinforcing the observation that the highest frequency, or Nyquist frequency, that can be reliably calculated from the computation of the FFT equals half the sampling frequency [23].

Although raw data is recorded as a function of time, much of the analysis in FFT is performed in the frequency domain. For this reason, FFT was considered to be a vital tool for signal analysis during the current study.

3.4 Material and methods

For testing, a laboratory-scale drill rig, 'Echidna rig', which is capable of simulating real rig conditions, was used in order to conduct seven 'step tests' to interrogate drilling performance and two 'wear tests' to examine bit wear. All tests were performed at the Australian Resource Research Centre (ARRC), CSIRO in Perth, WA.

The Echidna rig is able to exert either kinematic or dynamic variables control over the drilling operation. For the majority of the testing, the rig maintained kinematic variables control, a constant RPM and ROP in order to achieve a predefined depth of cut. The machine then switched to a dynamic variables condition in order to investigate the effects of WOB and TOB variations on the AE, while the depth of cut was kept constant. Sensors attached to the machine measured and recorded the variable magnitude for post-drilling analysis. Analysis of the results indicated that, despite the fact that the operational drilling parameters did not remain perfectly constant in the Echidna drill rig, the rig could maintain the parameters in a range sufficiently accurate to obtain meaningful AE signals in the context of drill bit testing. Drill bits 36 mm in diameter, drilled into rock samples approximately 32*32*32 cm were used. Two rock types are utilized in the drilling tests (see Table 3-1).

Table 3-1. Rock type characteristics

Rock Type	UCS (MPa)	Quartz (%)	Feldspar (%)	Biotite (%)	Grain size
American Black	300	3	97	0	Fine-medium
Radiant Red	180	35	53	18	Coarse

Two different drill bits were tested, both supplied by Dimatec Inc. (see Figure 3-2). They were, 'HR14', which has a soft matrix for hard, fine grained rock cutting and 'D2', which has a hard matrix for cutting soft, fracture rocks. Both bits were selected in order to meet their respective test requirements.

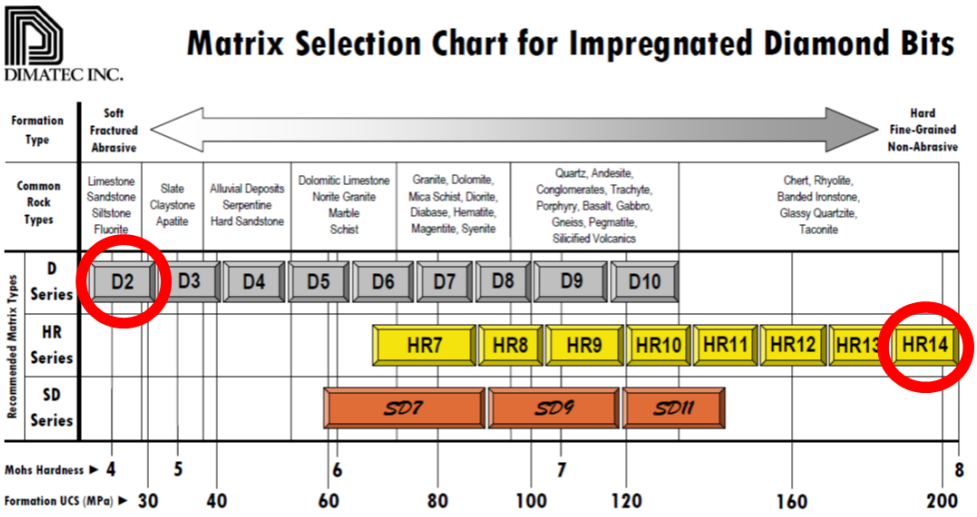

Figure 3-2. Matrix selection chart from Dimatec Inc. for ID bits [30].

The AE system for the tests consisted of one WDI sensor and one PICO sensor (with pre-amplifier) along with a data acquisition card (DAQ) and a LabView program developed at the University of Adelaide. The WDI AST wideband integral preamplifier sensors were equipped with 40 dB integrated preamplifiers and had a frequency bandwidth of 200–900 kHz. The PICO AE sensors had a frequency range of 200–800 kHz and required external preamplifiers to magnify the AE signals. The DAQ was a NI PCI-61333 (16 M Samples) S Series Multifunction DAQ Device, and was used to sample the AE data. The DAQ card had eight analogue channels, each of which was able to collect up to three million samples per second. Sampling rate for the AE was 800 kHz during all tests.

The PICO sensor was placed on a stationary part of the rig platform, as close as possible to the drill bit and as far away as possible from the machine motor. While the WDI sensor was placed on the upper surface of the rock sample, and at the edge furthest from drilling for safety reasons. The stress waves formed by the wear event propagated throughout the material and it was therefore not necessary to mount the sensor at the source of the waves [28]. Silicone gel was used as a medium between the sensors and the rock for even AE distribution across the sensors. Due to the large amount of drilling fluid outflow, however, the WDI sensor was attached with epoxy adhesive glue. For each test, data were initially saved in a binary '.dat' format. For ease of use, the files were converted to a double columned ASCII text

format with each column containing the voltage recorded from each sensor. Finally, data files were imported into MATLAB, where signal analysis was performed.

3.4.1 Step test

Initial testing involved a series of 'step' tests in which the depth of cut was steadily decreased. They were performed at 1600 RPM using a HR14 bit in American Black, with the WOB and TOB varying in order to maintain the predefined depth of cut. The drill bit was sharpened prior to the commencement of each test. In all, four tests were conducted using the sharp H14 bit. The depth of cut (d) started from 130 µm/rev to 50 µm/rev, reducing by 10 µm/rev steps. Then depth of cut started from 50 µm/rev to 5 µm/rev, reducing by 5 µm/rev steps.

In order to relate these tests to bit wear, similar tests were repeated using a worn D2 drill bit. Although the second set of bit wear tests had initially been programmed identically to the sharp bit tests, the WOB/TOB limits were quickly exceeded, meaning that drilling had to be stopped instantly for safety reasons. Two experimental tests were carried out to determine a depth of cut that would not exceed the WOB/TOB limits. 90 µm/rev was found to be the maximum achievable depth. Three step tests were therefore conducted using the worn D2 bit, beginning at 90 µm/rev and following steps similar to those adopted for the sharp H14 bit tests, but taking into account the issues discovered with the worn bit.

3.4.2 Wear test

Secondary testing was aimed at wearing the drill bits as much as possible in order to relate bit wear to AE. Bit mass loss was used to assess bit wear. The rock type was changed to Radiant Red, which has a higher abrasiveness resulting in an increased wear rate. Throughout the tests cutting speed was constant at 1600 RPM. Two types of wear tests were performed – one to induce matrix wear and one promoting diamond wear. At high depths of cut, matrix wear increased as there was more contact between the matrix and the rock, as well as more displacement of rock particles. At low depths of cut, on the other hand, the wearing flat of the diamonds became a prominent feature of the tests due to the grinding behaviour of the bit.

The matrix wear test used a HR14 drill bit with d=60 µm/rev while the diamond wear test was performed with the D2 bit. Due to the hardness of the matrix and the relatively low depth of cut, it was assumed that the matrix would experience minimal wear, while hopefully causing a polishing effect on the diamonds. The HR14 drill bit was sharpened and weighed before each of the tests. WOB/TOB limits were again reached, so the depth of cut had to be reduced to 50 µm/rev which provided a successful test for the diamond wear test.

3.5 Evaluation of the results

Prior to the analysis of the test results, the influence of background and machine noise, as well as correlation between the two signals coming from the two sensors had to be determined. As anticipated, both sensors were susceptible to background interference and detected vibrations coming from the rig motor and the laboratory environment. Being the noise source from which there were more vibrations, the rig motor had the greatest influence, especially in the rig sensor as it was closer to the source of noise than the rock sensor.

A spectral analysis of the recorded noise signals was conducted. As a result, a peak frequency of 30 kHz was detected, which suggests that the rig, the motor to be more specific, was producing this lower frequency range signal. Results from the spectral analysis were used in the filtering stage of the data processing.

As both sensors were recording simultaneously, it was expected that they would produce similar signals. Figure 3-3 illustrates the direct correlation between the signals recorded by both sensors during the matrix wear test. Circled are sections of the data which clearly highlight the correlation. While the signals were similar in structure, a large, approximately constant, difference in amplitude was observed due to the attenuation of the signals within the transferring mediums. However, the visual similarities of the two signals confirm the ability of a rig-based sensor to accurately detect rock–bit interaction.

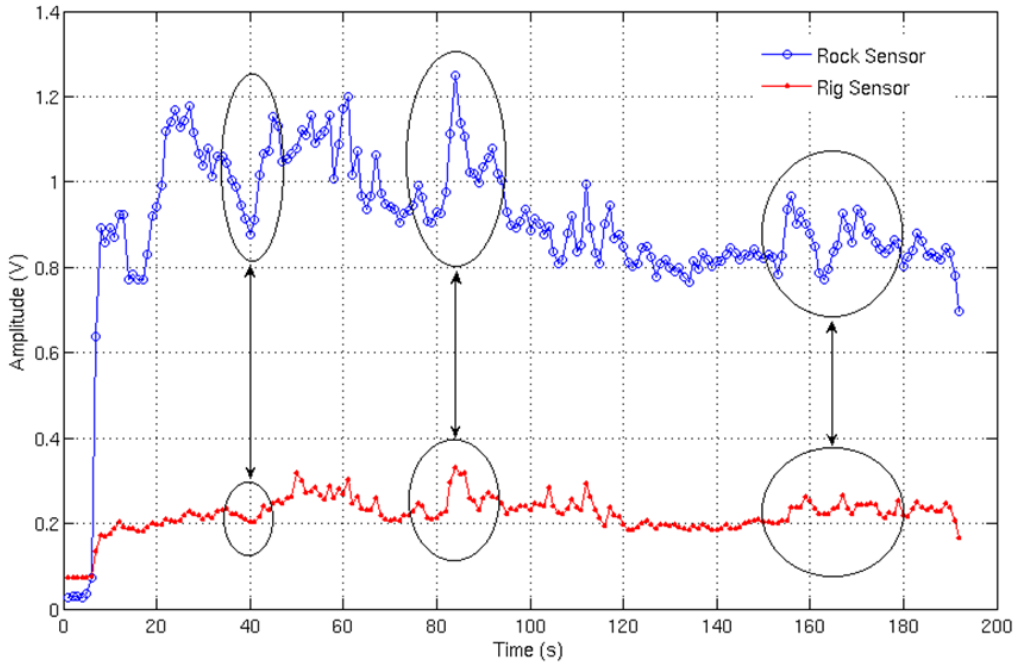

Figure 3-3. Matrix wear test correlation.

3.5.1 Step test results

The signal recorded during one of the sharp step tests is shown in Figure 3-4a. From these results, it is clear that the change in the depth of cut had a direct effect on the AE detected by both sensors. Each step reduction in the depth of cut clearly resulted in a reduction in amplitude of the two recorded signals. For depths of cut less than approximately 80 µm/rev, the steps are much clearer in the resultant signal amplitude. Above this level, the amplitude is more variable and it is difficult to determine the stepping trend. This large drop in amplitude occurring at approximately 80 µm/rev appeared in each of the sharp bit step test results. The drop can be attributed to a change in cutting behaviour as the depth of the cut varies.

The results indicate that above 80 µm/rev depth of cut, the drill bit cuts aggressively, causing macro cracking in both the diamonds and rock. Once the depth of the cut drops below approximately 80 µm/rev, the bit behaves less aggressively, acting in more of a grinding/rubbing manner. The less forceful drilling causes less cracking, less particle displacement and more of a steady rock–bit interaction, thus reducing movements and vibrations. There is an accompanying decrease in signal amplitude (see Figure 3-4a). In other words, at higher depths of

cut, the cutting mechanism is governed by the contact of the matrix with the rock, as well as with the rock chips formed; but as the depth of cut decreases, the diamond cutting mechanism dominates the interaction with the rock and the AE amplitude steadies.

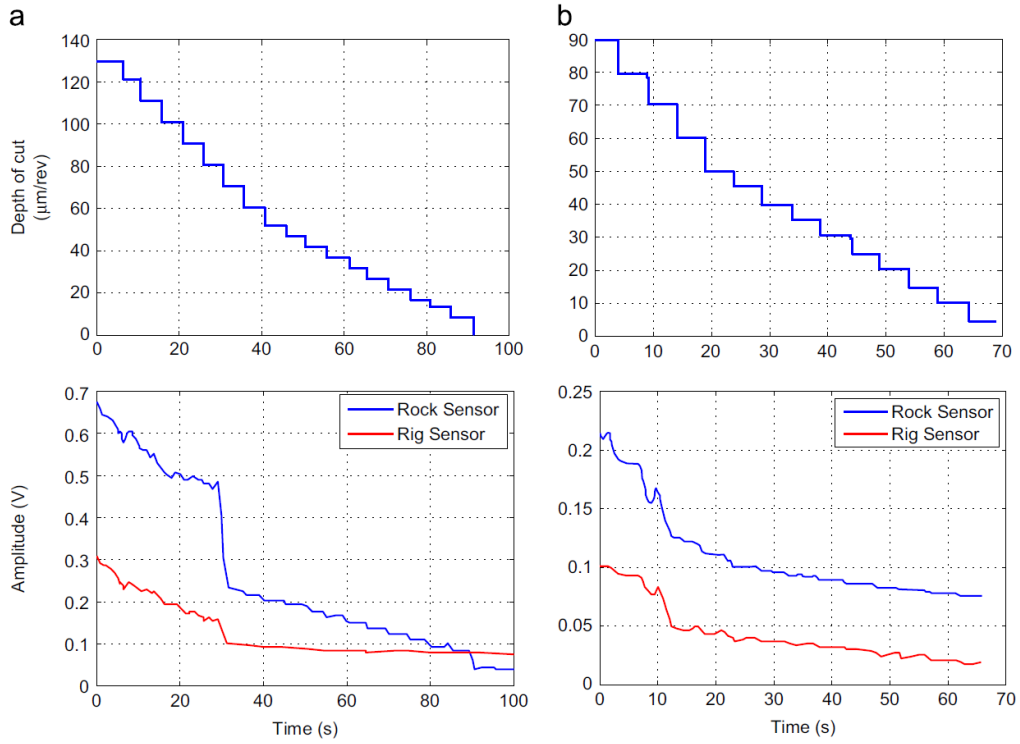

Figure 3-4. a-Sharp and b- blunt tests signal amplitude correlation with *d*.

Although for the step tests the depth of cut was the controlled parameter, in reality this is simply a measurement of bit performance and is directly controlled by the WOB and TOB. Therefore, relations between the depth of cut and the WOB and TOB have to be established. These relations were derived from drilling performance data recorded while drilling (see Figure 3-5).

Neither the (d) vs. WOB relation nor the (d) vs. TOB could accurately be described by a single linear equation. Instead, three linear different phases were identified (see Figure 3-5). These three phases correspond to the three cutting regimes described by Mostofi et al. [29].

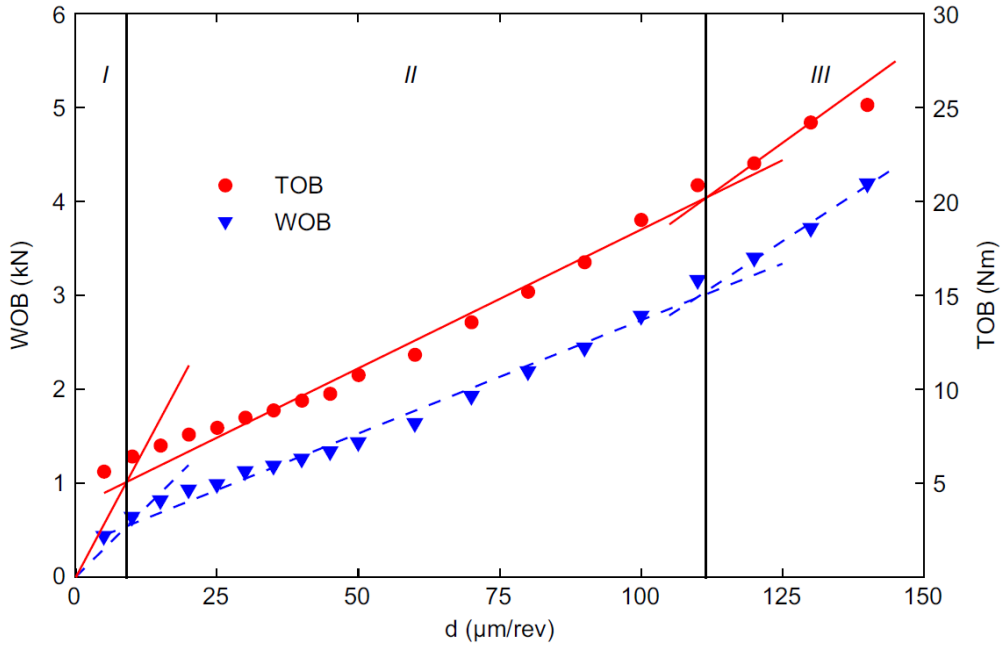

Figure 3-5. Drilling parameters relationships.

The variations in AE are therefore due to changes in dynamic variables applied to the bit. Direct relations between signal amplitude and operational drilling parameters were established. As the large increase in amplitude was common throughout the various sharp bit tests, separate relations were developed for the data above and below this value. The threshold depth of cut was estimated to be 80 µm/rev, corresponding to an approximate WOB and TOB of 2 kN and 14 Nm respectively.

Figure 3-6 illustrates the relationship between (d) and signal amplitude for sharp and blunt bits in the step tests. A similar plot would allow an operator to estimate the depth of cut solely by analysing the AE produced. Similar relations were developed which could be used to estimate, or as a secondary measure, to confirm, the WOB or TOB (see Figure 3-7 and Figure 3-8).

While these equations describe a direct relation between signal amplitude and drilling parameters, they are estimates for particular (d) ranges and the current experimental set up only. Changing the rock type, bit, RPM and drilling fluid would likely alter the results and hence the accuracy of these equations. Further testing

implementing the variation of these parameters is required to confirm their influence.

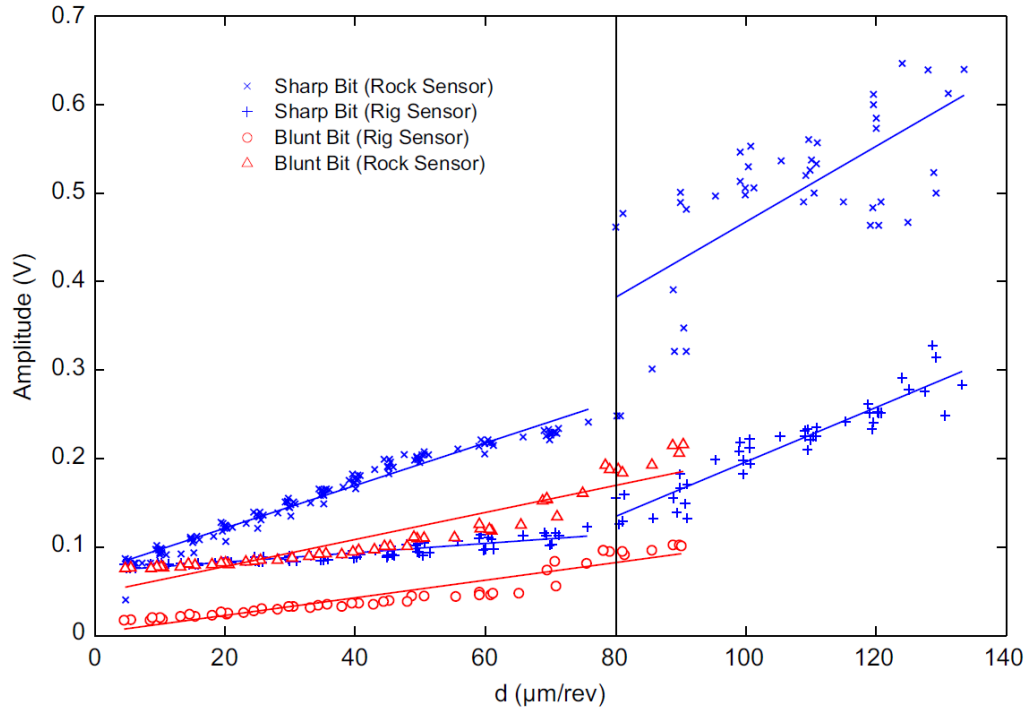

Figure 3-6. Signal amplitude of sharp/blunt bits varying depth of cut.

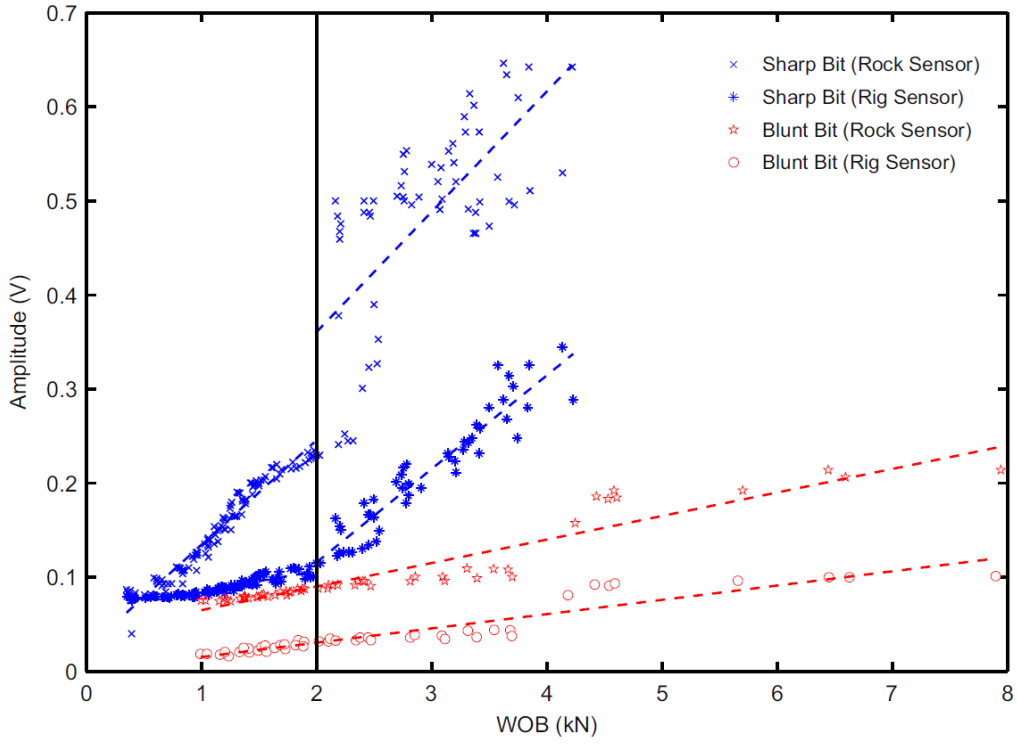

Figure 3-7. Signal amplitude of sharp/blunt bits varying WOB.

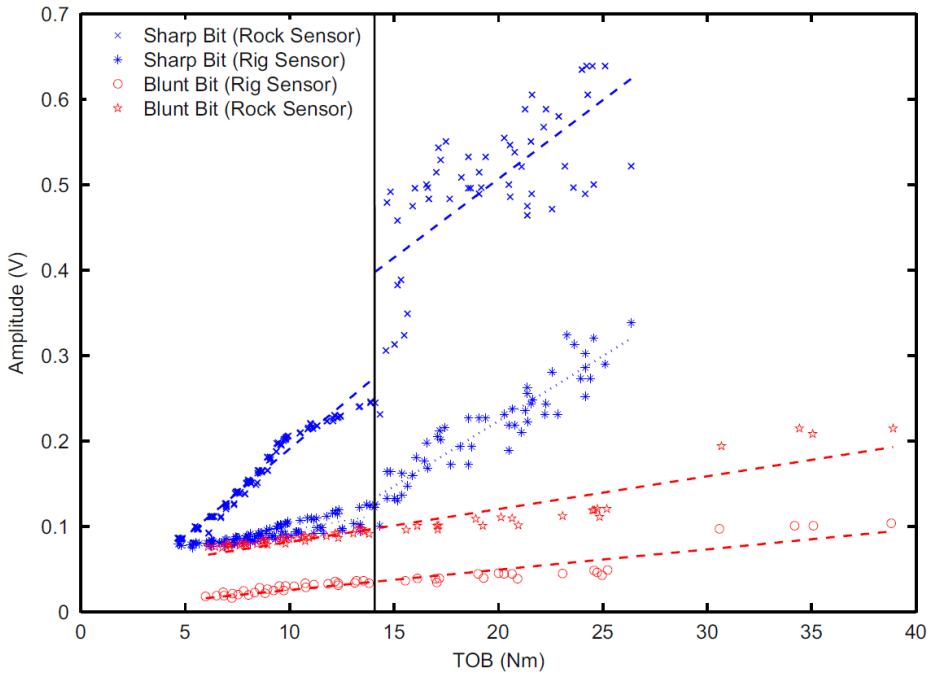

Figure 3-8. Signal amplitude of sharp/blunt bits varying TOB.

After the completion of the sharp bit step tests, the tests were repeated using a blunt bit in order to establish the effect of bit wear on AE. These tests revealed similar results (see Figure 3-4), with well-defined step like features corresponding to decreases in depth of cut. The primary observation from these tests was that a worn bit results in a lower average signal amplitude. This is likely due to the inability of the worn bit to aggressively cut the rock surface.

While the worn bit used in these tests was of the same dimensions as the sharp HR14 bit, the matrix was much harder, meaning that it was difficult to confirm the change in the AE was due solely to the different wear stages of the bit. Another important difference was the absence of the drop that existed at 80 µm/rev depth of cut for sharp bit tests. It was believed that this was due to the less aggressive cutting behaviour. This observation highlights the fact that the wear state of the bit is a significant variable affecting the AE emitted.

3.5.2 Wear test results

The secondary stage of testing focused on relating drill bit wear directly to the recorded AE. As bit wear is a relatively slow process, the amount of wear that could be caused was limited by the practical capabilities of the Echidna rig. Two primary

tests were developed. The first was designed to cause rapid wear of the bit matrix, while the second targeted diamonds' wear flat development. Due to the small scale of bit wear incurred, it proved difficult to assess and quantify the wear caused during drilling.

The signals recorded during the matrix wear test are depicted in Figure 3-9. Both amplitudes fluctuated during the length of the test, with the small scale variations likely due to factors, such as small changes in drilling parameters WOB and TOB, vibrations of particles at the cutting face, or the encountering of irregularities in the rock.

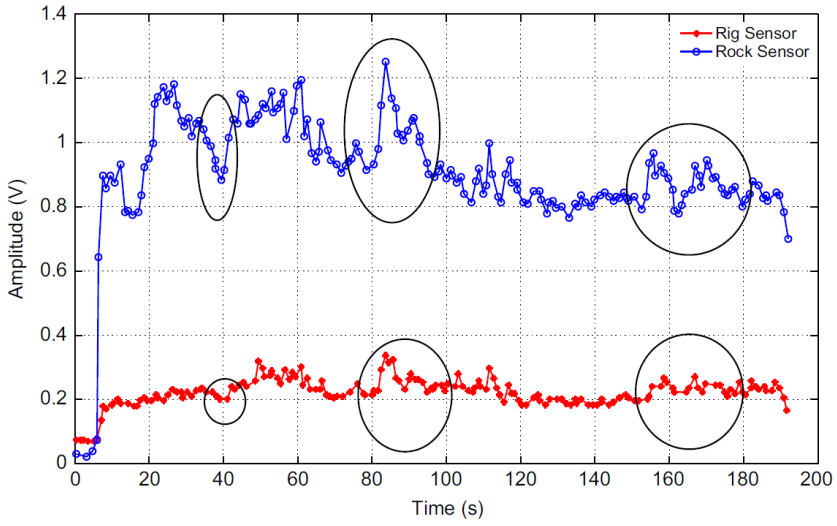

Figure 3-9. Matrix wear test.

As the drilling parameters remained constant throughout the test, the decrease in amplitude could be attributed to the bit becoming worn and hence producing less AE. The bit incurred a total mass loss of 1.42 g during the three minutes test. The cyclic trend of the amplitude may be due to the cyclic sharpening of the drill bit. At the beginning of the test, with the matrix worn away, fresh diamond cutting faces were revealed. The fresh cutting face began operation by cutting the rock aggressively, resulting in a peak of signal amplitude. As the diamonds were stripped away by the abrasive rock, cutting efficiency and signal amplitude both decreased. This cycle repeats as fresh diamonds are revealed following each breakdown of the

worn matrix. It was difficult to confirm this theory due to the small sample time, however.

In order to further investigate the effect of bit wear on AE, the FFT was used to determine the frequency domain of the signal. These FFTs were carried out during one second windows every 10 s in order to determine any changes in the frequency content of the signal as the drill bit became more worn. Once the FFT was calculated and plotted (see Figure 3-10) for 18 windows, the frequency range and peak frequency were collected.

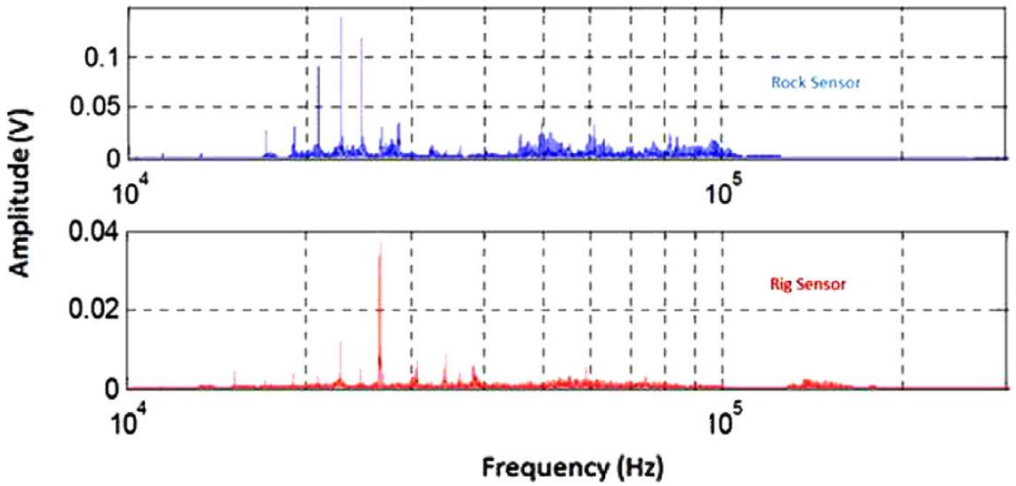

Figure 3-10. Typical frequency spectrum in wear tests.

Analysing the collected results (Table 3-2), it proved difficult to derive any significant conclusion regarding the relationship between peak frequency and progressive bit wear. Table 3-2 shows no observable trend relating peak frequency to the time or wear of the bit. This might be due to the small scale of the induced wear, however, and continuous drilling over longer periods might possibly reveal more conclusive results.

Table 3-2. Matrix wear test peak frequencies and frequency range.

Beginning of window	Rig sensor			Rock sensor		
	Peak frequency (kHz)	Frequency range (kHz)		Peak frequency (kHz)	Frequency range (kHz)	
		From	To		From	To
10	30	16	45	32	18	32
20	30	16	62	22	18	32
30	30	16	62	25	19	34
40	31	24	62	25	22	52
50	31	16	62	25	19	46
60	28	16	62	31	16	62
70	26	22	62	31	16	62
80	31	16	62	31	18	51
90	31	16	62	31	16	62
100	31	16	62	31	16	62
110	31	16	62	28	18	33
120	31	27	39	28	18	33
130	31	27	39	29	17	45
140	31	16	62	25	17	52
150	31	16	62	29	18	52
160	31	27	39	25	17	52
170	31	22	62	25	19	32
180	31	22	62	25	19	35

The aim of the next wear test was to cause diamond wear-flat development while minimizing matrix wear. The harder D2 bit lost 1.20 g over the 90-s drilling period. While the results appeared similar to those of the matrix test, four prominent peaks were detected by the rock sensor, as shown in Figure 3-11.

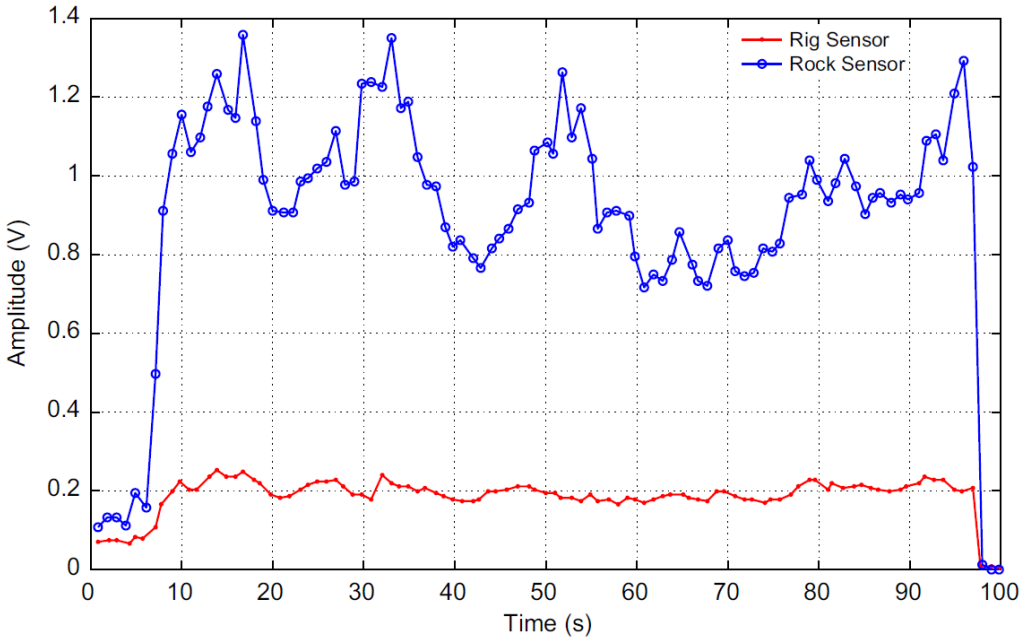

Figure 3-11. Diamond wear test.

A possible explanation for these observations could be the progressive wear of the diamonds with the highest protrusion. At the beginning of the test, only a small number of diamonds are in direct contact with the rock. As the test proceeds, these diamonds begin cutting, increasing the signal amplitude. Due to the highly abrasive radiant red rock and the low depth of cut, these diamonds rapidly wear flat, resulting in a reduction of signal amplitude. As the initial diamonds flatten out, their protrusion from the matrix surface decreases, allowing other protruding diamonds to initiate contact with the rock surface. These fresh diamonds cut until they too are worn flat, allowing other diamonds to begin cutting. This cycle repeats until all diamonds on the surface of the bit are worn flat, greatly reducing any remaining cutting efficiency. While this theory explains the continuous sharp fluctuations in signal amplitude, longer cutting times could possibly confirm it. Frequency analyses were performed on the diamond wear tests, as they had been for the matrix tests, and following the same procedure. But the results were inconclusive (Table 3-3). The wear mode of the drill bit had little effect on peak frequency. Despite the use of two different bits, and changes in depth of cut, it is possible that the bit was wearing in the same fashion in both tests, explaining the similarity of results.

Table 3-3. Diamond wear test peak frequencies and frequency range.

Beginning of window	Rig sensor			Rock sensor		
	Peak frequency (kHz)	Frequency range (kHz)		Peak frequency (kHz)	Frequency range (kHz)	
		From	To		From	To
10	27	16	38	24	17	28
20	27	16	38	25	17	40
30	38	23	38	23	21	26
40	27	16	38	52	17	52
50	26	23	35	25	17	28
60	27	23	38	25	17	40
70	27	23	38	52	17	61
80	27	23	38	25	17	65
90	27	23	38	25	17	70

3.6 Conclusions

The outcomes of this research indicate that AE monitoring techniques are a feasible option to optimize diamond core drilling performance. Changes in drilling conditions and the effect of drilling parameters can be accurately mapped by analysing AE. The results from the findings can be summarized as follows.

Preliminary ‘step tests’ have concluded that there is a direct link between AE amplitude and drilling parameters. A series of linear relations have concluded that the signal amplitude alone could accurately estimate the current depth of cut, WOB or TOB in real time.

Step tests also indicated that at a certain depth of cut, approximately 80 µm/rev, AE amplitude behaves erratically before decreasing voltage suddenly. This can be explained as a change in cutting behaviour of the bit, from an aggressive nature, to a more stable, grinding mechanism.

Under accelerated wear, AE amplitude decreased over drilling time. A relationship could not be established since the decrease could be due to variation of other drilling parameters, which did not remain constant.

Frequency analysis was performed on the AE at accelerated wear, which revealed that there was little variation in the AE's peak frequency and frequency range over time. From the frequency spectrum, we found that fundamental frequencies ranged from 20 to 50 kHz.

Further investigations performed under both laboratory and field conditions are required to accurately relate AE and bit wear. Overall, the conclusions drawn from this research shed further light on the field of AE monitoring of impregnated diamond drill bits, but more work is required.

3.7 Acknowledgements

The work has been supported by the Deep Exploration Technologies Cooperative Research Centre whose activities are funded by the Australian Government's Cooperative Research Centre Programme. This is DET CRC Document DET CRC 2014/376. The authors would like to thank to Gary Cavanough from Queensland Centre for Advanced Technologies (QCAT), CSIRO, and Luiz Franca and Stephen Banks from the Australian Resource Research Centre (ARRC), CSIRO Perth, WA. Special thanks go to lab technicians Ian Cates, Simon Golding, T. May and D. Ollerenshaw from School of Civil, Environmental and Mining Engineering, The University of Adelaide. Mrs. Barbara Brougham is also gratefully acknowledged for reviewing the manuscript.

3.8 References

[1] Australian bureau of statistics 2012. Mineral and Petroleum Exploration. 8412.0 ed. ⟨http://www.abs.gov.au/ausstats/abs@.nsf/mf/8412.0⟩ [accessed 04.04.13].

[2] Hardy HR. Acoustic emission/microseismic activity. Principles, Techniques and Geotechnical Applications, vol. 1. Rotterdam: Balkema; 2003.

[3] Chen X, Li B. Acoustic emission method for tool condition monitoring based on wavelet analysis. Int J Adv Manuf Technol 2007;33:968–76.

[4] Sun XQ. A study of acoustic emission in drilling applications. In: The 37th US Symposium on Rock Mechanics: Rock mechanics for industry (USRMS), Vail, Colo, Rotterdam: Balkema; 1999: p. 983–90.

[5] Carpinteri A, Dimastrogiovanni L, Pugno N. Fractal coupled theory of drilling and wear. Int J Fract 2005;131:131–42.

[6] Wang Y, Luo H. Ways to improve the drilling effectiveness of rock bits by a tribological method. J Tribol 1988;110:212–5.

[7] Rao KUM, Bhatnagar A, Misra B. Laboratory investigations on rotary diamond drilling. Geotech Geol Eng 2002;20:1–16.

[8] Tian X, Tian S. The wear mechanisms of impregnated diamond bits. Wear 1994;177:81–91.

[9] Maurer WC. The state of rock mechanics knowledge in drilling. In: Fairhurst C, editor. Failure and breakage of rock: Proceedings of the 8th US Rock Mechanics Symposium, Minneapolis: AIME; 1966: p. 355–95.

[10] Miller D, Ball A. The wear of diamonds in impregnated diamond bit drilling. Wear 1991;141:311–20.

[11] Bullen GJ. Rock-hard tribology. Ind Lubr Tribol 1985;37:44–76.

[12] Baranov V, Kudryavstev E, Sarychev G, Schavelin V. Acoustic emission in friction. Amsterdam: Elsevier; 2007.

[13] Huang SL, Wang ZW. The mechanics of diamond core drilling of rocks. Int J Rock Mech Min Sci 1997;34(134):e1–14.

[14] Hanchi J, Klamecki BE. Acoustic emission monitoring of the wear process. Wear 1991;145:1–27.

[15] Dong WP, Au YHJ, Mardapittas A. Characteristics of acoustic emission in drilling. Tribol Int 1994;27:169–70.

[16] Sudev LJ, Ravindra HV. Tool wear estimation in drilling using acoustic emission signal by multiple regression and GMDH. Proceedings of the ASME International Mechanical Engineering Congress and Exposition (IMECE). Boston, New York: ASME; 2008; 97–106.

[17] Gómez MP, Hey AM, Ruzzante JE, D'Attellis CE. Tool wear evaluation in drilling by acoustic emission. Phys Procedia 2010;3:819–25.

[18] Kannatey-Asibu Jr E, Dornfeld DA. A study of tool wear using statistical analysis of metal-cutting acoustic emission. Wear 1982;76:247–61.

[19] Jung SJ, Prisbrey K, Wu G. Prediction of rock hardness and drillability using acoustic emission signatures during indentation. Int J Rock Mech Min Sci 1994;31(5):561–7.

[20] Chandrashekhar S, Osuri RH, Chatterjee S. Preliminary investigation into the prediction of drill wear using acoustic emission. Proceedings of the Winter Annual Meeting of the ASME. Dallas, New York: ASME; 1990; 123–37.

[21] Jemielniak K, Otman O. Tool failure detection based on analysis of acoustic emission signals. J Mater Process Technol 1998;76:192–7.

[22] Williams E, Hagan P. Monitoring acoustic emission levels with changes in rock cutting conditions; 2002. ⟨http://www.mining.unsw.edu.au/sites/default/files/hagan4.pdf⟩ [accessed 02.04.13].

[23] Shiavi R. Introduction to applied statistical signal analysis. 3rd ed. San Diego: Academic Press; 2007.

[24] Heideman M, Johnson D, Burrus CS. Gauss and the history of the fast Fourier transform. Arch Hist Exact Sci 1985;34:265–77.

[25] Bath M. Spectral analysis in geophysics. Amsterdam: Elsevier; 1974.

[26] Reddy V. On fast Fourier transform – a popular tool for spectrum analysis. Resonance 1998;3:79–88.

[27] Li CJ, Li SY. Acoustic emission analysis for bearing condition monitoring. Wear 1995;185:67–74.

[28] Everson CE, Cheraghi SH. The application of acoustic emission for precision drilling process monitoring. Int J Mach Manuf 1999;39:371–87.

[29] Mostofi M, Franca LFP, Richard T. Drilling response of impregnated diamond bits: an experimental investigation. In: Proceedings of the 47th US Rock Mechanics Symposium, San Francisco, Paper ARMA 13-440; 23–26 June 2013.

[30] Dimatec Inc. Matrix Selection Chart. ⟨http://www.dimatec.com/images/mat_chart.pdf⟩ [accessed 02.04.13].

Statement of Authorship

Title of Paper	Development of a tool condition monitoring system for impregnated diamond bits in rock drilling applications under laboratory conditions
Publication Status	☐ Published ☑ Accepted for Publication ☐ Submitted for Publication ☐ Unpublished and Unsubmitted work written in manuscript style
Publication Details	Accepted for publication in Rock Mechanics and Rock Engineering journal.

Principal Author

Name of Principal Author (Candidate)	Santiago Perez		
Contribution to the Paper	Data analysis, paper write-up and data collection		
Overall percentage (%)	90		
Certification:	This paper reports on original research I conducted during the period of my Higher Degree by Research candidature and is not subject to any obligations or contractual agreements with a third party that would constrain its inclusion in this thesis. I am the primary author of this paper.		
Signature		Date	

Co-Author Contributions

By signing the Statement of Authorship, each author certifies that:

iv. the candidate's stated contribution to the publication is accurate (as detailed above);

v. permission is granted for the candidate in include the publication in the thesis; and

vi. The sum of all co-author contributions is equal to 100% less the candidate's stated contribution.

Name of Co-Author	Murat Karakus		
Contribution to the Paper	Manuscript evaluation		
Signature		Date	

Chapter 4

Development of a tool condition monitoring system for impregnated diamond bits in rock drilling applications

Abstract

The great success and widespread use of impregnated diamond (ID) bits are due to their self-sharpening mechanism, which consists of a constant renewal of diamonds acting in the cutting face as matrix wear takes place. This mechanism, however, can be altered by the blunting of the bit. Therefore, this paper aims at investigating the applicability of artificial intelligence (AI) based techniques to monitor tool condition of ID bits, sharp or blunt. Accordingly, topologically-invariant tests are performed with sharp and blunt bits while recording acoustic emissions (AE) and measuring-while-drilling variables. These are then used as inputs variables to create two approaches for the prediction of bit bluntness. The first is based on the aforementioned variables and the second is by using the concept of specific energy in drilling. Acceptable pattern recognition rates were obtained for both approaches with different pattern recognition algorithms, particularly, that composed by AE_{rms} and torque-on-bit.

4.1 Introduction

In the last few decades, the rock cutting industry has experienced economic advantages with the introduction of diamond bits. Impregnated diamond (ID) bits are part of that introduction and they are mainly used for drilling hard and abrasive rock formations. Performance in ID drilling operations is based on the experience of the operator who controls the operational parameters of the drill rig in order to achieve optimal drilling conditions. This increases the susceptibility to errors during the process.

An important part of the success of the ID bits is due to the so-called self-sharpening mechanism. Considerable amounts of research have been devoted to better understand this mechanism of ID bits [1-5]. It is widely accepted that the wear process of ID bits is, ideally, composed of three sequential stages. Initially, active diamonds are worn because of their contact with the rock (polishing process). Then, blunted diamonds are stripped off the matrix bonding. Finally, the matrix is worn until fresh diamonds are exposed again (or self-sharpening mechanism). It is also known that any interruption in the replacement of blunt diamonds can alter the balance between wear rate of diamonds and matrix, resulting in an unstable response or bluntness of the bit [6]. This bluntness can eventually lead to a less than optimal performance of the bit which is reflected in lower rates of penetration. Therefore, the importance of on-line identification of the wear state, sharp or blunt, at which the bit is so that the drilling process can be performed in optimal conditions, that is, going constantly through the three aforementioned stages.

Since direct assessment of the bit wear condition is difficult and time consuming in deep drilling, alternative techniques must be developed in order to evaluate, in real time, the wear condition of the bit. It is for this reason that in this work we use acoustic emission (AE) along with measuring while drilling (MWD), that is depth of cut (d) and torque (TOB) and weight on bit (WOB), variables as an alternative methodology in order to find a solution for such a problem.

Laboratory and field-scale drilling researches have been done in order to monitor tool condition in rock drilling applications using artificial intelligence (AI) based approaches. On the one hand, field-scale drilling experiments have been performed to evaluate the wear state of regular carbide drill bits [7]. It was found that useful information referring to bit wear and impending bit failure can be extracted with an AI-based approach from the AE waveforms. On the other hand, laboratory-scale drilling experiments have also shown that tool condition monitoring can be effectively carried out in rock drilling using AI based methods such as decision trees [8]. Furthermore, Karakus and Perez [9] found clear differences on the AE signatures generated when drilling with different bit wear conditions. Although they did not attribute such difference to uniquely the tool condition of the ID bits used, such a study provides the basis for the current research.

For the above reasons we, in this paper, primarily aim at developing and evaluating the performance of multiple tool condition monitoring systems for classifying ID tool wear state, namely sharp and blunt, using different pattern recognition techniques based on multiple time-domain input parameters at laboratory scale under same ID bit properties. Successful adoption of this methodology may lead to constant optimal conditions in the drilling operation.

4.2 Materials and methods

For testing, a laboratory-scale drill rig labelled ‘Echidna rig’, which can simulate real rig conditions, is utilized. All tests were performed at CSIRO Drilling Mechanics Laboratory. Figure 4-1 shows the general setup of the AE equipment and drilling apparatus used during the topologically-invariant, as defined in [6], cutting experiments.

The testing program included a series of sharp and blunt tests in which the depth of cut was steadily decreased. 54 sharp tests were performed, at 1600 RPM, using kinematic control while recording $AE_{rms,}$ WOB and TOB. Similarly, 42 blunt tests were performed using a worn (blunt) drill bit under the same conditions. Although blunt tests had initially been programmed similarly to the sharp tests, the dynamic

variable limits of the drilling system were reached, ceasing drilling instantly due to safety reasons.

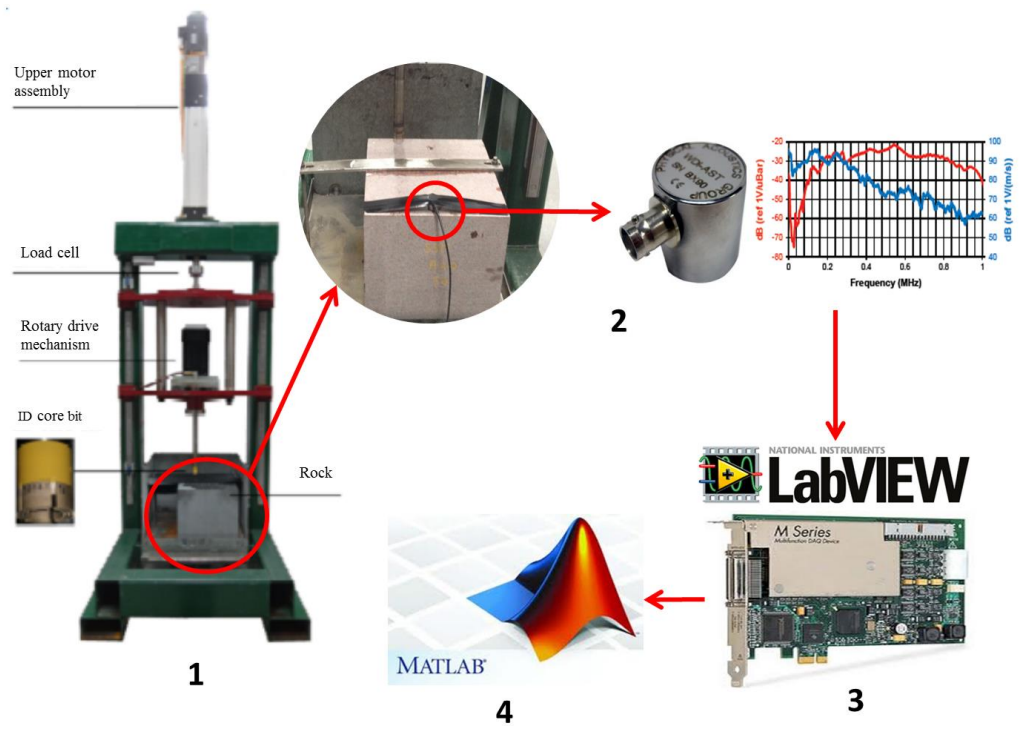

Figure 4-1. Experimental setup

Figure 4-2 shows the characteristics of both, sharp and blunt, topologically-invariant drilling tests in a *depth of cut vs. time* space.Blunting and sharpening process are part of a pre-conditioning phase carried out before testing. The former is achieved by drilling at high Ω and low ROP, whilst the latter is achieved by drilling with larger than the maximum *d* so that the diamond protrusion increases [6]. The duration of each test is approximately 5 s, or about 130 revolutions, which guarantees a topologically invariant response of the ID bit.

In total 96 drilling tests were carried out in granite called “American Black” under laboratory conditions. This rock has a uniaxial compressive strength of 300 MPa and 3% of quartz content. HR14 drill bits, sourced from Dimatec Inc., were utilized since they are recommended for hard, fine grained rock cutting.

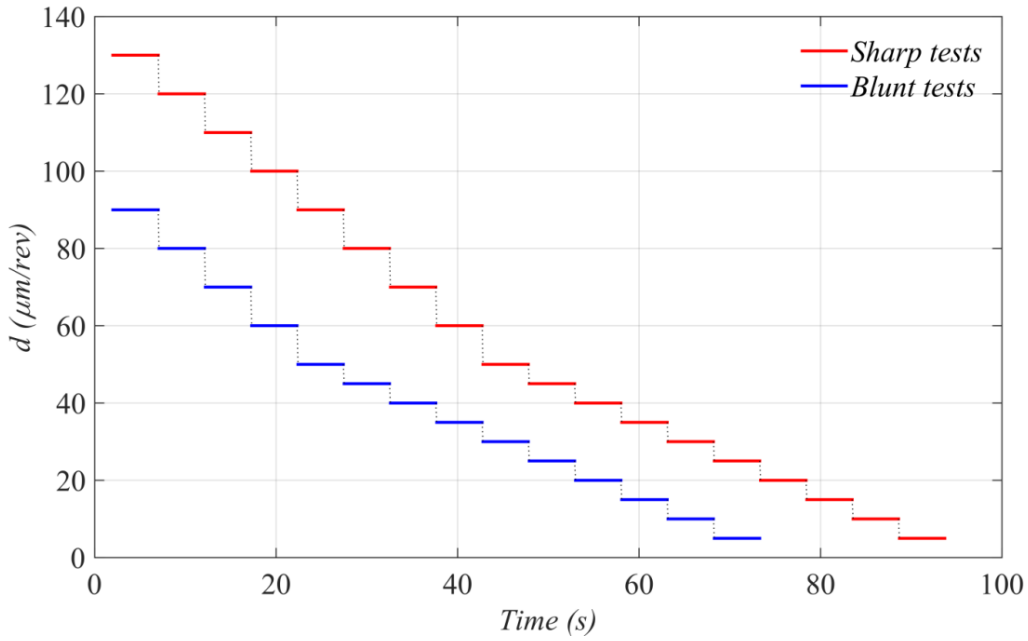

Figure 4-2. Drilling tests under controlled *d*.

Although there is no explicit answer in the literature for the number of prototype patterns (topologically-invariant tests) required to obtain good generalization properties with the classifiers, Tou and Gonzalez [10] recommend a rule of thumb in which the number of prototype patterns (topologically-invariant tests) required is of the order of ten times C_k, where C_k equals to twice the number of weights in the decision function (θ^T). In our worst case scenario (subset 1), C_k=8, therefore the number of prototype patterns required should be of the order of 80, which is less than the 96 drilling tests performed.

4.2.1 Drilling apparatus

Echidna is a computer controlled laboratory drilling rig that is utilized to investigate the drilling action of ID bits. Kinematic controlled tests are exerted with this setup, that is, Ω and V are imposed via a rotary drive mechanism and an upper motor assembly respectively (Figure 4-1). A linear actuator and a geared brushless electrical servo-motor compose the upper motor assembly. This assembly has a load capacity of up to 40 kN and can provide a precise V ranging from 0.1 to 13 mm/s. Weight on bit, *WOB* is measured by a uniaxial force transducer placed on the end of the actuator shaft. The rotary drive mechanism consists of an electrical brushless

servo-motor, a timing belt pulley system and a torque sensor (sprocket pulley sensor). The maximum TOB capacity of this system is 94 Nm and provides rotary speed, Ω, ranging from 10 to 250 rad/s. Accurate depth of cuts from 1 to 200 μm/rev can be exerted by combining these two systems, the rotary drive system and the upper motor assembly. Further details on the Echidna rig can be found in [11].

4.2.2 AE instrumentation

The AE system used consists of a WDI-AST sensor along with a data acquisition card (DAQ) and a LabView program developed in-house at the University of Adelaide. The WDI-AST is a wide band AE sensor with 40 dB gain integrated pre-amplifier and an operating frequency range of 200-900 kHz. The DAQ is a NI PCI-61333 (16M Samples) S Series Multifunction DAQ Device. The DAQ card has eight analogue channels each of which was able to collect up to 3 million samples per second. Sampling rate for the AE_{rms} during drilling tests was 0.8 MHz. The WDI sensor was placed on the upper surface of the rock sample, and for safety reasons, at the furthest edge from drilling (Figure 4-1). Silicone gel is used as ultrasonic couplant between the sensors and the rock surface.

4.2.3 Data analysis

All data processing was performed off-line using Matlab R2015a ®. Two statistical techniques are mainly employed in the signal processing: root mean square (quadratic mean) and mean. The former is utilised in the AE signal processing and the latter is utilised for the WOB and TOB signal processing. Once this is completed, bias removal and normalization are applied to the dataset following a similar procedure to that of [7]. Normalization and bias removal give a more general meaning to the results. This study will be based on the normalized dataset.

K-fold cross-validation was used before training the different algorithms. Five divisions (k=5) are used to partition the data. Each division is held out to test the model while the training phase is carried out with the rest of the data. The final result of the pattern recognition classifiers is the average of the results from the five divisions. For performance evaluation of the pattern recognition system, the

confusion matrix is utilised (see Table 4-1). In fact, the performance values display in Table 4-2 and Table 4-3 are calculated as per Equation 4.1.

$$Performance\ (\%) = \frac{TP+TN}{TP+TN+FP+FN} * 100 \quad (4.1)$$

where TP, TF, FP, and FN are the components of the confusion matrix. Table 4-1 represents the confusion matrix for our study.

Table 4-1. Confusion matrix components

	Sharp (Predicted)	Blunt (Predicted)
Sharp (actual)	True positive (TP)	False negative (FN)
Blunt (actual)	False positive (FP)	True negative (TN)

The typical architecture used during the ANN analyses is as follows: input neurons varies accordingly to the number of input variables in each subset, the number of hidden neurons was fixed at six neurons for all subset analyses, output neurons and transfer function were hyperbolic tangent and gradient descent respectively for all subsets.

4.3 Theory

Extended and more detailed information regarding the three main components (i) impregnated diamond drilling, (ii) acoustic emission and (iii) machine learning/pattern recognition is given as follows.

4.3.1 Impregnated diamond drilling

Impregnated diamond rock drilling is a technology commonly used for core retrieval in medium to hard rocks environments. A typical ID bit consists of several matrix crowns or segments, typically made out from mixtures of tungsten, tungsten carbide and bronze, with synthetic diamonds uniformly embedded over its volume. This crown is normally attached to a steel cylindrical body [4]. ID bits are designed to act as grinders. As such, they gradually wear away, exposing sharp and fresh

diamonds to come in contact with the rock being cut. This cycle characterized by the renewal of the bit face is known as self-sharpening [12].

ID drilling can be characterized by a set of relations between four operational variables: torque-on-bit (TOB), weight-on-bit (WOB), rate of penetration (V) and rotary speed (Ω) [13, 14]. TOB, WOB and V, Ω can be classified into dynamic variables and kinematic variables respectively (see Figure 4-3). In the current work, assuming that processes taking place at the bit-rock interface are rate-independent [14], a variable name as the depth of cut (d), measured in micrometres per revolution of the drill bit (μm/rev), will be extensively used (Eq. 4.2).

$$d = \frac{2\pi V}{\Omega} \tag{4.2}$$

The depth of cut, d, is an important variable since it controls the magnitude of the forces acting on the tool. For our experiments, d is the variable that will be pre-set whilst TOB and WOB will be measured. In addition, defining d in this length scale makes it comparable to other parameters such as rock grain size and diamond grit size.

ID drilling can be considered as a rotary mechanism in which a normal force keeps the new (fresh) diamonds in contact with the rock, whilst a torsional force rotates the bit parallel to the rock surface. This mobilization generates both tensile and shear stresses in the rock, which eventually induce failure in the rock by a combination of scratching, grinding, crushing and cutting [15, 16]. Gradually new diamonds begin to wear until they are stripped off the matrix and removed by the flushing media, thus, exposing again new diamonds.

Thus in optimal drilling conditions, sharp diamonds wear to transitory wear-flats that are later remove from the matrix. However, in less than optimal conditions wear-flats developed in the diamonds are not transitory and, since they no longer protrude from the matrix, the effectiveness of the ID is greatly compromised due to the bluntness of the bit. We will define to this undesirable phenomenon as a blunt bit. According to Bullen [17], optimal drilling condition can only be achieve again

by physically breaking the diamonds or re-dressing the bit face since increasing WOB, which is consider to be the most influential wear factor [18], is not sufficient to cause rock drilling in optimal conditions.

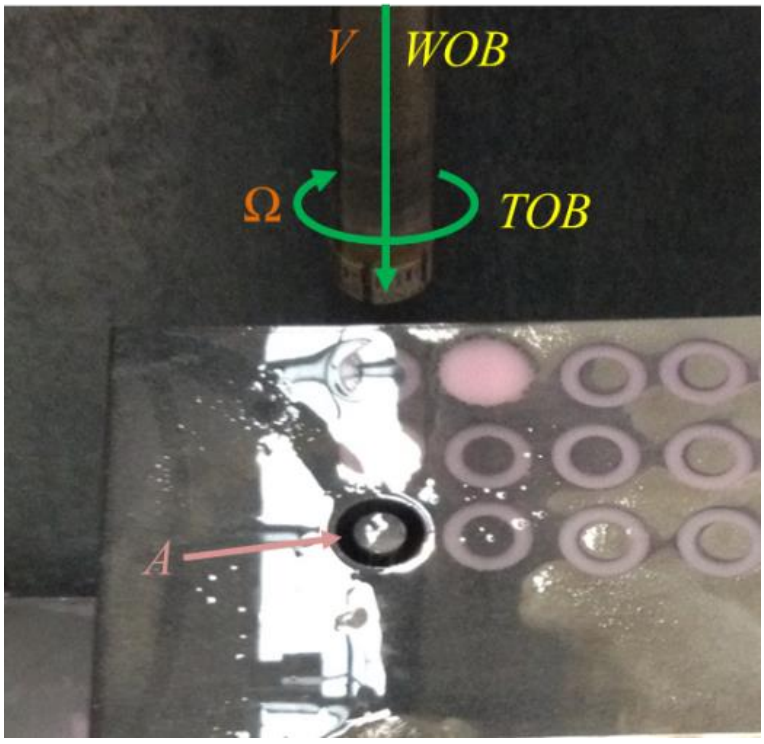

Figure 4-3. Drilling variables

An alternative and widely accepted approach to characterise the drilling process is with the concept of specific energy (SE) introduced to drilling by Teale [19]. SE is defined as the amount of work required to break a unit volume of rock (see Eq. 4.3). The specific energy can be expressed as shown below:

$$SE = \frac{wob}{A} + 2\pi \frac{tob}{A\,d} \tag{4.3}$$

where A is the area of the bit/rock interface (see Figure 4-3), TOB is torque-on-bit, WOB refers to weight-on-bit and d is depth of cut. Energy resulting from TOB is the main part of the drilling specific energy. Investigations have shown that the value of the second term (TOB) is about 10–200 times greater than the first (WOB) in Eq. 4.3[20].

4.3.2 Acoustic emission/micro-seismic

Transient stress waves generated when the deformation state of a body changes are known as Acoustic Emissions (AE), "rock talk" or microseismic activity [21, 22]. AE can be detected as two different types of signals: continuous emissions or burst (discrete) emissions. Continuous emissions are characterized by lower amplitude and least separation of occurrence (higher frequency). Whilst discrete emissions are characterized by a sudden increase of amplitude or pulses and are therefore registered as a burst-type AE [23].

Sources of AE encountered while drilling can be from several different natures: changes in friction surface structure, elastic deformation, changes in stress-strain state of a local volume of solid surface layer, plastic deformation, energy liberation at repeated deformation, phase hardening-weakening, damage on surface layer, formation and propagation of micro cracks and appearance of wear debris or surface spalling [23, 24].

The advantage of utilising acoustic signal for on-line detection of tool wear is that the frequency range of the signal (100kHz-1MHz) is far above that of drill rig vibration (0-20kHz) and other sources of noise. Thus, a high pass filter can easily remove unwanted noise and vibration components [25].

It is important to extract relevant information regarding the drilling process from the large amounts of information contained within continuous AE generated at the rock-bit interface. Statistical methods are used in AE signal analysis since AE signals are of stochastic nature [22]. Amongst these methods, there is one in particular, root mean square (AE_{rms}), that we will be using in this study since it has been demonstrated that has a high sensitivity to the wear state of the drilling tools [9, 26 27]. AE_{rms}, estimated via Eq. 4.4, generally makes any present trend in the data more noticeable. It works akin a moving average smoothing the data.

$$AE_{rms} = \sqrt{\frac{1}{n}(x_1^2 + x_2^2 + \cdots + x_n^2)} \tag{4.4}$$

where x_i is the instantaneous value of the voltage and n is the number of points.

The analysis of AE signals generated during the drilling process has been suggested as both a technique for further studying the rock drilling process [9, 28] as well as a technique for detecting tool wear and failure on line [7, 29]. Although Karakus and Perez [9] found clear differences on the AE signatures generated at different states of wear, they did not attribute such difference to the wear state uniquely since ID bits used had different properties. However, AE signatures generated in a field experiment carried out with regular carbide rotary drilling by Sun [7] can be clearly attributed to the different states of bit wear.

4.3.3 Machine learning

Machine learning is a subfield of artificial intelligence (AI) [30] that incorporates pattern recognition [31]. The objective of machine learning is to develop algorithms that allow computers to learn from data. These algorithms are of particular importance because they are able to induce models that continually improve their performance over time as new data is available [32]. In the context of machine learning, two main classes of learning algorithms can be distinguished based upon their application and functionality:

Supervised learning: these algorithms learn from a labelled set of data. They analyse the training data and produce decision functions that are used to classify the response of new data. These sorts of algorithms are commonly used in classification and regression problems.

Unsupervised learning: those algorithms learning from non-labelled data. Their goal is to recognized different groups of data that share similar characteristics amongst themselves. These groups are the so-called clusters.

Hence, pattern recognition can be understood as the categorization of input data into identifiable classes through the extraction of significant features or attributes of the data. Formally, pattern recognition assigns new data into different discrete categories and/or classes. This is achieved by using a multidimensional input vector $X=[x_1, x_2, ..., x_n]$, where x_i are components associated to the vector X in an n-dimensional feature space, in order to calculate the optimal vector $\theta=[\theta_0, \theta_1, ..., \theta_n]$,

where θ_i are the weight coefficients components of vector θ. These two vectors constitute the so-called decision boundaries when their product equals to zero, $\theta^T X=0$ (See Figure 4-4). Decision boundaries can be linear or non-linear functions of the vector X [31].

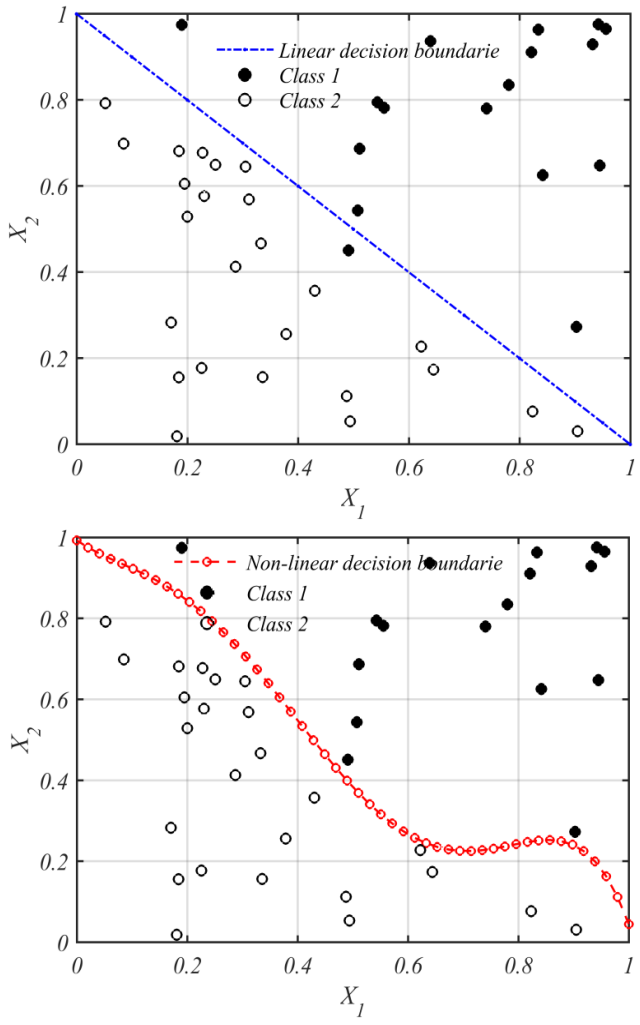

Figure 4-4. Schematic of the essential components of a PR system

Accordingly, decision boundaries can be interpreted as functions that divide the feature space into different discrete regions (See Figure 4-4). Ideally, each region corresponds to one and only one of the discrete classes, as can be seen in the lower space of Figure 4-4.

Implementation of a pattern recognition system consists of two phases, training phase and classification phase. In training, the vector of weight coefficients (θ^T) of

the decision boundary is obtained from the training dataset using an algorithm, which helps finding the decision boundary that minimises the classification error. Whilst in classification phase, the pattern classifier, which consists of decision boundaries, classifies incoming signal into one of the predefined classes. As the focus of this work is on the application of tool condition monitoring systems to ID drilling, more details on the theoretical background of pattern recognition and how to choose the parameters of vector θ via different algorithms can be found in [31, 32].

Pattern recognition algorithms have been extensively used in metal cutting as pointed out in different reviews [33-35] for the detection of wear states of the cutting tools. Conversely, in rock cutting these algorithms have been barely used [7, 8]. Researchers have studied, under laboratory conditions, the AE signals generated during rotary coal cutting and concluded that AE techniques are feasible to monitor coal cutting and dust generation in underground mines [28]. Similarly, Sun [7] studied in a field experiment the technical feasibility for AI-based AE monitoring for bit-wear during regular carbide rotary drilling. He concluded that useful information pertaining to degree of bit-wear, formation change and impending bit failure can be extracted via pattern recognition analyses from the AE signals generated at the rock/bit interface. Also, Klainc, et al. [8] developed a system for tool condition monitoring of small diameter twist drill using features extracted from the force sensor and feed drive current sensors. These features were extracted from both time and frequency domain of the signals generated with drilling the rock. Two tool conditions, namely sharp and worn, were monitor with such a system.

Most pattern recognition applications in drilling rely on using features derived from the frequency spectra of AE signals [7, 28. 36, 37]. The present paper aims at developing a system based on time domain output of the drilling variable and AE signals. For this investigation, different patter recognition algorithms are used i.e. simple trees (ST), support vector machine (SVM) [38], K-nearest neighbour (KNN)

with k=1 [21, 28], boosted trees (BT) [39] and artificial neural networks (ANN) [21,37].

4.4 Experimental results

Topologically-invariant drilling tests were conducted under kinematic control, which is by imposing *d*, as mentioned earlier. The signals, AE_{rms}, WOB, and TOB, for each drilling test were recorded in a personal computer using a DAQ.

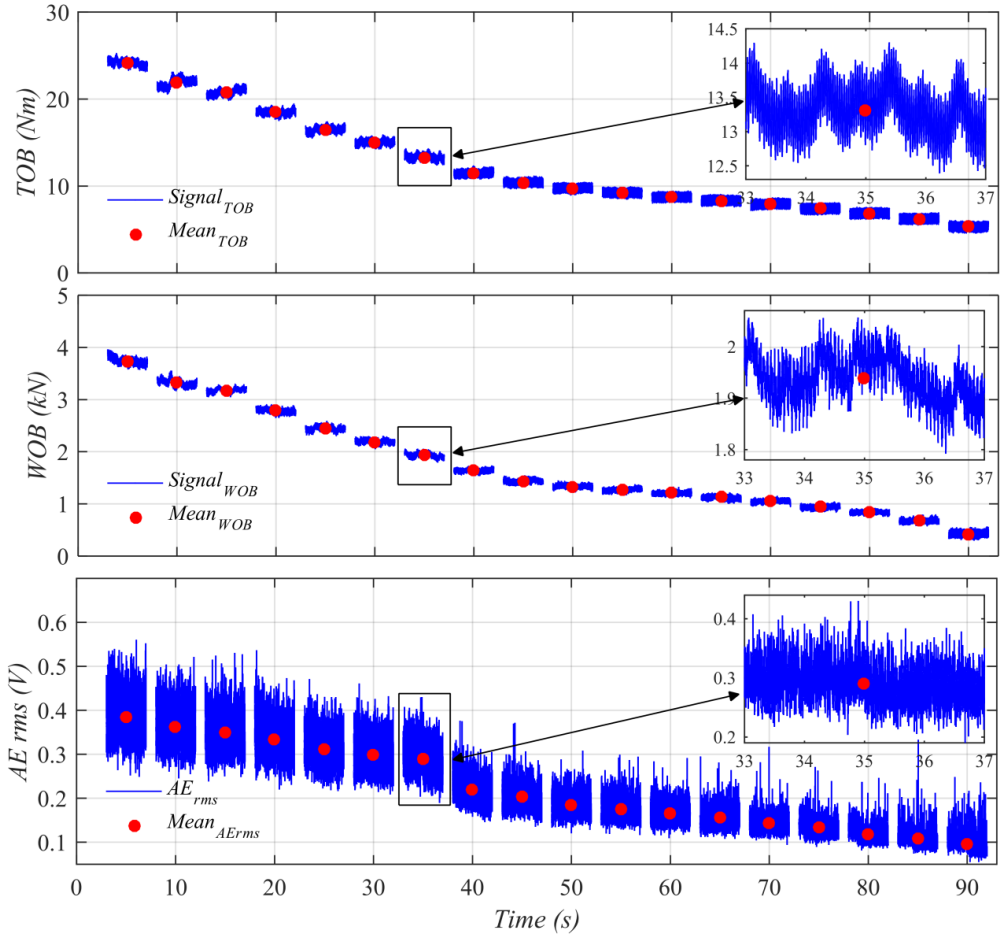

Figure 4-5. TOB, WOB and AE_{rms} responses for sharp tests.

Figure 4-5 shows AE_{rms} and the drilling dynamic variables waveforms for sharp tests plotted in the time space. AE_{rms}, WOB, and TOB responses follow a similar trend to that of the imposed d, meaning that there is certain pattern that can be revealed by the different techniques applied with pattern recognition system. The three waveforms behave as a typical random stationary process as seen in the

zoomed-in graphs. However, AE_{rms} signal is significantly more variable, this is attributed to the higher sensibility that AE_{rms} has to rock chip formation compared to WOB and TOB waveforms. The red dots in Figure 4-5 represent, as discussed earlier, the mean and the RMS (or quadratic mean) of drilling variables and AE respectively for total duration of each test.

Two different approaches are taken into considerations for the development of the pattern recognition system. The first approach consists on taking AE_{rms}, d, WOB and TOB individually as inputs of the system. Whereas the second approach gathers d, WOB and TOB into one single input variable, SE. Results of the two approaches are given next.

4.4.1 First pattern recognition approach-drilling variables

Figure 4-6 shows a matrix of two-dimensional spaces of the inputs of the pattern recognition system. Two-dimensional plots are shown rather than three-dimensional since they provide more clarity to the representation. Results of the pattern recognition systems in Table 4-2 are based on the normalised data (see Section 4.2.3) in spite of original data being displayed in Figure 4-6.

It can be foreseen from some of the two-dimensional spaces of the matrix (Figure 4-6) that the pattern recognition system can be successfully implemented. The reason for this is that tests belonging to the two classes (sharp and blunt) are clearly scattered in separable regions of the two-dimensional space. For instance, data points belonging to sharp class, red dots, can be separated from data point of blunt class, blue triangles, by a straight line in the AE_{rms} *vs.* TOB space. Similarly, AE_{rms} *vs.* d, and AE_{rms} *vs.* WOB spaces possess a similar regionalization of the data. Such observations are confirmed with the results obtained in Table 4-2.

As mentioned earlier, different pattern recognition algorithms were applied to different combination of input variables (subsets) in order to find the subset and pattern recognition algorithm for wear state classification of ID drilling.

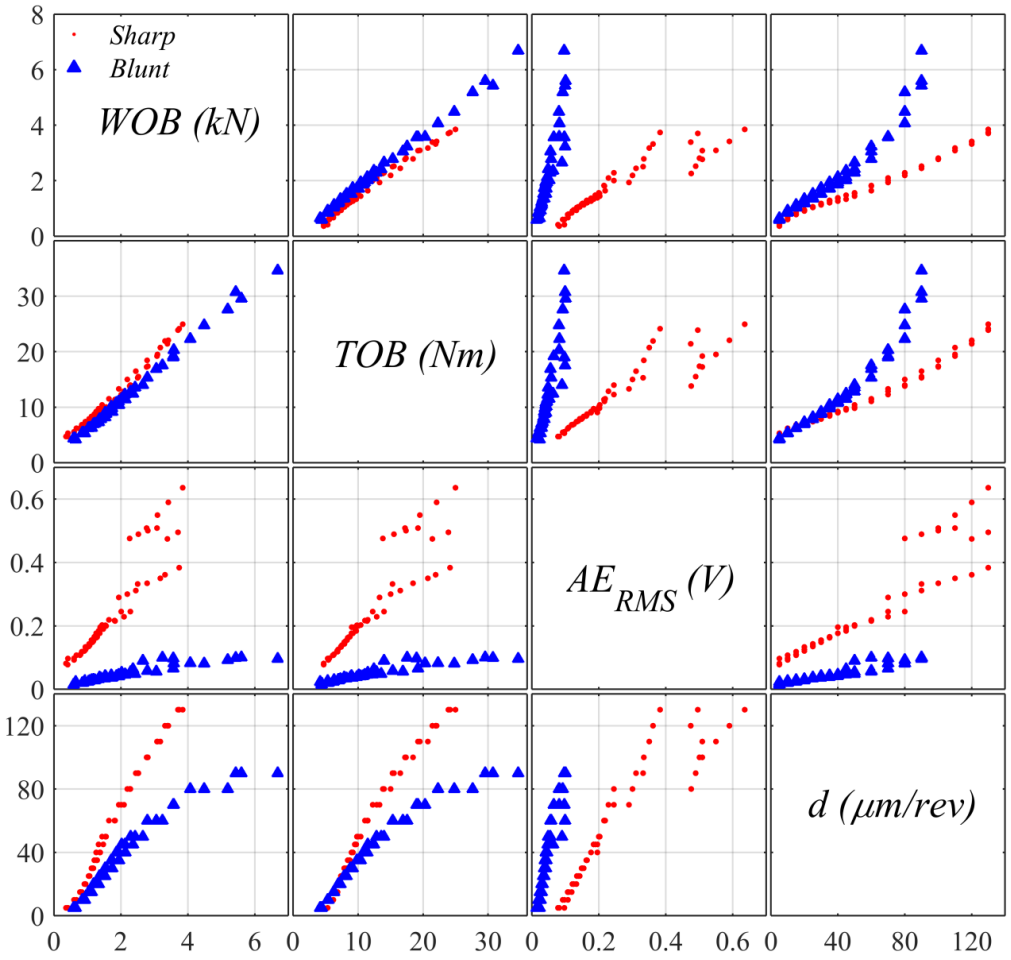

Figure 4-6. Two-dimensional plot matrix for drilling variables.

Table 4-2 shows the performances of different algorithms throughout the various subsets. When it comes to the classification algorithm accuracy, SVM is closely followed by KNN (*k=1*) which on average have performances of 97.92% and 97.35% respectively. SVM performance ranges from 81.25% to 100% making it the pattern recognition algorithm that has a slightly better performance. In the same way, the subset that better classifies the two topologically-invariant classes is subset 1 which includes the four input variables (AE_{rms}, d, WOB, TOB). However, it is important to note that subset 4 has a fairly good average recognition performance of 98.54% considering that it only requires two input variables *(*AE_{rms} and TOB*)* for adequate classification. This is a remarkable finding since it replicates the same that has previously been found in tool wear evaluation of drill bits for metal cutting [40].

Table 4-2. Performance of different PR techniques using AE and MWD.

Subset	Selected variables				Performance (%)				
	AE_{rms}	d	WOB	TOB	ST	SVM	KNN	BT	ANN
1	✓	✓	✓	✓	95.79	100	100	98.96	100
2	✓	✓			91.67	100	100	97.92	100
3	✓		✓		91.67	100	100	97.92	100
4	✓			✓	94.79	100	100	97.92	100
5	✓	✓	✓		91.67	100	91.67	97.92	100
6	✓	✓		✓	94.79	100	100	97.92	100
7	✓		✓	✓	94.79	100	100	97.92	100
8		✓	✓		70.83	81.25	87.50	61.46	61.46
9		✓		✓	75	98.96	100	60.42	100
10		✓	✓	✓	75	98.96	100	66.67	51.04
11			✓	✓	51.04	97.92	91.67	60.42	97.92

4.4.2 Second approach-specific energy

In a similar manner as the drilling variable approach, the specific energy approach results are displayed in two-dimensional spaces (see Figure 4-7). By looking at Figure 4-7, it is expected that the general performance of the pattern recognition algorithms should decrease compared to the first approach. That is because the two classes, sharp and blunt, are spatially scattered around similar regions of the spaces.

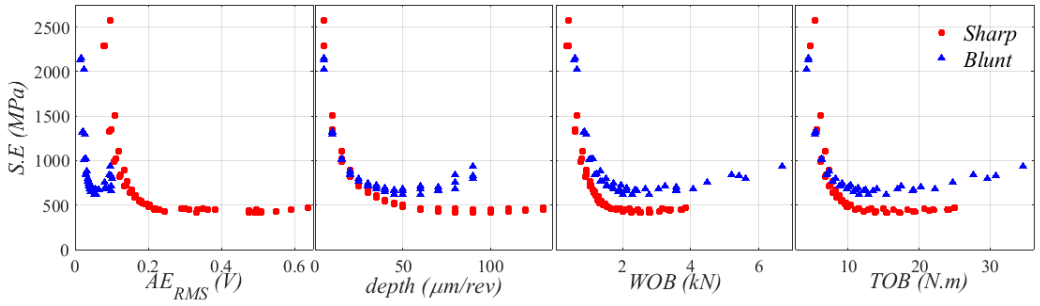

Figure 4-7. Two-dimensional spaces for specific energy approach

Table 4-3 shows the results of the different pattern recognition algorithms applied to four different subsets of inputs. As *SE* gathers information of the drilling

variables, only two-dimensional pattern recognition systems are implemented in the following approach. Successful classification performance for this energy-based approach ranged between 41.67% and 100%. For our second approach, the KNN (k=1) is again the algorithm that better classifies, on average, the two classes wear states on the two-dimensional spaces. Its classification performance ranged from 89.58% to 100% for the four subsets.

In regard to the most appropriate subset of the second approach, subset 1 composed by SE and AE_{rms} is by far the subset in which pattern recognition algorithms better perform the classification task. On average the successful recognition performance was 98.33%.

Table 4-3. Performance of different PR techniques (second approach).

Subset	Selected variables					Performance (%)				
	SE	AE_{rms}	d	WOB	TOB	ST	SVM	KNN	BT	ANN
1	✓	✓				94.79	100	98.96	97.92	100
2	✓		✓			82.29	55.21	89.58	80.21	42.71
3	✓			✓		91.67	60.42	100	82.29	90.63
4	✓				✓	82.29	62.50	89.58	80.21	41.67

4.5 Conclusions and recommendations

Large numbers of ID drilling experiments were conducted at laboratory-scale to demonstrate the ability of AE_{rms} along with measuring-while-drilling variables as variables as input parameters in a tool condition monitoring system of ID bits. Initial results obtained demonstrate that pattern recognition/machine learning can be successfully implemented in order to predict the ID drilling tool wear state. This was achieved via a testing program that included two important topologically-invariant states of the ID bits, sharp and blunt bits.

Performance rates for the various input variables subsets and different pattern recognition techniques ranged between 51.04% and 100% for the drilling variables approach and between 60.42% and 100% for the specific energy approach. Overall,

AE_{rms} and TOB are considered the most adequate input variables for a wear monitoring system of ID bits because of the simpler and more accurate classification performance of all the different pattern recognition algorithms. Their performances for ST, SVM, KNN, BT and ANN were 94.79%, 100%, 100%, 97.92% and 100% respectively. Further, this finding is consistent with what has already been found for wear evaluation in metal drilling as well as with the major contribution in terms of specific energy that TOB provides when compared to WOB in MWD.

ID drilling may be improved by implementing this proposed tool condition monitoring system and using it as an early warning system to prevent bit bluntness, in other words, to keep the sequence of self-sharpening process continuously occurring under optimal operational conditions. Application of this methodology may be limited to this particular instrumentation setup and despite bias removal and normalization being applied with the purpose of making the findings more general, more tests are required to ensure the validity and the potential filed application of the proposed methodology.

Further studies could be undertaken by utilising different bit configurations (size and properties), bit geometries as well as different rock types so that robustness of the models increases and so does its predictability.

4.6 Acknowledgements

The work has been supported by the Deep Exploration Technologies Cooperative research Centre whose activities are funded by the Australian Government's Cooperative Research Centre Programme.

4.7 References

[1] A. Borri-Brunetto, A. Carpinteri, S. Invernizzi, Characterization and mechanical modeling of the abrasion properties of sintered tools with embedded hard particles, Wear, 254 (2003) 635-644.

[2] G.J. Bullen, Hard rock drilling-Some recent test results, Industrial Diamond Review, 44 (1984) 270-275.

[3] D. Miller, A. Ball, The wear of diamonds in impregnated diamond bit drilling, Wear, 141 (1991) 311-320.

[4] X. Tian, S. Tian, The wear mechanisms of impregnated diamond bits, Wear, 177 (1994) 81-91.

[5] M. Mostofi, Drilling Response of Impregnated Diamond Bits: Modelling and Experimental Investigations, Department of Petroleum Engineering, Curtin University2014.

[6] L.F.P. Franca, M. Mostofi, T. Richard, Interface laws for impregnated diamond tools for a given state of wear, Int. J. Rock Mech. Min. Sci., 73 (2015) 184-193.

[7] X.Q. Sun, A study of acoustic emission in drilling applications, The 37th U.S. Symposium on Rock Mechanics: Rock mechanics for industry (USRMS), A Balkema, Vail, CO, 1999, pp. 983-990.

[8] M. Klaic, T. Staroveski, T. Udiljak, Tool Wear Classification Using Decision Trees in Stone Drilling Applications: A Preliminary Study, Procedia Engineering, 69 (2014) 1326-1335.

[9] M. Karakus, S. Perez, Acoustic emission analysis for rock–bit interactions in impregnated diamond core drilling, Int. J. Rock Mech. Min. Sci., 68 (2014) 36-43.

[10] D. Miller, Rock drilling with impregnated diamond micro bits, university of Cape Town1986.

[11] E. Detournay, P. Defourny, A phenomenological model for the drilling action of drag bits, Int. J. Rock Mech. Min. Sci., 29 (1992) 13-23.

[12] E. Detournay, T. Richard, M. Shepherd, Drilling response of drag bits: Theory and experiment, Int. J. Rock Mech. Min. Sci., 45 (2008) 1347-1360.

[13] W.C. Maurer, The state of rock mechanics knowledge in drilling, in: C. Fairhurst (Ed.) Failure and breakage of rock: proceedings of the 8th Symposium on Rock Mechanics, AIME, University of Minnesota, 1966, pp. 355-395.

[14] Y. Wang, H. Luo, Ways to improve the drilling effectiveness of rock bits by a tribological method, J Tribol, 110 (1988) 212-215.

[15] G.J. Bullen, Rock-hard tribology, Indust Lubr Tribol, 37 (1985) 44-76.

[16] S.L. Huang, Z.W. Wang, The mechanics of diamond core drilling of rocks, Int. J. Rock Mech. Min. Sci., 34 (1997) 131-134.

[17] R. Teale, The concept of specific energy in rock drilling, International Journal of Rock Mechanics and Mining Sciences & Geomechanics Abstracts, 2 (1965) 57-73.

[18] Z. Li, K.-i. Itakura, An analytical drilling model of drag bits for evaluation of rock strength, Soils and Foundations, 52 (2012) 216-227.

[19] H.R. Hardy, Acoustic Emission/Microseismic Activity, Taylor & Francis2003.

[20] E. Kannatey-Asibu Jr, D.A. Dornfeld, A study of tool wear using statistical analysis of metal-cutting acoustic emission, Wear, 76 (1982) 247-261.

[21] V. Baranov, E. Kudryavstev, G. Sarychev, V. Schavelin, Acoustic emission in friction, Elsevier2007.

[22] S. Perez, M. Karakus, The influence of mineral contents of granitic rock on the acoustic emission during single contact abrasivity test, 13th International Symposium on Rock Mechanics International Society for Rock Mechanics, Montreal, Canada, 2015.

[23] S. Damodarasamy, S. Raman, An inexpensive system for classifying tool wear states using pattern recognition, Wear, 170 (1993) 149-160.

[24] K. Jemielniak, O. Otman, Tool failure detection based on analysis of acoustic emission signals, J Mat Process Technol, 76 (1998) 192-197.

[25] S.J. Jung, K. Prisbrey, G. Wu, Prediction of rock hardness and drillability using acoustic emission signatures during indentation, Int. J. Rock Mech. Min. Sci., 31 (1994) 561-567.

[26] H.W. Shen, H.R. Hardy, A.W. Khair, Laboratory study of acoustic emission and particle size distribution during rotary cutting, Int. J. Rock Mech. Min. Sci., 34 (1997) 121.e121-121.e116.

[27] C. Gradl, A.W. Eustes, G. Thonhauser, An Analysis of Noise Characteristics of Drill Bits, Journal of Energy Resources Technology, 134 (2011) 013103-013103.

[28] S.J. Russell, P. Norvig, Artificial intelligence: a modern approach, 3rd ed., Prentice Hall, Sydney, 2010.

[29] C.M. Bishop, Pattern recognition and machine learning, Springer, USA, 2007.

[30] T.M. Mitchell, Machine Learning, McGraw-Hill, New York, 1997.

[31] X. Li, A brief review: acoustic emission method for tool wear monitoring during turning, Int J Mach Manuf, 42 (2002) 157-165.

[32] A.A. Kassim, Z. Mian, M.A. Mannan, Connectivity oriented fast Hough transform for tool wear monitoring, Pattern Recognition, 37 (2004) 1925-1933.

[33] G. Byrne, D. Dornfeld, I. Inasaki, G. Ketteler, W. König, R. Teti, Tool Condition Monitoring (TCM) — The Status of Research and Industrial Application, CIRP Annals-Manufacturing Technology, 44 (1995) 541-567.

[34] S. Perez, M. Karakus, An artificial neural network approach for the prediction of abrasivity of hard rocks using acoustic emission, in: W. Schubert, A.

Kluckner (Eds.) Eurock 15 & 64th Geomechanics colloquium, Salzburg, Austria, 2015, pp. 285-290.

[35] S. Perez, M. Karakus, E. Sepulveda, A preliminary study on the role of acoustic emission on inferring Cerchar abrasivity index of rocks using artificial neural network, Wear, 344–345 (2015) 1-8.

[36] C. Cortes, V. Vapnik, Support-Vector Networks, MLear, 20 (1995) 273-297.

[37] J.H. Friedman, Greedy Function Approximation: A Gradient Boosting Machine, The Annals of Statistics, 29 (2001) 1189-1232.

[38] J.T. Tou, R.C. Gonzalez, Pattern recognition principles, Addison-Wesley, Reading, Massachusetts, 1974.

[39] M. Mostofi, L.F.P. Franca, T. Richard, Drilling response of impregnated diamond bits: An experimental investigation, 47th US Rock Mechanics / Geomechanics Symposium, San Francisco, CA., 2013.

[40] M.P. Gómez, A.M. Hey, J.E. Ruzzante, C.E. D'Attellis, Tool wear evaluation in drilling by acoustic emission, Phys Procedia, 3 (2010) 819-825.

Statement of Authorship

Title of Paper	A preliminary study on the role of acoustic emission on inferring Cerchar abrasivity index of rocks using artificial neural network
Publication Status	☑ Published ☐ Accepted for Publication ☐ Submitted for Publication ☐ Unpublished and Unsubmitted work written in manuscript style
Publication Details	Perez, S, Karakus, M & Sepulveda, E, 2015. A preliminary study on the role of acoustic emission on inferring Cerchar abrasivity index of rocks using artificial neural network, *Wear,* 344–3451-8.

Principal Author

Name of Principal Author (Candidate)	Santiago Perez		
Contribution to the Paper	Data analysis, paper write-up and data collection		
Overall percentage (%)	80		
Certification:	This paper reports on original research I conducted during the period of my Higher Degree by Research candidature and is not subject to any obligations or contractual agreements with a third party that would constrain its inclusion in this thesis. I am the primary author of this paper.		
Signature		Date	

Co-Author Contributions

By signing the Statement of Authorship, each author certifies that:

i. the candidate's stated contribution to the publication is accurate (as detailed above);

ii. permission is granted for the candidate in include the publication in the thesis; and

iii. The sum of all co-author contributions is equal to 100% less the candidate's stated contribution.

Name of Co-Author	Murat Karakus		
Contribution to the Paper	Manuscript evaluation		
Signature		Date	

Name of Co-Author	Exequiel Sepulveda		
Contribution to the Paper	Implementation of data analysis codes		
Signature		Date	

Chapter 5

A preliminary study on the role of AE on inferring Cerchar abrasivity index of rocks using artificial neural network

Abstract

The wear rate of working tools during the cutting and drilling of rocks is closely related to the abrasiveness of those rocks. As the contact area of the tools increases, due to wear, the specific cutting energy will also increase, and that directly affects the overall consumption of excavation tools. A new artificial intelligence (AI) based model has been developed. It utilizes acoustic emission (AE) and rock properties as main indicators of rock abrasivity, estimated by Cerchar Abrasivity Index (CAI). AE sensors are attached to both the Cerchar testing apparatus and the rock in question while conducting scratch tests using hardened steel pins of 42 and 56 HRC. Prior to the implementation of Artificial Neural Network (ANN) modelling, the selection of independent variables was carried out via Gamma test and V-ratio analyses. As a result, AE parameters, such as total number of events and root mean square of signal, in addition to testing parameters (i.e. uniaxial compressive strength, Young's Modulus, quartz content and pin hardness) are found to be the optimum model input combination needed to accurately predict CAI.

5.1 Introduction

Rock abrasivity is an important factor to be considered in rock excavation. It is directly related to wearing processes taking place at the rock–tool interface. As such, rock abrasivity has a high impact on lifespan of drilling; tunnelling and excavation tools utilized in mineral exploration, oil and gas industry and infrastructure projects. Due to high costs associated with excavation tools and limited understanding of the laws governing the wearing process, it is important for engineers to constantly monitor rock abrasivity during rock cutting. This allows better excavation tool selection, decreases downtime caused by tool failure and reduces project costs and duration. In mechanical rock cutting, four tests are commonly used to assess rock abrasivity. They were developed at different laboratories and thus their names:

- Centre d'Études et Recherches des Charbonnages (Cerchar) test [1],
- Gouging abrasion test [2],
- Laboratoire des Ponts et Chaussées (LCPC) abrasivity test [3],
- Norwegian University of Science and Technology (NTNU) test [4].

Many researchers and engineers use Cerchar abrasivity index (CAI) as an abrasivity measurement because it has been recommended by the American Society for Testing and Materials (ASTM) [5] and the International Society of Rock Mechanics (ISRM) [6]. CAI was developed in France for the coal mining industry in the 1970s [1] and was defined as the length of the wear flat induced at the top of a conic steel pin after being scratched along 10 mm of the rock surface; one CAI is equivalent to 0.1 mm of wear flat [5–7]. Various researchers have proposed linear and non-linear models to indirectly predict the amount of wear exerted on the pin from a geomechanical standpoint. Such models have used different geomechanical and geological rock properties, i.e. uniaxial compressive strength (UCS) [8,9], Young's modulus (E_{tan}) [10–12] and quartz content (C_{qtz}) [13,14], as inputs to predict CAI. However, none of these models have addressed the matter from a tool condition monitoring viewpoint.

Tool condition monitoring in metal machining has long utilized AE features as a successful methodology in order to infer wear of single/multiple-contact cutting tools [15–18]. For instance, Yao et al.[19] described, by means of a fuzzy neural network, the relation between tool wear and AE features derived from a wavelet analysis. Also, Rangwala and Dornfeld [20] utilized a feedforward neural network with error back-propagation for monitoring wear state from AE parameters and cutting forces. More detailed and complete descriptions of AE as a means of tool condition monitoring can be found in review papers by [21–23].

Majority of research covering tool condition monitoring using AE is devoted to metal cutting. Fewer studies are focused on the application of those techniques to monitor the wear of rock cutting tools [24–28], however, they have been more focused in wear of drill bits. In summary, tool condition monitoring through AE and rock abrasivity via CAI are two individually well-studied fields that could be linked provided that CAI is alternatively understood as a tool condition monitoring problem.

Thus, the primary aim of this study is to analyse various AE features that could potentially correlate to the length of the wear flat induced at the top of the steel pin, CAI, and to develop an alternative approach to predict CAI from a tool condition monitoring point of view using the previously selected AE features and rock properties at laboratory scale. The secondary aim is to gain more insight into the main mechanisms generating AE during Cerchar abrasivity tests. This work is primarily an academic study that looks to set the basis of a relatively new research field, applications of tool condition monitoring techniques to rock cutting, and currently is at an early stage of development towards a fully AE-based CAI prediction model.

5.2 Materials and methods of analysis

A series of 88 tests has been carried out in 11 different rock types. The surface of the rock specimens used can be considered smooth as specimens were diamond sawn according to ASTM [5]. Tests on the modified Cerchar apparatus are carried

out under static load of 70 N. One CAI is equivalent to 0.1 mm measured at the top of the conical pin (see Figure 5-1).

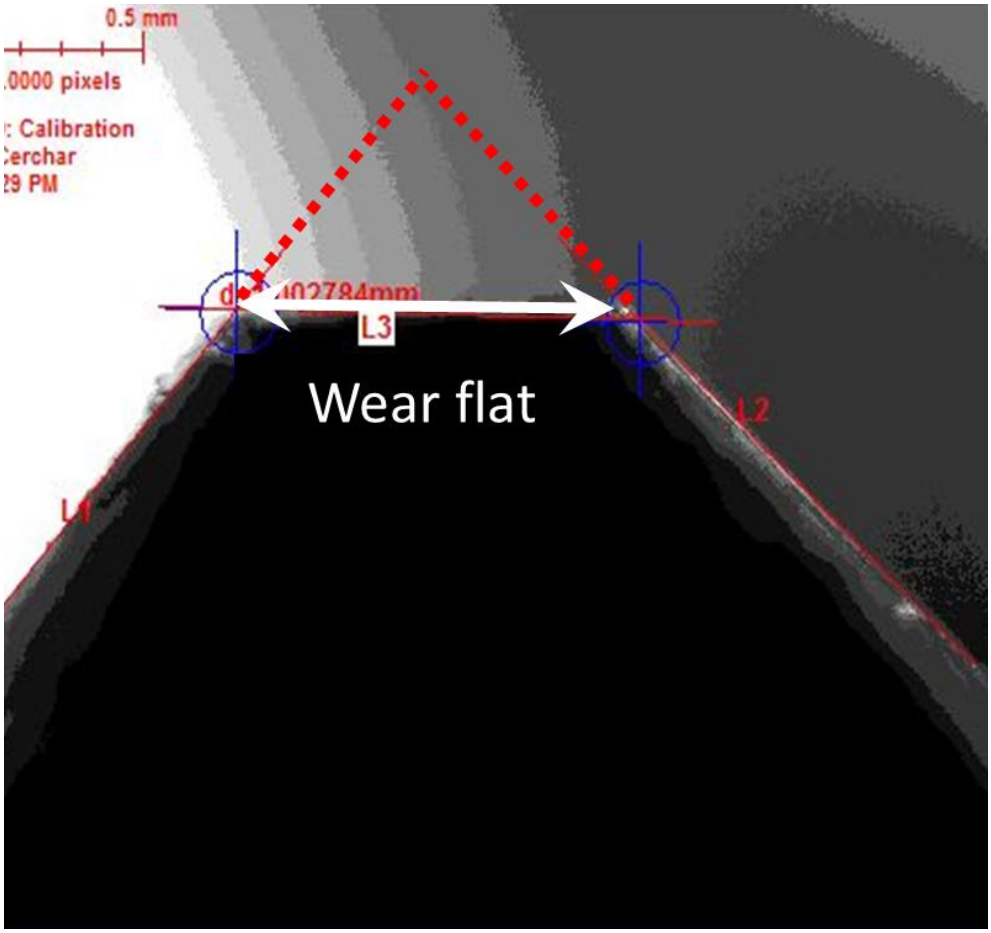

Figure 5-1. Wear flat incurred at top of a pin.

A Philips XL40 scanning electron microscope (SEM) is utilized to find out the nature of the acoustic emission. Secondary electron and backscattered electron images are respectively used to scan the surface for damage and to identify the minerals along the groove left by the pin.

5.2.1 Test method and Materials

For testing, a conventional West Cerchar apparatus has been used (see Figure 5-2). It has been equipped with a stepper motor. The stepper motor has been directly installed to one of the two hand cranks driving the screws in the two-axis cross table. The purpose of the modification that has been carried out is not only to match

acoustic emission with the spatial location in the rock specimen but also to ensure constant velocity of scratching in the tests.

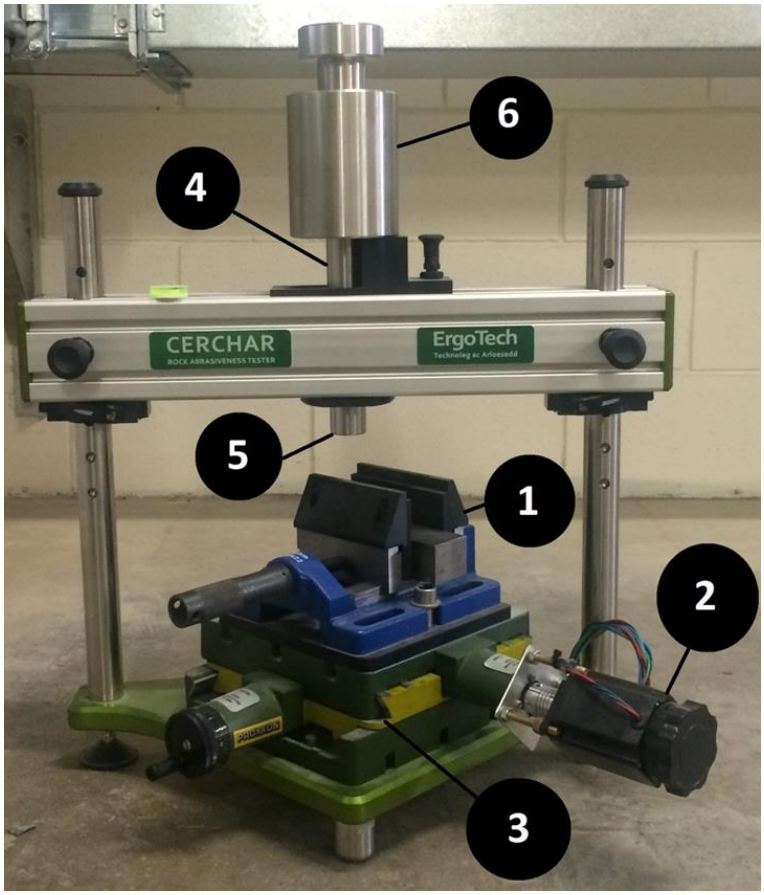

Figure 5-2. Modified Cerchar apparatus: 1-Sample holding vice, 2-Electric motor, 3-Two axis cross table, 4-Tool holder, 5-Pin and 6-Normal force.

Some discrepancies exist amongst the scientific community regarding adequate Cerchar test parameters. The most notable are test velocity and the hardness of the pin used during testing. In terms of pin hardness, there is a lack of agreement on unique pin hardness. Some researchers claim that 56 HRC should be used [6,10,29,30] unlike others suggest that 42 HRC must be used during abrasivity tests [9,13,31]. In this study, 56 HRC and 42 HRC pins will be used in order to avoid such a discrepancy.

Additionally, test velocity is another important testing parameter that presents discrepancy. The different proposed velocities vary within an order of magnitude.

Some researchers suggest testing velocity of 10 mm/s [14,32] in contrast with the slower velocities of 1 mm/s proposed in [29] or even as slow as 10 mm/min [13]. However, Plinninger, et al.[12] suggest that the values of CAI estimated from the different velocities and apparatus setups do not vary significantly. Hence, the adopted velocity for the current series of tests is 1 mm/s.

Rock properties

UCS tests were carried out on core samples with height to diameter ratio of approximately 2 [33]. They were conducted using a servo-controlled stiff testing machine (Instron 1342) with 300 kN load capacity. This machine consists of a compression loading frame, an axial dynamic loading system and a data acquisition card. Core samples were loaded at 0.04 mm per minute under displacement controlled.

During uniaxial compressive strength tests, deformation measurements were also performed with dual axial extensometers and a circumferential extensometer, model MTS 632.11F-90 and model MTS 632.12F-20 respectively. Tangent Young modulus (E_{tan}) values were calculated from the stress–strain curves.

As mentioned earlier, rock properties also influence the CAI values to some extent. There is agreement on that the "classical" rock properties that have more influence on CAI are UCS [9,10], E_{tan} [10–12] and C_{qtz} [9,13]. The three previously mentioned rock properties, thus, are considered as inputs for our model.

AE setup

AE are transient stress waves, which are generated when the deformation state of a body changes [34]. Other sources of AE that are expected to occur during Cerchar testing are: elastic deformation, plastic deformation in the work piece and the chips, collisions between chips and tool, frictional contact between tool face and rock surface, damage on rock surface, formation of micro cracks and appearance of wear debris or surface spalling [22,35].

AE is a technique that has previously been used under certain condition to monitor CAI [25], rock cutting processes [24, 28, 36] and tool condition monitoring in metal cutting [15–23]. Amongst the AE parameters that have been used by researchers are: a-value [25], b-value [25], total number of events (∑N) [28] and root mean square (RMS) [24]. a-value and b-value are computed from the amplitude–frequency distribution analysis [37]. Total number of events (∑N) is defined as the number of times that the amplified AE signal crosses the 5 mV pre-set trigger voltage during a finite time, which in our case is about 10 s [38]. RMS as described in Eq. 5.1 provides an indication on the magnitude of the signal, in spite of the shape of the waveform [39].

$$V_{RMS} = \sqrt{\frac{1}{T}\int_0^T {V_i}^2 \, dt} \tag{5.1}$$

where T is period of the waveform and Vi is the instantaneous voltage. More information on acoustic emission can be found in [40,41].

Regarding AE system used for testing, AE sensors and their respective preamplifiers are utilized along with a data acquisition card (DAQ) and LabVIEW program as seen in Figure 5-3. Two PICO AE sensors with flat frequency response of approximately 200–750 kHz are utilized. One is firmly attached to rock sample for capturing the acoustic signals generated at the pin–rock interface and the other to the frame of the apparatus so that vibration emitted from the motor can be captured. The latter signals are utilized for high-pass digital filtering at 30 kHz. Silicone gel is used as couplant between sensors and their respective attachment points. Both Pico sensors are equipped with external 20 dB preamplifiers that magnify the AE signal. This magnified signal is then transmitted to a NI PCI-61333 (16 MS/s) S series multifunction DAQ. Sampling rate used in the DAQ is 1.5 MHz for all tests. Finally, a LabVIEW program developed at the University of Adelaide and commercially available software, Matlab, are utilized for signal post-processing.

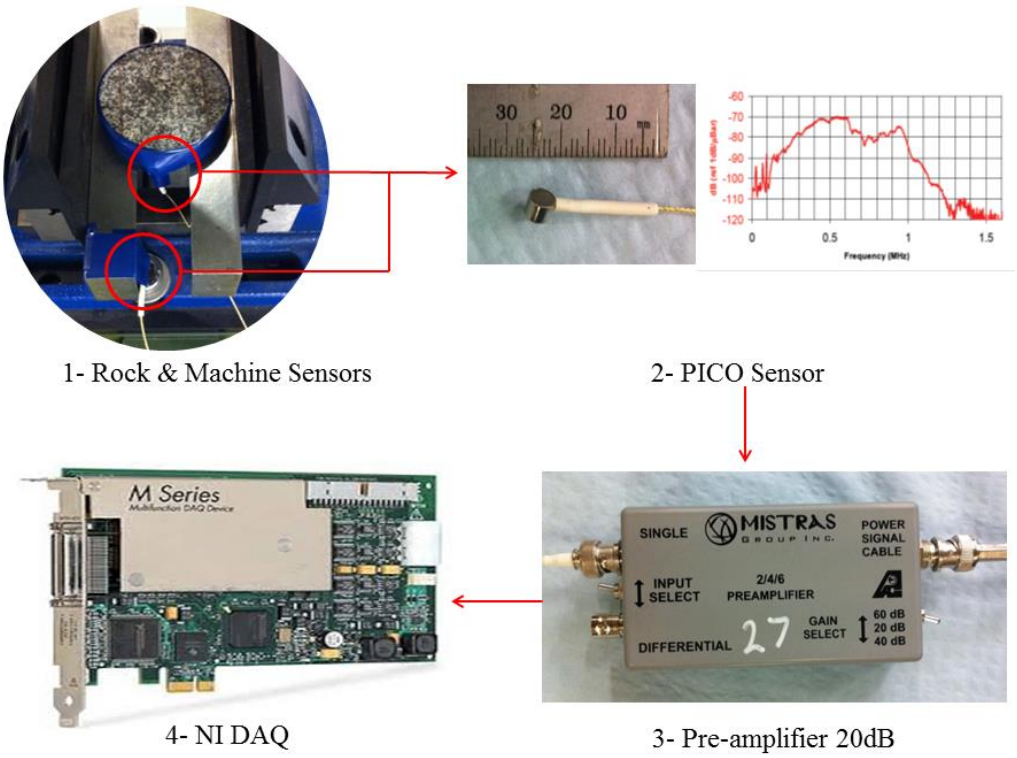

Figure 5-3. Acoustic signals capturing and post-processing setup.

5.2.2 Data analysis

Selection of independent variables

In a multivariate scenario, a regression model uses a set of independent variables to predict a dependent variable, in our case is CAI. Although all independent variables, AE features and rock properties, can contribute to the model, there are some variables that have more significant contribution compared to others. It is therefore better to include only the most relevant variables for simpler modelling. Since we have multiple AE features, it is important to apply feature selection to our work.

Gamma test is a data analysis routine that can measure the noise level of any smooth model of the following form (Eq. 5.2) [42].

$$y = f(x) + \epsilon \tag{5.2}$$

where f(x) is a smooth function (non-linear) and ϵ is the noise component following a normal distribution with zero mean and v variance. The gamma statistic uses the

data neighbourhood to estimate the noise variance. The V-ratio, defined as the ratio between the gamma statistic and the total variance of the dependent variable, is an indicator of model. As V-ratio approximates to zero, the prediction accuracy of the model is expected to be higher. More details on this test can be found in [43]. A practical use of the Gamma test is feature selection since we can calculate the gamma statistic for all input variables combinations in small input variables datasets. The independent variables of the combination with the lowest V-ratio are considered for further modelling.

Artificial neural networks

ANNs are extensively used in different engineering applications due to their well-known capabilities of performing non-linear modelling amongst multiple variables with unknown relations. They are smooth models therefore the gamma statistic is suitable to estimate the error variance of some specific ANN architecture. ANNs imitate the behaviour of the real neural system. The basic principle is given by the neuron activation mechanism, where a neuron is activated by an input and only responds if the input magnitude is greater than a determined threshold [44]. The type of neural network used in this study is termed Multi Layered Perception (MLP). A MLP neural network consists of an input layer, a hidden layer and an output layer. The input layer represents all selected AE features and rock properties, the hidden layer contains non-linear relationships and finally, the output layer corresponds to the prediction neurons, CAI (see Figure 5-4). Each layer contains one or more processing units (neurons). Each neuron has a set of weights and an activation function in order to emulate the threshold activation that exists on real neural systems. The output of one weighted processing unit (neuron) can be calculated using Eq. (5.3).

$$y = f(\sum_{k=1}^{n} w_k x_k) \tag{5.3}$$

where f is the activation function, w_k is the weight for the k-input and x_k is the k-th independent variable [44]. For the most problems, sigmoid or hyperbolic tangent function can be considered a good activation function.

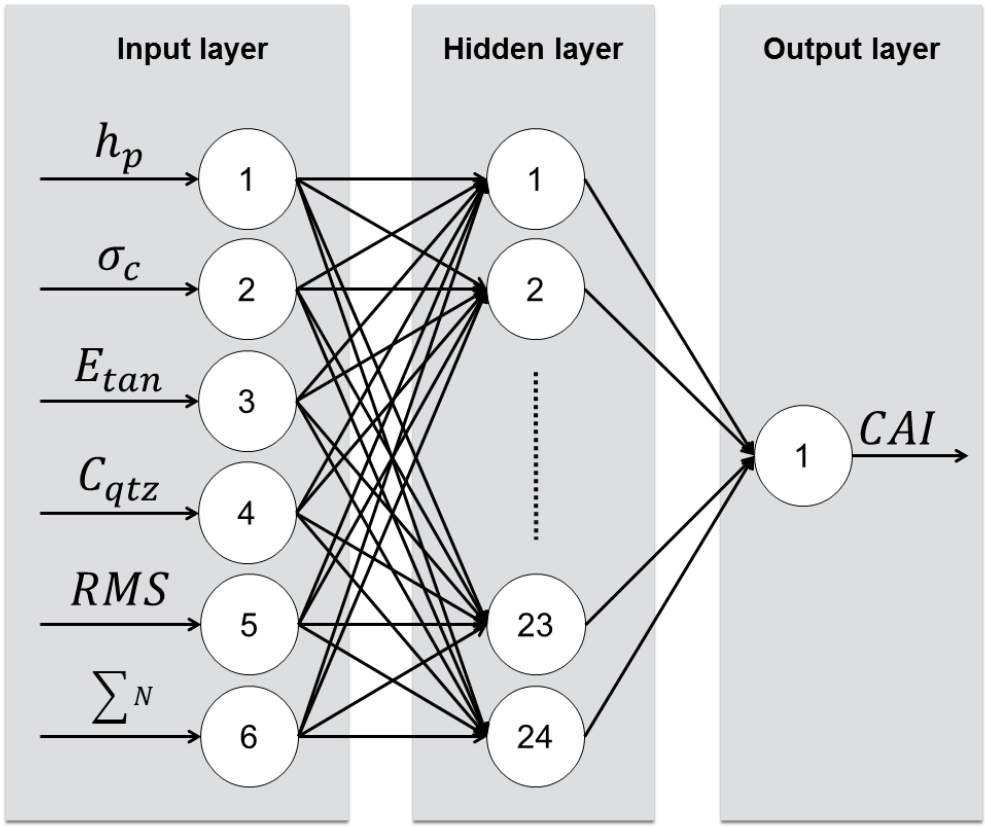

Figure 5-4 Artificial neural network (ANN) architecture.

The weights are the interconnection between layers that contribute to the prediction and classification power of the ANN. During the learning phase, these interconnections learn from experimental data by optimizing the quadratic error between the prediction and real value of the output variable. A widely used optimization method is the gradient descendent method. For performance assessment of the ANN model, three datasets are required: training, validation and testing datasets. The training dataset is used to find the optimal weights. Validation dataset is utilized in order to avoid overfitting, which occurs when the ANN memorizes and replicates the training dataset. Finally, the ANN performance is evaluated using the unseen testing dataset.

ANN has been extensively used in tool condition monitoring as described by Sick [23]. However, there is no rule to determine the architecture parameters of an appropriate ANN, i.e. number of neurons and activation function in the hidden

layer, learning rate and regularization term. Therefore, several ANN were tested varying these parameters. The Python library PyBrain [45] was used to train the ANN and 70%, 15% and 15% of the dataset is used for training, validation and testing of the network, respectively, preserving the mean and standard deviation of the dependent variable in the three sets as much as possible to avoid some bias on the dataset selection.

For the prediction performance assessment of the ANN model, four different indicators are computed between measured and predicted CAI values. Coefficient of determination (r^2) quantifies the explained variance of the model; the model has better predictions as it approximates 1. Root Mean squared Error (RMSE) is the estimator in charge of measuring the magnitude of the estimation errors (Eq. 5.4). The closer to zero, the more accurate the model is. Mean Absolute Error (MAE) measures how close predictions are to measured data. Similarly to RMSE, the smaller MAE is, the more accurate the model (Eq. 5.5). Finally, Variance Account For (VAF) indicator is calculated (Eq. 5.6). This is used to verify the correctness of the model and is commonly used in rock properties modelling to control model prediction performance.

$$RMSE = \sqrt{\frac{1}{N}\sum_{i=1}^{N}(y - y')^2} \tag{5.4}$$

$$MAE = \frac{1}{N}\sum_{i=1}^{N}|y - y'| \tag{5.5}$$

$$VAF = \left[1 - \frac{var(y-y')}{var(y)}\right] \times 100 \tag{5.6}$$

where y and y' are the measured and predicted values respectively, N is number of samples and "var" is the variance function.

5.3 Results and discussion

A total of 88 CAI tests were performed on 11 different rocks (see Table 5-1). They consisted of six igneous, one metamorphic and four sedimentary rocks. The softest rock has UCS of 8 MPa and the hardest rock 250 MPa approximately.

Table 5-1. Classification of rocks under study.

Rock Name	Rock type	σ_c (MPa)	E_{tan} (GPa)	C_{qtz} (%)	Grain size
American black	Granitoid	250	97.68	3	Fine-medium
Granodiorite	Granitoid	170	47.50	24	Medium
Monzogranite	Granitoid	112	15.60	29	Medium-coarse
Radiant red	Granitoid	249	75.49	39	Medium-coarse
Riverina	Granitoid	159	46.31	32	Medium-coarse
Hawkesbury	Sandstone	43	6.23	65	Fine
Castlegate	Sandstone	16	2.67	60	Fine
Mountain gold	Sandstone	34	5.08	75	Fine
Brukunga	Phyllite	108	39.10	30	Fine
Mantina	Basalt	240	66.37	50	Fine
Tuffeau	Tuff	8	3.41	10	Fine

5.3.1 Gamma test

Prior to conducting ANN analysis, a set of independent variables, namely, signal AE_{rms}, a-value, b-value, total number of events (ΣN), UCS (σ_c), quartz content (C_{qtz}), Young's modulus (E_{tan}), and pin hardness (h_p), was chosen to be included as potential inputs.

In Table 5-2, the result of seventeen possible variable combinations that were Gamma tested can be read. It was found that combination of variables given in sub-set 10 has the lowest gamma test value and V-ratio at 0.361 and 0.222 respectively (see Table 5-2). As a result, optimum input variables are found to be as per Eq. 5.7. These variables allow us to simplify the model as well as to avoid overfitting.

$$CAI = f\left(h_p, \sigma_c, E_{tan}, C_{qtz}, AE_{rms}, \sum N\right) + \epsilon \tag{5.7}$$

Table 5-2. Gamma test results.

Subset	h_p	σ_c	C_{qtz}	E_{tan}	AE_{rms}	a value	b value	$\sum N$	Gamma (Γ)	V Ratio
1	✓	✓	✓	✓					0.845	0.520
2					✓	✓	✓	✓	0.54	0.33
3	✓	✓	✓	✓	✓	✓	✓	✓	0.373	0.230
4	✓	✓	✓	✓	✓				0.647	0.398
5	✓	✓	✓	✓		✓			0.720	0.443
6	✓	✓	✓	✓			✓		0.684	0.421
7	✓	✓	✓	✓				✓	0.585	0.360
8	✓	✓	✓	✓	✓	✓			0.543	0.334
9	✓	✓	✓	✓	✓		✓		0.574	0.353
10	✓	✓	✓	✓	✓			✓	0.361	0.222
11	✓	✓	✓	✓		✓	✓		0.608	0.374
12	✓	✓	✓	✓		✓		✓	0.497	0.306
13	✓	✓	✓	✓			✓	✓	0.522	0.321
14	✓	✓	✓	✓	✓	✓	✓		0.493	0.303
15	✓	✓	✓	✓	✓	✓		✓	0.363	0.223
16	✓	✓	✓	✓	✓		✓	✓	0.373	0.229
17	✓	✓	✓	✓		✓	✓	✓	0.465	0.286

In Table 5-3, the correlation matrix of the optimum variables can be seen. Although σ_c and E_{tan} are not statistically independent (correlation=0.96), they both were kept as independent input variables since they have been previously considered as important rock properties affecting CAI.

Table 5-3. Correlation matrix of independent input variables.

	CAI	E_{tan}	h_p	C_{qtz}	AE_{rms}	$\sum N$	σ_c
CAI	1	0.55	-0.13	-0.19	0.42	-0.02	0.64
E_{tan}		1	0	-0.48	0.36	-0.33	0.96
h_p			1	0	0.29	0.02	0
C_{qtz}				1	-0.31	0.51	-0.38
RMS					1	-0.09	0.37
$\sum N$						1	-0.31
σ_c							1

5.3.2 Artificial neural network

After training different network configurations, it is found that the network with better performance has 6 independent input variables, 24 neurons in the hidden layer and 1 output neuron for predicting flat wear length, CAI. It is important to highlight that the network increases its complexity from 6 neurons in the input layer to 24 neurons in the hidden layer. This increment provides the capability of finding complex non-linear relations amongst input variables and wear flat measured during testing. The architecture of the proposed ANN is illustrated in Figure 5-4. Training parameters and algorithm of the neural network can be read from Table 5-4.

Table 5-4. The architecture of the ANN model.

IN*	HN**	ON***	Transfer function	Training algorithm	Learning rate	Epochs	Weight decay
6	24	1	Hyperbolic tangent	Gradient descent	0.01	125	0.01

**IN*, input neurons; ***HN*, hidden neurons; ****ON*, output neurons

In Figure 5-5, estimated flat wear measurements are plotted against their respective measured values to confirm the prediction capability of the model. As the points are uniformly scattered along the 1:1 line (diagonal line), it can be said that the model is accurate. These plots are sorted according to the three different phases, i.e. training, validation and testing. Their respective coefficient of

determination (r^2), RMSE, MAE and VAF can be found in Table 5-5. In general, it can be said that there is a high consistency between measured and predicted CAI for the ANN model.

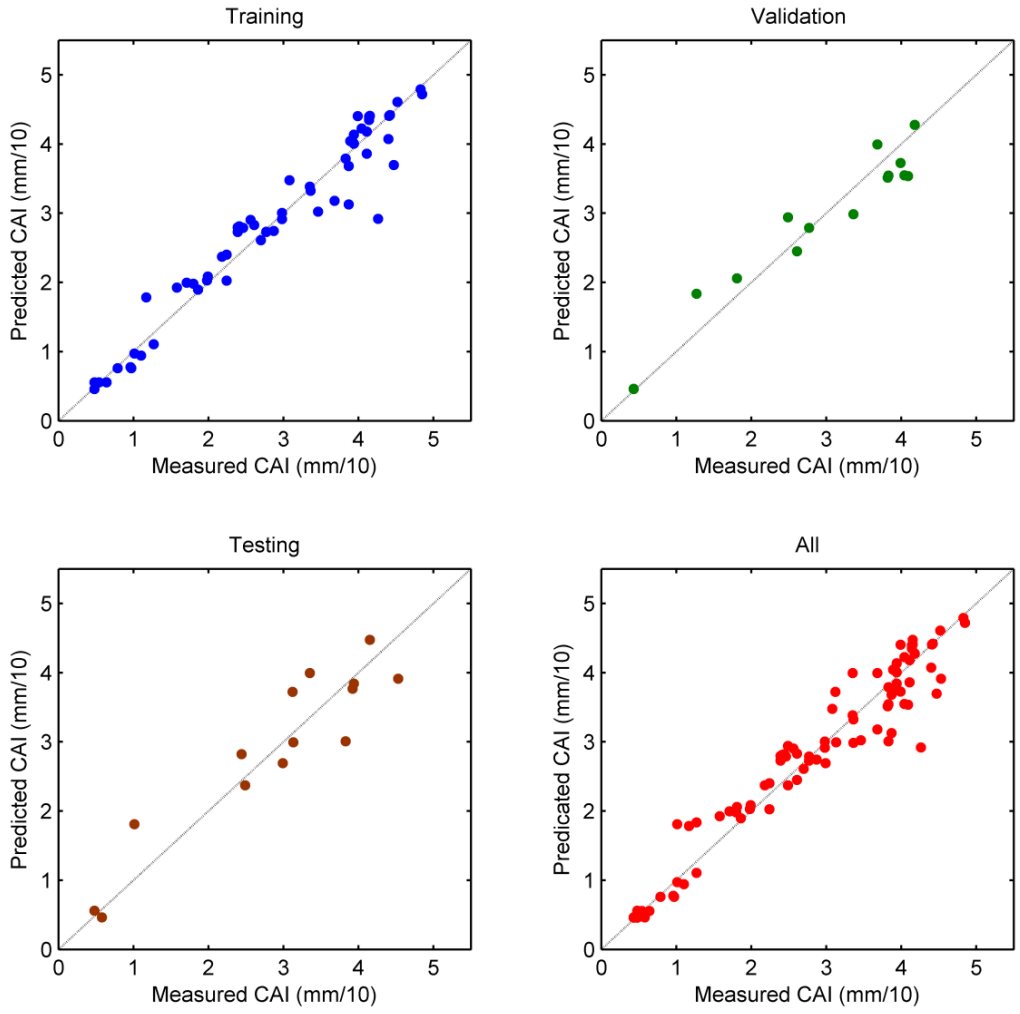

Figure 5-5. ANN values against experimental values at different stages.

Also in Table 5-5, the r^2, RMSE, MAE and VAF of the multivariate linear regression model can be read which allows us to demonstrate that the predictions derived from an ANN are more accurate than traditional multi-linear modelling. The proposed model enhances the coefficient of determination performance in approximately 36% compared to a multivariate linear regression, which is a significant improvement for the tool condition monitoring system.

Table 5-5. Coefficients of determination and prediction performance of the estimate for ANN model compared to a linear regression.

Model	r^2	RMSE	MAE	VAF (%)
Training	0.94	0.32	0.22	93.9
Validation	0.93	0.32	0.27	93.3
Testing	0.87	0.46	0.37	87.3
All Data	0.93	0.34	0.25	92.7
Linear regression	0.57	0.82	0.67	58.3

In addition, Figure 5-6 shows the prediction errors distribution for the ANN predictions. It can be seen that errors are normally distributed which ensures that the prediction model is unbiased. Therefore, the tool condition monitoring using AE features along with rock properties can be considered a sensible approach to estimate the length of the flat wear, CAI.

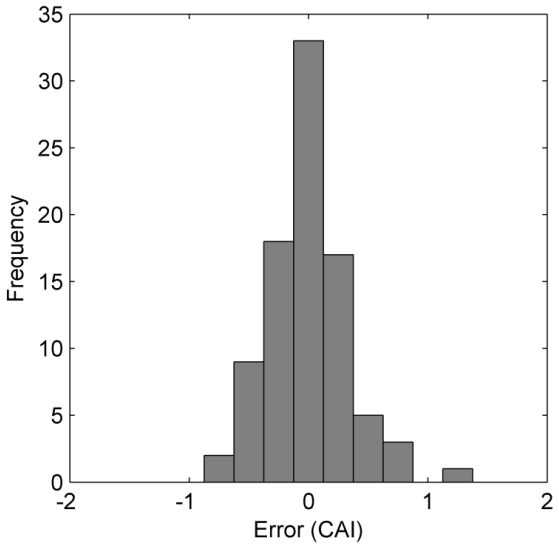

Figure 5-6 Distribution of estimation errors.

5.3.3 Nature of AE

In order to explore the main source of the AE, scanning electron microscopic (SEM) images were carried out, after each abrasivity test, in the grooves created by the pin during scratching the rock surface. Figure 5-7 correlates the AE signature with the

mineral content and damage generated on the surface of a monzogranite sample. In the secondary electrons surface image (Figure 5-7a), the damage generated by the pin on the rock surface can clearly be seen. Different types of fracture patterns can be identified. From Figure 5-7b, a backscattered electron image, it is seen that such damage patterns are associated to different rock minerals. There are clear distinctions on the acoustic signal characteristics (Figure 5-7c) generated by the different fracture patterns.

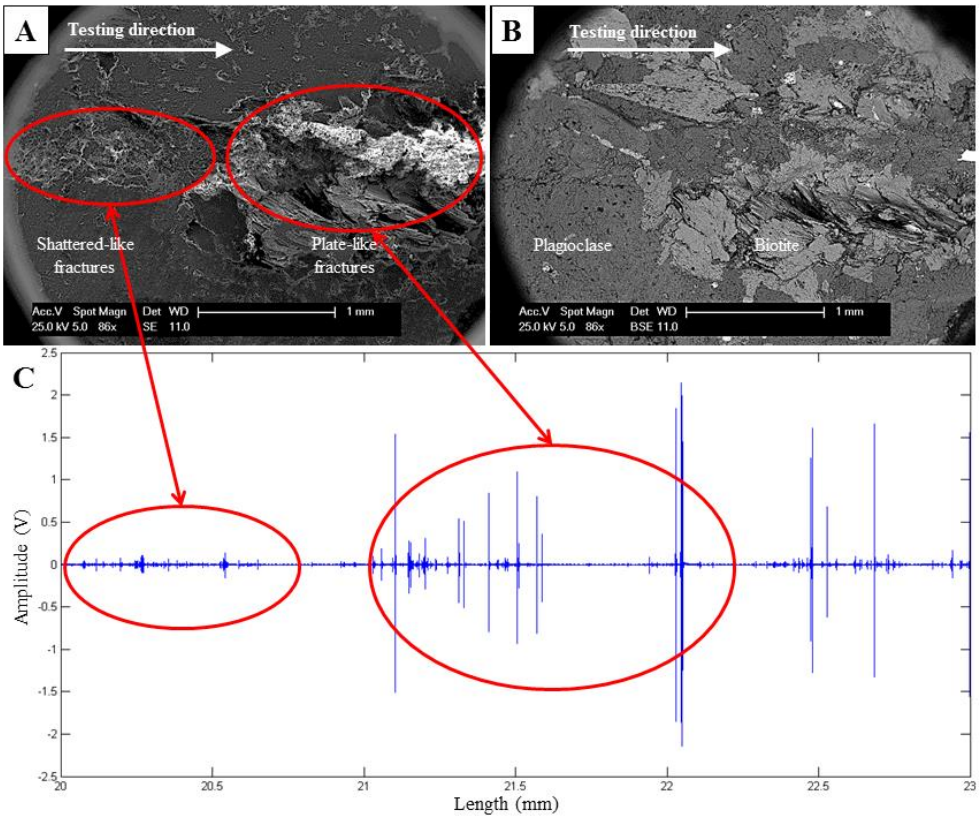

Figure 5-7. A-Secondary electrons surface image, B-BSE image and C-Amplitude vs. time signal corresponding to the sample.

In spite of being widely accepted that 85% of the wear occurs in the first 2 mm of the test [10], the AE activity recorded during testing is randomly distributed throughout the total length of the groove. This means that wear is not the main AE source present in the tests. Therefore, it is believed that the main sources of AE for crystalline rocks are the fracture generation and propagation processes taking place in the steel pin–rock interface (see Figure 5-7). For sedimentary rocks, on the other

hand, it is believed that grain dislocation is the main source of AE. This can be evidenced from granular character of the rock debris generated during the tests.

5.4 Conclusions

In this paper, we discuss from a tool condition monitoring viewpoint the applicability and the role of AE as an alternative monitoring technique in order to predict rock abrasivity via CAI. The amount of flat wear in the conic steel pin, CAI, was accurately predicted from AE parameters, rock properties and Cerchar testing parameters using the newly proposed approach. The findings from this research can be summarized as follows:

Gamma test and V-ratio analyses demonstrated that including rock properties along with AE features as input variables significantly reduced the noise or error variance in the prediction. AE features such as RMS and total number of events are found to produce less variance in the CAI prediction model.

It has also been demonstrated that predicting CAI from a tool condition monitoring viewpoint is a feasible approach. This new approach opens up a promising research field. Consequently, tool condition monitoring based on AE features and rock properties was implemented as a new valid means to estimate the length of wear flat in 42 and 56HRC steel pins.

Finally, the main sources of AE during CAI abrasivity tests are fracture generation and propagation for crystalline rocks and grain dislocation and appearance of wear debris for sedimentary rocks.

Further research is required as the current work just sets the basis of the applications of tool condition monitoring to rock cutting applications. At present the research is on-going and more work is required in the field in order to develop the first tool condition monitoring system that may predict CAI from AE features exclusively. Although this methodology is still far from having industry application, it is a promising field of research.

5.5 Acknowledgments

The work has been supported by the Deep Exploration Technologies Cooperative research Centre whose activities are funded by the Australian Government's Cooperative Research Centre Programme (2015/781). Special thanks to Henry Munoz for the discussions and providing of some rock samples. The authors would also like to thank to Simon Golding and Adam Ryntjes from the University of Adelaide.

5.6 References

[1] A. Valantin, Examen des differens procedes classiques de determination de la nocivite des roches vis-a-vis de l'attaque mecaniqe, 1973, pp. 133–140.

[2] V.A. Golovanevskiy, R.A. Bearman, Gouging abrasion test for rock abrasiveness testing, Int. J. Miner. Process. 85 (2008) 111–120.

[3] N.F. P18-579, Granulats-mesure d'abrasivité et de broyabilité, AFNOR Association Française de Normalisation, Paris, 1990.

[4] B. Nilsen, F. Dahl, J. Holzhauser, P. Raleigh, New test methodology for estimating the abrasiveness of soils for TBM tunneling, in: M.T. Traylor, J.W. Townsend (Eds.) Proceedings of the Rapid Excavation and Tunneling Conference on Society for Mining, Metallurgy and Exploration (SME), 2007, pp. 104–116.

[5] ASTM, Standard Test Method for laboratory determination of abrasiveness of rock using the CERCHAR method, D7624-10, American Society for Testing and Materials, 2010.

[6] M. Alber, O. Yaralı, F. Dahl, A. Bruland, H. Käsling, T. Michalakopoulos, M. Cardu, P. Hagan, H. Aydın, A. Özarslan, ISRM suggested method for determining the abrasivity of rock by the CERCHAR abrasivity test, Rock Mech. Rock Eng. 47 (2014) 261–266.

[7] Centre d'Études et des Recherches des Charbonnages de France-Cerchar, The Cerchar abrasivity index, (1986).

[8] A.H. Deliormanli, Cerchar abrasivity index (CAI) and its relation to strength and abrasion test methods for marble stones, Construct. Build. Mater. 30 (2012) 16–21.

[9] J. Rostami, A. Ghasemi, E. Alavi Gharahbagh, C. Dogruoz, F. Dahl, Study of dominant factors affecting Cerchar Abrasivity Index, Rock Mech. Rock Eng. (2013) 1–15.

[10] R. Plinninger, H. Käsling, K. Thuro, G. Spaun, Testing conditions and geomechanical properties influencing the CERCHAR abrasiveness index (CAI) value, Int. J. Rock Mech. Min. Sci. 40 (2003) 259–263.

[11] S. Kahraman, M. Alber, M. Fener, O. Gunaydin, The usability of Cerchar abrasivity index for the prediction of UCS and E of Misis Fault Breccia: regression and artificial neural networks analysis, Exp. Syst. Appl. 37 (2010) 8750–8756.

[12] R. Plinninger H. Kasling K. Thuro, Wear prediction in hardrock excavation using the CERCHAR abrassivenes index (CAI) EUROCK, in: Proceedings of the 53rd Geomechanics Colloquim 2004.

[13] G. West, Rock abrasiveness testing for tunnelling, Int. J. Rock Mech. Min. Sci. Geomech. Abstr. 26 (1989) 151–160.

[14] O. Yaralı, E. Yaşar, G. Bacak, P.G. Ranjith, A study of rock abrasivity and tool wear in coal measures rocks, Int. J. Coal Geol. 74 (2008) 53–66.

[15] L. Xiaoli, Y. Zhejun, Tool wear monitoring with wavelet packet transform—fuzzy clustering method, Wear 219 (1998) 145–154.

[16] H.V. Ravindra, Y.G. Srinivasa, R. Krishnamurthy, Acoustic emission for tool condition monitoring in metal cutting, Wear 212 (1997) 78–84.

[17] D.A. Dornfeld, M.F. DeVries, Neural network sensor fusion for tool condition monitoring, CIRP Ann.-Manuf. Technol. 39 (1990) 101–105.

[18] J. Hanchi, B.E. Klamecki, Acoustic emission monitoring of the wear process, Wear 145 (1991) 1–27.

[19] Y. Yao, X. Li, Z. Yuan, Tool wear detection with fuzzy classification and wavelet fuzzy neural network, Int. J. Mach. Manuf. 39 (1999) 1525–1538.

[20] S. Rangwala, D.A. Dornfeld, Sensor intregration using neural networks for intelligent tool condition monitoring, J. Manuf. Sci. Eng. 112 (1990) 219–228.

[21] E. Jantunen, A summary of methods applied to tool condition monitoring in drilling, Int. J. Mach. Manuf. 42 (2002) 997–1010.

[22] X. Li, A brief review: acoustic emission method for tool wear monitoring during turning, Int. J. Mach. Manuf. 42 (2002) 157–165.

[23] B. Sick, On-line and indirect tool wear monitoring in turning with artificial neural networks: a review of more than a decade of research, MSSP 16 (2002) 487–546.

[24] M. Karakus, S. Perez, Acoustic emission analysis for rock–bit interactions in impregnated diamond core drilling, Int. J. Rock Mech. Min. Sci. 68 (2014) 36–43.

[25] S. Perez, M. Karakus, The influence of mineral contents of granitic rock on the acoustic emission during single contact abrasivity test, in: Proceedings of the 13th International Symposium on Rock Mechanics International Society for Rock Mechanics, Montreal, Canada, 2015.

[26] S.Perez, M. Karakus, An artificial neural network approach for the prediction of abrasivity of hard rocks using acoustic emission (in press), Eurock 15 in: Proceedings of the 64th Geomechanics Colloquium, Salzburg, Austria, 2015.

[27] M. Klaic, T. Staroveski, T. Udiljak, Tool wear classification using decision trees in stone drilling applications: a preliminary study, Proced Eng 69 (2014) 1326–1335.

[28] X. Q. Sun, A study of acoustic emission in drilling applications, in: Proceedings of the 37th U.S. Symposium on Rock Mechanics: Rock mechanics for Industry (USRMS), A Balkema, Vail, CO, 1999, pp. 983–990.

[29] T.N. Michalakopoulos, V.G. Anagnostou, M.E. Bassanou, G.N. Panagiotou, The influence of steel styli hardness on the Cerchar abrasiveness index value, Int. J. Rock Mech. Min. Sci. 43 (2006) 321–327.

[30] M. Suana, T. Peters, The Cerchar Abrasivity Index and its relation to rock mineralogy and petrography, Rock Mech. 15 (1982) 1–8.

[31] J. Stanford P. Hagan, An assessment of the impact of stylus metallurgy on Cerchar Abrasiveness Index, in: Proceedings of the Coal opereators' Conference, 2009, Univesity of Wollongong, pp. 347–355.

[32] M. Alber, Stress dependency of the Cerchar abrasivity index (CAI) and its effects on wear of selected rock cutting tools, Tunnel. Undergr. Sp. Technol. 23 (2008) 351–359.

[33] C. Fairhurst, J.A. Hudson, Draft ISRM suggested method for the complete stress-strain curve for intact rock in uniaxial compression, Int. J. Rock Mech. Min. Sci. 36 (1999) 279–289.

[34] E. Kannatey-Asibu Jr, D.A. Dornfeld, A study of tool wear using statistical analysis of metal-cutting acoustic emission, Wear 76 (1982) 247–261.

[35] V. Baranov, E. Kudryavstev, G. Sarychev, V. Schavelin, Acoustic Emission in Friction, Elsevier, Oxford, 2007.

[36] H. Vardhan, B.R. Kumar, Rock Engineering Design: Properties and Applications of Sound Level, CRC Press-Taylor & Francis Group, Boca Raton, FL, 2013.

[37] B. Gutenberg, C.F. Richter, Seismicity of the Earth and Associated Phenomena, Princeton University Press, Princeton, New Jersey, 1949.

[38] C.E. Everson, S.H. Cheraghi, The application of acoustic emission for precision drilling process monitoring, Int. J. Mach. Manuf. 39 (1999) 371–387.

[39] S.J. Jung, K. Prisbrey, G. Wu, Prediction of rock hardness and drillability using acoustic emission signatures during indentation, Int. J. Rock Mech. Min. Sci. 31 (1994) 561–567.

[40] H.R. Hardy, Acoustic Emission/Microseismic Activity, Taylor & Francis, Amsterdam, 2003.

[41] C. Grosse, M. Ohtsu, Acoustic Emission Testing, Basics for Research-Applications in Civil Engineering, Springer Berlin Heidelberg, 2008.

[42] A. Stefánsson, N. Končar, A. Jones, A note on the gamma test, Neural Comput. Appl. 5 (1997) 131–133.

[43] S.E. Kemp, I.D. Wilson, J.A. Ware, A tutorial on the gamma test, Int. J. Simul.: Syst. Sci. Technol. 6 (2004) 67–75.

[44] H. Vardhan, B.R. Kumar, Application of Artificial Neural Networks Rock Engineering Design, CRC Press, Florida (2013), p. 105–130.

[45] T. Schaul, J. Bayer, D. Wierstra, Y. Sun, M. Felder, F. Sehnke, T. Ruckstiess, J. Schmidhuber, PyBrain, J. Mach. Learn. Res. 11 (2010) 743–746.

Statement of Authorship

Title of Paper	The influence of mineral content of granitic rocks on the acoustic emission during single contact abrasivity test
Publication Status	☑ Published ☐ Accepted for Publication ☐ Submitted for Publication ☐ Unpublished and Unsubmitted work written in manuscript style
Publication Details	Perez, S & Karakus, M 2015, The influence of mineral contents of granitic rock on the acoustic emission during single contact abrasivity test. *13th International Symposium on Rock Mechanics* Montreal, Canada: International Society for Rock Mechanics.

Principal Author

Name of Principal Author (Candidate)	Santiago Perez		
Contribution to the Paper	Data analysis, paper write-up and data collection		
Overall percentage (%)	85%		
Certification:	This paper reports on original research I conducted during the period of my Higher Degree by Research candidature and is not subject to any obligations or contractual agreements with a third party that would constrain its inclusion in this thesis. I am the primary author of this paper.		
Signature		Date	

Co-Author Contributions

By signing the Statement of Authorship, each author certifies that:

i. the candidate's stated contribution to the publication is accurate (as detailed above);

ii. permission is granted for the candidate in include the publication in the thesis; and

iii. The sum of all co-author contributions is equal to 100% less the candidate's stated contribution.

Name of Co-Author	Murat Karakus		
Contribution to the Paper	Manuscript evaluation		
Signature		Date	

Chapter 6

The influence of mineral content of granitic rocks on the acoustic emission during single contact abrasivity test

Abstract

Core drilling is a fundamental process in the mineral exploration industry. As deep exploration in hard rocks is accelerated due to the depletion of near ground mineral resources, deep-drilling operations need to reduce their reliance in operators experience and begin to implement new technologies in order to increase efficiency and cost-effectiveness of the overall process. Currently, lack of real-time information on the bit/rock interaction is a major problem. Therefore, the mechanism behind the acoustic emission, which is a proven technique for remote monitoring, generation in mechanical rock cutting must be understood in order to provide real time information about the rock. This paper is aimed at identifying the influence of mineral composition of granitic rocks on the Acoustic Emission (AE) whilst scratching rocks with a single contact tool and evaluating the feasibility of AE as a means to infer Cerchar Abrasivity Index (CAI). Single contact tool is utilised since it allows a better understanding and identification of the mechanism generating the AE waves. A Cerchar apparatus that was modified to provide constant scratching speed is utilized to monitor AE during rock/tool interaction.

HRC-56 steel pins are used for scratching the rocks. Two AE PICO sensors with an operating frequency range of 200-750 kHz were used. One of the AE sensors was attached onto the Cerchar frame and the other sensor was on the rock sample. Continuous AE signals were recorded with 1 MHz sampling rate during scratching. Tests on the modified Cerchar apparatus are carried out under the static load of 70N and cutting speed of 1 mm/s. A Scanning Electron Microscope (SEM) is utilized to visualize the groove in the rock and to identify the mineral composition through Back-Scattered Electrons (BSE) reflected from the rock sample. Based on the microscope images, particular rock minerals have been associated with different types of AE signals during their fracturing process. These different types of signals are in turn evidence of different cutting responses in the respective minerals. For instance, biotite shows a larger groove area and plate-like fractures accompanied with burst-type AE signal, whereas plagioclase and quartz, which are characterized by similar hardness and BSE brightness, possess shattered-like fractures and more continuous-type AE signals. Also, A-value of the Gutenberg-Richter scale has been found to well correlate with CAI.

6.1 Introduction

Automation and remote sensing, which are a relatively new trend in the mining industry, require new techniques and strategies for real-time detection of rock properties. AE is considered as one of these novel techniques whereby engineers and researchers can sort out the newly presented challenges derived from automation and remote sensing. Rock cutting, by mechanical means, is a common practise not only in mining industry but also in exploration and oil and gas industry. As such it is important to understand and identify rock characteristics that affect AE while cutting. Amongst the different rock properties there is one which stands out, abrasivity, as affecting the process and tool cutting tool life the most. Different scratching/cutting configurations clearly generate particular and different acoustic signatures. This can even be evidenced when cutting at home through a wall. It sounds different when cutting in pure cement than when doing so through a block or reinforced concrete. Does the generated sound in rock scratching/cutting behave

in a similar manner under different scratching/cutting conditions? Some researchers have demonstrated that differences do exist under different cutting conditions [1-4] and also that rock properties can be extracted via AE [5, 6]. However, the mechanism generating the acoustic waves has not been clearly defined yet and CAI from AE has not either been attempted.

Although this paper is part of a broader research project that focuses on the study of acoustic emission as a means to remotely identify particular conditions of the rock cutting process and rock properties, for this particular case we will be focusing in a very specific type of rocks. It is therefore that this paper aims at:

- Determining the effect that the mineral content of granitic rocks has in the acoustic signature generated while cutting rock.
- Determining the applicability of AE technique to infer CAI of granitic rocks.
- Characterising the phenomena generating the AE at the rock/tool interaction between cutting and friction.

6.1.1 Cerchar Apparatus

Cerchar abrasion index (CAI) is widely used in mining and excavation projects. Although it is utilised in different applications, for instance, estimation of rock cutting tool mean lifetime, project timing and costing, proper selection of rock cutting tool, there are some discrepancies with the test results. These are mainly attributed to the test subjectivity and, more important, to the lack of repeatability of the tests. The latter has been an important focus of research, since the test was first introduced in the early 70s, more specifically, test parameters. They are reviewed in the following sections. From all the different Cerchar test parameters, the ones with more variability and influence in the test results are the test velocity and the hardness of the pin used during testing.

Pin hardness

After an exhaustive review of literature in regard to stylus hardness, it has been found that previous tests have predominantly been carried out with two different

pins hardness since the CAI was first introduced. To be precise, 56 HRC [7-9] and 42 HRC stylus pins [10-12]. Due to this inconsistency, a study completed at the University of new south Wales by Stanford and Hagan [11] has come up with a useful relation between pin hardness and CAI values (Eq. 6.1).

$$CAI = -0.0766HRC + 5.80 \tag{6.1}$$

where HRC is Rockwell hardness of the steel pin and CAI stands for Cerchar abrasivity index.

Velocity

As mentioned earlier, one of the more important parameters affecting the CAI is the test velocity. The different proposed velocities vary within an order of magnitude which is why it is considered as an important source of discussion. Some Being the more notorious one the higher velocities of 10mm/s [13, 14] in contrast with the slower velocities of 1mm/s proposed by Michalakopoulos *et al.* [8] or even as slow as 10mm/min [10]. However, Plinninger *et al*. [15] suggest that the values of CAI estimated from the different velocities and setups do not vary significantly.

Number of tests

The result of the tests is also sensitive to number of tests performed in each specimen albeit to a less degree that other parameters. In the Cerchar standard, it is recommended to perform 5 tests and average the results to evaluate the abrasivity of the rock. with 2 tests in perpendicular direction to the other 3 [16]. However, Plinninger *et al.* [9] consider average grain size as the main feature to determine the number of tests. Thus, for fine-grained rocks are subjected to 2-3 tests and for coarse-grained 5 or more tests. According to West [10], care must be taken when rock present veins or are banded. This situation should be accompanied with an increase in the number of tests in order to avoid single mineral or band CAI values.

Wear measurement and rock surface quality

Sample surface is the variable that in quantitative terms still needs more detailed research. Due to the fact that Plinninger et al. [9] only qualitatively mentions “rough

surface" and/or "smooth surface" regardless of how smooth and/or rough the actual surface is. Despite this, their relation (Eq. 6.2) is suggested by ASTM (2010) to be used in order to normalise the CAI values. Rostami et al. [12] have come up with their own relation and analyses between indexes of different surface condition, reinforcing the influence that surface quality has on CAI values.

$$CAI = 0.99CAI_s + 0.48 \tag{6.2}$$

where CAI = Cerchar abrasivity index in natural surface, CAIs = Cerchar abrasivity index in smooth surface.

Lastly, Although CAI unit has been defined by as a 100 μm wear flat diameter measured in the stylus wear flat [10], there is ambiguity and lack of information on the details of wear flat measurement procedure. Plinninger et al. [9] used a reflected light microscope with 50x magnification, whilst the Cerchar standard suggests a microscope with minimum 30x magnification [16]. Other discrepancy that exists in terms of wear is whether the measurement should be performed looking at the pin tip sideways [17] or from the top [10].

6.1.2 Acoustic Emission

Transient elastic waves released during fracture, plastic transformation or changes in the internal structure of materials are conventionally defined as AE. Sources of AE concerning this study are of mainly of two different natures: material behaviour related and friction related. Material related waves include those generated by the result of rapid release of strain energy during fracturing, dynamic external force presence, plastic deformation, changes in internal structure [18] whilst the friction related are due to changes in friction surface structure, surface spalling or appearance of wear [19].

AE is a technique that possesses multiple parameters. These parameters can all be utilised to describe the different processes to which AE is applied. In Figure 6-1, the two typical types of emissions and some of their parameters are shown

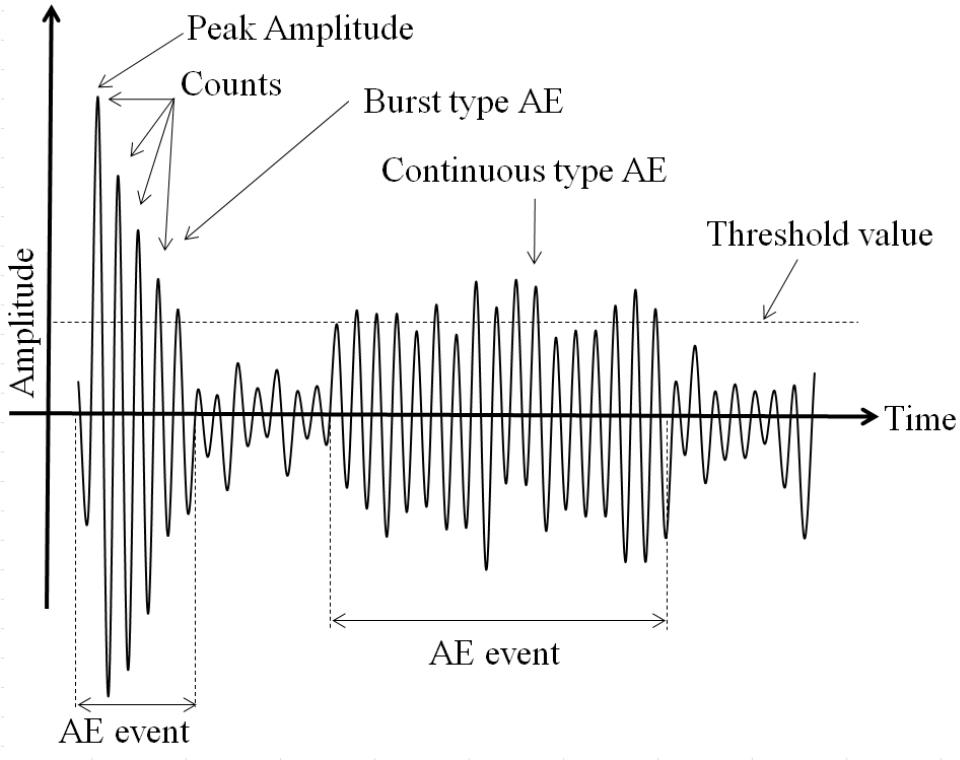

Figure 6-1. Schematic representation of AE

In the past, different researchers have used AE to monitor processes closely related to CAI. For instance, Karakus and Perez [1] found that a direct relation between AE amplitude and drilling parameters such as thrust, torque and depth of cut in impregnated diamond core drilling under kinematic control. Sun [4] used AE to monitor predefined bit wear conditions using tricone bits. He concluded that different drilling situations may be identified by the characteristics of AE signals generated at the rock/bit interaction and also extracted useful information pertaining to bit wear and rock formation changes.

Furthermore, AE has been found to correlate with different rock properties and rock fracture. Indentation hardness, in a study by Jung et al. [5], was found to relate with some AE parameters. They found a direct relation amongst peak Root Mean Square (RMS), number of events and integrated RMS with indentation hardness. Considering the correlation between peak RMS and indentation hardness as the more pronounced and significant finding from the previously mentioned.

6.2 Methods

A conventional West Cerchar apparatus has been modified for testing. The apparatus has been equipped with a stepper motor. The stepper motor has been directly installed instead of one of the two hand cranks driving the screws in the two-axis cross table (see Figure 6-2). The purpose of the modification that has been carried out is not only to better understand and match acoustic emission with its source in the microscopic analysis but also to avoid discrepancies in regard to velocity of the test. The adopted velocity for the current series of tests is, as suggested by Michalakopoulos et al. [8], 1 mm/s.

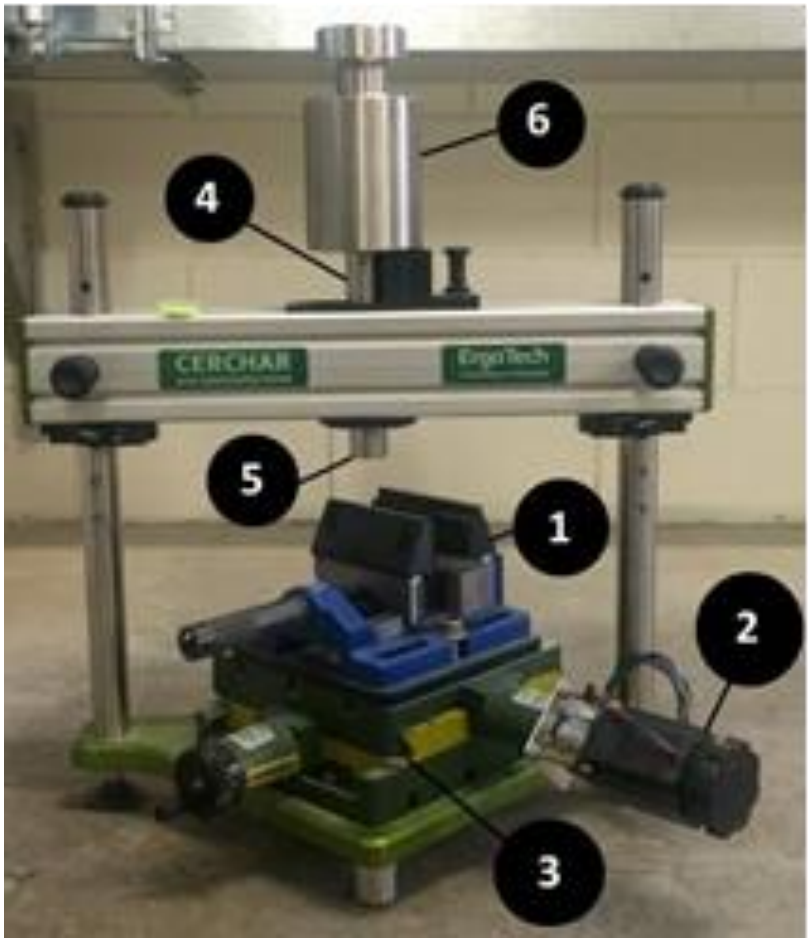

Figure 6-2. Modified Cerchar apparatus: 1-Sample holding vice, 2-Electric motor, 3-Two axis cross table, 4-Tool holder, 5-Pin and 6-Normal force.

56 HRC pin hardness is utilised. Number of tests performed on each rock sample equals to four. Two different granitic rocks, named monzogranite and granodiorite

of which mineral content analyses are shown in Table 1 [20, 21], are subjected to tests. These granitic rock samples used are considered “smooth” surfaces since they have been diamond sawn [9] and surface grinded. As a result, a flat surface sample with an approximate roughness of less than 10 μm, which is considered appropriate to conduct the test, is achieved. The mineral composition was carried out by a series of thin section microscopic analyses.

Table 6-1. Mineral composition of granitic rocks

Mineral	Monzogranite		Granodiorite	
	Average content (%)	St. dev.	Average content (%)	St. dev.
Quartz	29.2	0.748	24	1.265
Orthoclase	19.6	3.826	5	3.098
Plagioclase	17.8	5.845	27.2	7.222
Biotite	12.8	1.166	37	14.142
Others	20.6	11.360	6.8	2.926

In terms of AE system (Figure 6-3) used for testing, AE sensors and their respective preamplifiers are utilised along with a data acquisition card (DAQ) and LabView program. Two PICO AE sensors with flat frequency response of approximately 200-750 kHz are utilised. One is firmly attached to rock sample for capturing the acoustic signals generated at the pin-rock interface and the other to the frame of the apparatus so that vibration emitted from the motor can be captured. Silicone gel is used as couplant material between sensors and their respective attaching parts. Then, the signal conditioning procedure is undertaken as follows. Both Pico sensors are equipped with external 20 dB pre-amplifiers that magnify the AE signal. This magnified signal is then transmitted to a NI PCI-61333 (16 MS/s) S series multifunction DAQ. Sampling rate used in the DAQ is 1 MHz for all tests. Finally, a LabView program developed at the University of Adelaide and commercially available software, Matlab, are utilised for post-processing.

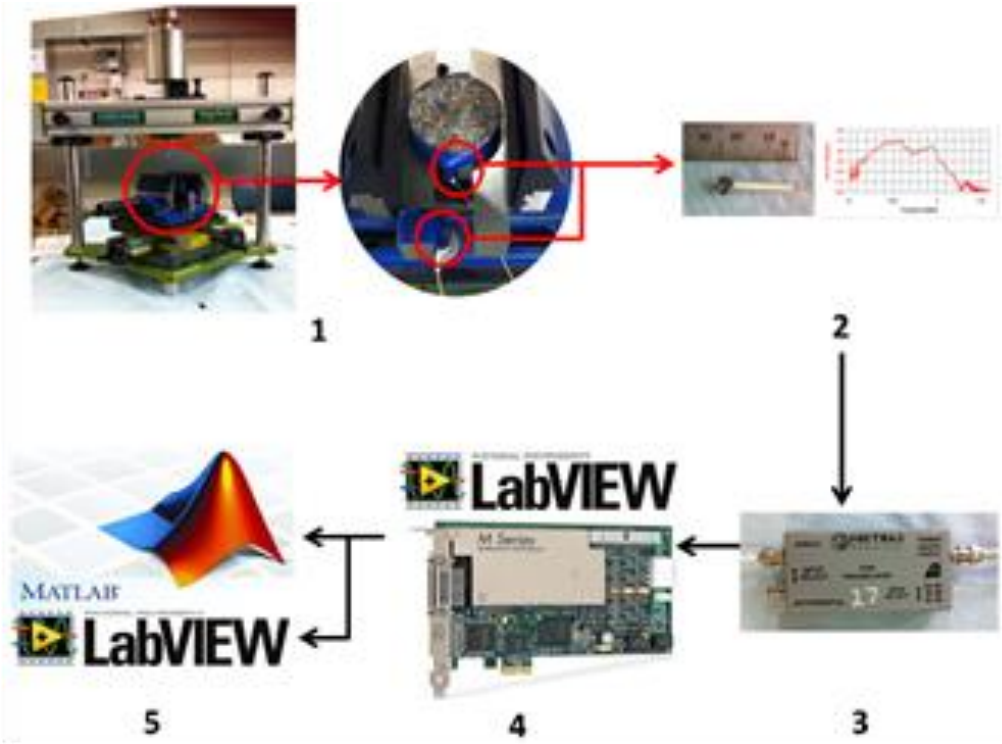

Figure 6-3. Acoustic emission capturing setup

A Philips XL40 scanning electron microscopy is utilised for examining the groove surfaces and their associated mineral composition. Granitic rocks are silver coated so that the secondary electrons (SEl) produced by the beam can be properly reflected from the surface. Also, backscatter electrons (BSE) are detected in order to identify the mineral content of the specimen surface. Finally, wear flat measurement of the pins is carried out after testing. An optical measurement unit provided by ErgoTech is used. Calibration is done prior to measurement. Five digital measurements are averaged for every wear flat. In cases when there is a burr in the pins, the measurements are carried out, as suggested by Rostami, Ghasemi, Alavi Gharahbagh, Dogruoz and Dahl [12], from the point of intersection of the wear flat with the original shape of the pin.

6.3 Results

6.3.1 Cerchar Abrasivity Index

Individual wear flat measurements can be visualized in Figure 6-4. Average values of the five digitised wear flats of the pins used in testing monzogranite and granodiorite can be seen in Figure 6-4a and Figure 6-4b respectively. Average CAI value for monzogranite is 5.0 and granodiorite possesses an average CAI value equal to 3.5, which according to Stanford and Hagan [11] can be classified as "extremely abrasive" and "highly abrasive" rocks respectively.

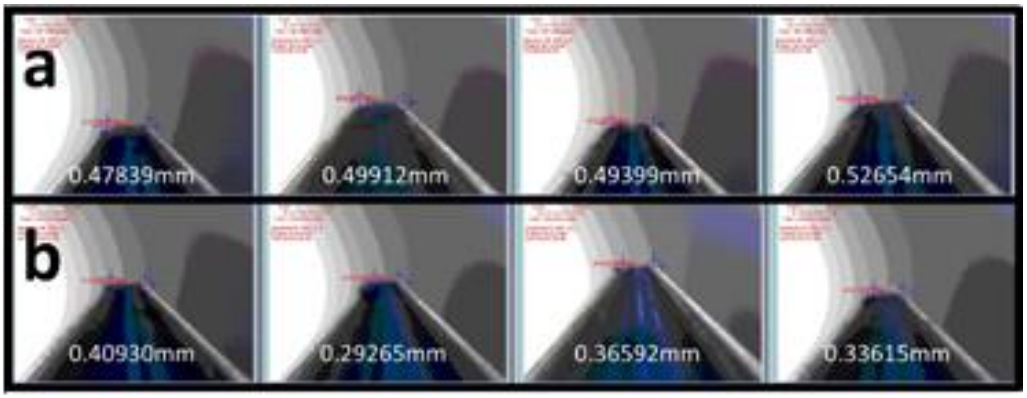

Figure 6-4. Individual wear flat: a) Monzogranite and b) Granodiorite.

6.3.2 Acoustic signals

Signals recorded from the tests can predominantly be considered as burst type AE. However, there are some short time intervals in the signals in which the frequency of the generated emissions is so high that the signal can be regarded as continuous during such periods. The similarity of the pattern between signals recorded by the sensor on the apparatus and on the rock can be visually distinguished, though there is a high degree of attenuation on the signal recorded at the apparatus sensor. The attenuation of the signal amplitude is of approximately two orders of magnitudes (Figure 6-5).

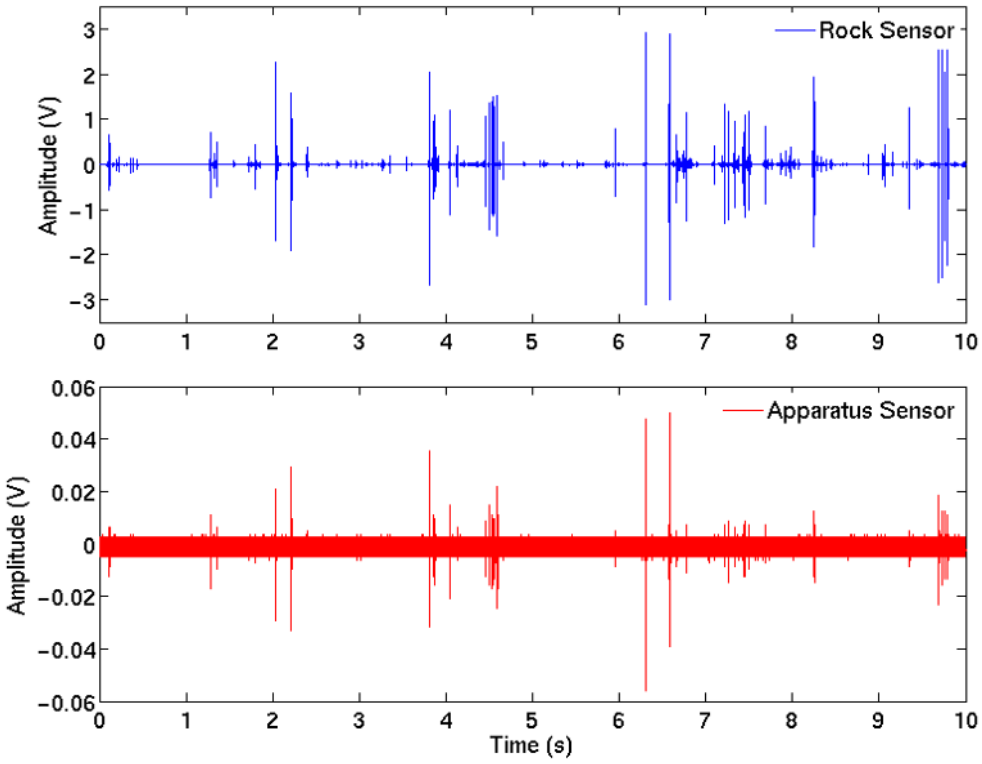

Figure 6-5. Apparatus and rock signals in a typical monzogranite test.

a- and b-value

An important degree of self-similarity within the signals was recognised after carefully analysing the signals. So cumulative hit-amplitude distributions are plotted for both rocks and the best linear regression is fitted to each dataset by least square method (Figure 6-6).

The linear best fits for both rocks obey the Gutenberg-Richter law, in which, N, provides the number of AE events with amplitude, M, and a and b are the positive constants of the linear regression of the form of Eq. 6.3. In this research, a-value is related to the total number of events that occur during the testing length and b-value indicates the relation that exists between larger and smaller events.

$$Log\ N = a - bM \tag{6.3}$$

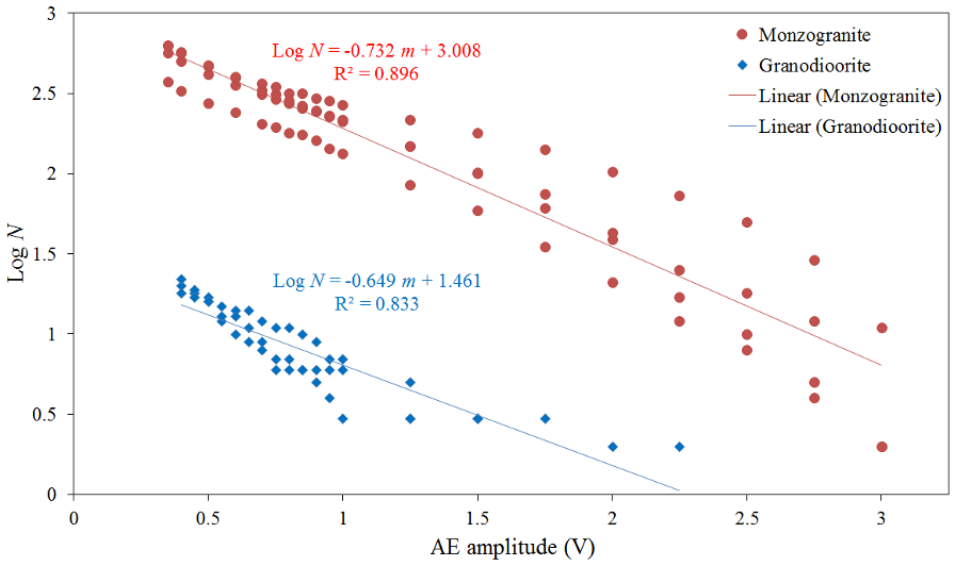

Figure 6-6. Cumulative hits-amplitude distributions for granitic rocks.

6.3.3 Relations between AE signals and CAI

As a-value is directly associated with total number of events generated, it has been used for obtaining an equivalent of the AE energy released during a test. Hence, eliminating the dependency of AE energy value in the characteristics of the AE monitoring facilities [22] i.e. sampling frequency.

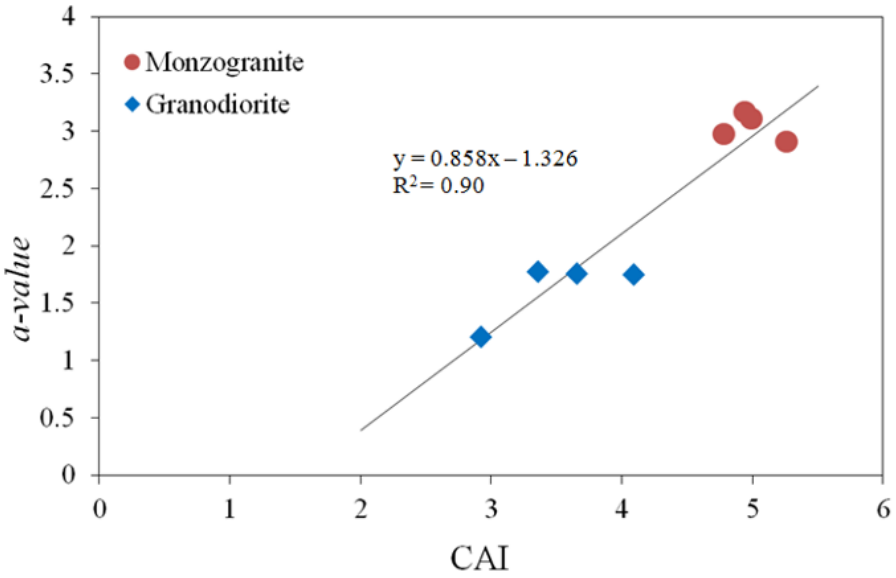

Figure 6-7. a-value vs. CAI for granitic rocks

Surface analysis

SEM analyses are carried out in the grooves left by the abrasivity tests in the granitic rock samples. Figure 6-8a depicts a typical SEl surface image. In this surface image, the damage generated by the pin can be clearly seen. Further, different types of fractures can be identified. On Figure 6-8b, it is seen a BSE image from which the different minerals in the rock granitic surface are identified and their respective damage qualified. Finally, Figure 6-8c shows the correspondent acoustic signature.

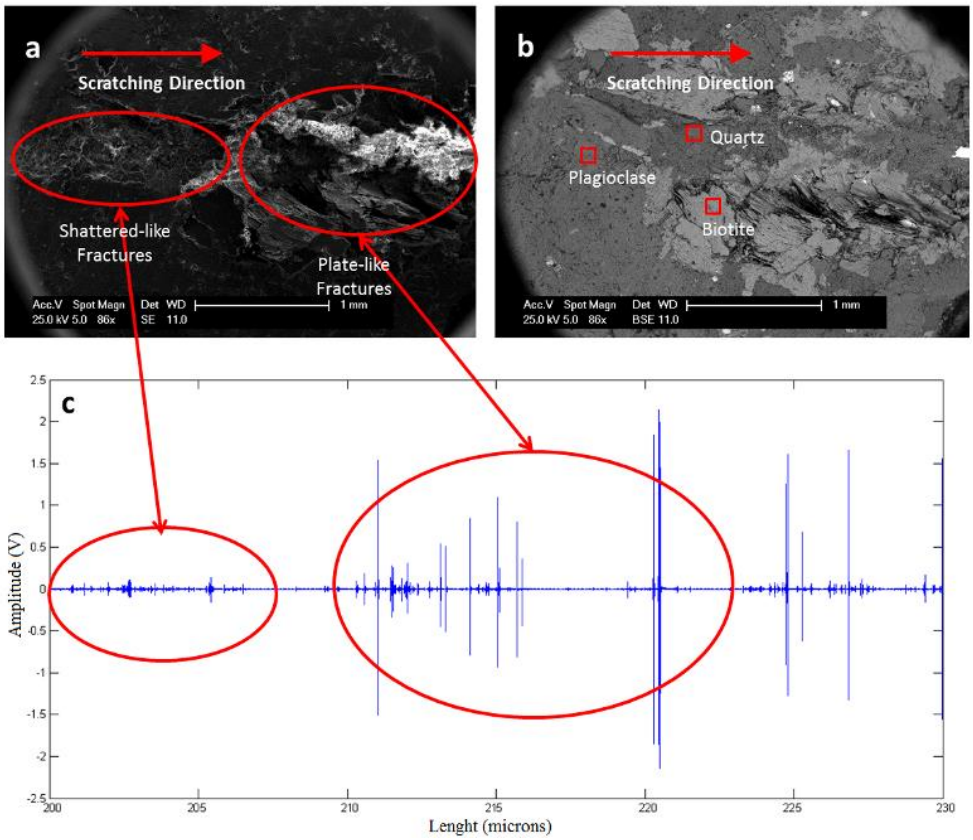

Figure 6-8. Rock surface analysis with scanning electron microscopy.

6.4 Discussion

Despite the fact that apparatus sensor based measurement was deemed inappropriate for this type of test due to the high degree of attenuation of the waves traveling to the apparatus sensor, the very few high energy events that can be detected in the apparatus signals (Figure 6-5) serve to validate the signals detected at the rock sensor. The high degree attenuation may be explained by the fact that

the rock sample is mounted in a rubber band in order to isolate it from the motor vibration, hence, causing an important loss of energy in the signal.

From the linear best fit (Figure 6-6), in which, N, provides the number of micro-seismic events with amplitude, M, and a and b are positive constants, it is important to highlight that both rock obey the Richter-Gutenberg law. In regard to a-value, which describes the amount of micro-seismic activity, it was expected to be higher for more abrasive rocks as an increase in the activity takes place at the rock/pin interaction resulting in more AE generation. In fact, a-value is the AE parameter that best correlates with the CAI because (Figure 6-7). This result confirms that the interaction between pin and rock can be monitored by AE, however it is important to highlight that the result may be restricted to certain values of CAI in our case this relation can be used in rocks with CAI larger than 1.5 (CAI $\geq$ 1.5), most granitic rock lie in that range. When it comes to b, it is known that b-value, which is a measure of the relation amongst the different size events occurring at the interface, is highly affected by the heterogeneity of the rock. In this particular case, b-values registered during monzogranite, whose average crystal size is smaller, testing are larger than those from granodiorite.

It is widely accepted that 85% of the wear occurs in the first 2 mm of the test. However, the AE activity recorded during testing is randomly distributed through the total length of the groove. There are two main explanations for such finding. They are that either the AE signals generated from the wear are in a different frequency range or the friction process occurring at the interface is not an important contributor to the AE generation during the tests.

Based on the microscope images, particular rock minerals have been associated with different types of AE signals during the tests. These different types of signals are in turn evidence of different fracturing responses in the respective minerals. For instance, biotite (Figure 6-8b) shows a larger groove area and plate-like fractures (Figure 6-8a) accompanied with burst-type AE signal (Figure 6-8c). Understanding by plate-like fracture the process in which cracks grow large enough so that there is chip formation, that is to say material removal. In the particular case of biotite,

this fracturing type may have been enhanced by the mineral cleavage and its lower hardness in the Mohs scale, 2.5-3. On the other hand, plagioclase and quartz, which are characterized by similar Mohs scale hardness, 6-6.5 and 7 respectively, and BSE brightness (Figure 6-8b), possess shattered-like fractures (Figure 6-8) and more continuous-type AE signals (Figure 6-8c). Here, shattered-like fractures are defined as superficial cracks that expanded and formed a network of cracks without removing material. These harder materials require more energy in order to be cut. The generation of the crack network is the process that generates the higher frequency and low amplitude signal generated at the rock/pin interface.

6.5 Conclusion

Laboratory tests have been performed with the modified Cerchar apparatus in granitic rocks. Results indicated that there was a correlation between CAI and AE parameters using a-value and b-value. The former, which is related to total number of events, has stronger correlation with CAI and the latter corresponds to event size and therefore is more related to grain size. The main conclusions draw from this research are as follows: A-value is the parameter that is recommended to express CAI of granitic rocks through AE as it best correlates with CAI. SEM analyses point out fractures propagation as the main source generating the AE in granitic rocks during CAI testing. And, finally, apparatus based monitoring is not feasible in this type of test since generated waves are of high frequency, thus they suffer higher attenuation rate.

6.6 Acknowledgments

The work has been supported by the Deep Exploration Technologies Cooperative Research Centre whose activities are funded by the Australian Government's Cooperative Research Centre Programme. This is DET CRC Document DET CRC 2014/548. The authors would like to thank Mr. Ian Cates and Mr. Simon Golding at the University of Adelaide.

6.7 References

[1] M. Karakus, S. Perez, Acoustic emission analysis for rock–bit interactions in impregnated diamond core drilling, Int. J. Rock Mech. Min. Sci., 68 (2014) 36-43.

[2] C. Gradl, A.W. Eustes, G. Thonhauser, An Analysis of Noise Characteristics of Drill Bits, Journal of Energy Resources Technology, 134 (2011) 013103-013103.

[3] M. Karakus, T. May, D. Ollerenshaw, Acoustic Emission (AE) signatures of rock cutting response of an impregnated diamond drill bit, the 2013 International Conferences of mechanical Engineering, London, 2013.

[4] X.Q. Sun, A study of acoustic emission in drilling applications, The 37th U.S. Symposium on Rock Mechanics: Rock mechanics for industry (USRMS), A Balkema, Vail, CO, 1999, pp. 983-990.

[5] S.J. Jung, K. Prisbrey, G. Wu, Prediction of rock hardness and drillability using acoustic emission signatures during indentation, Int. J. Rock Mech. Min. Sci., 31 (1994) 561-567.

[6] A. Lavrov, The Kaiser effect in rocks: principles and stress estimation techniques, Int. J. Rock Mech. Min. Sci., 40 (2003) 151-171.

[7] M. Suana, T. Peters, The Cerchar Abrasivity Index and its relation to rock mineralogy and petrography, Rock Mechanics, 15 (1982) 1-8.

[8] T.N. Michalakopoulos, V.G. Anagnostou, M.E. Bassanou, G.N. Panagiotou, The influence of steel styli hardness on the Cerchar abrasiveness index value, Int. J. Rock Mech. Min. Sci., 43 (2006) 321-327.

[9] R. Plinninger, H. Käsling, K. Thuro, G. Spaun, Testing conditions and geomechanical properties influencing the CERCHAR abrasiveness index (CAI) value, Int. J. Rock Mech. Min. Sci., 40 (2003) 259-263.

[10] G. West, Rock abrasiveness testing for tunnelling, International Journal of Rock Mechanics and Mining Sciences & Geomechanics Abstracts, 26 (1989) 151-160.

[11] J. Stanford, P. Hagan, An assessment of the impact of stylus metallurgy on Cerchar Abrasiveness Index, Coal opereators' conference, Univesity of Wollongong, 2009, pp. 347-355.

[12] J. Rostami, A. Ghasemi, E. Alavi Gharahbagh, C. Dogruoz, F. Dahl, Study of dominant factors affecting Cerchar Abrasivity Index, Rock Mech. Rock Eng., (2013) 1-15.

[13] O. Yaralı, E. Yaşar, G. Bacak, P.G. Ranjith, A study of rock abrasivity and tool wear in Coal Measures Rocks, Int. J. Coal Geol., 74 (2008) 53-66.

[14] M. Alber, Stress dependency of the Cerchar abrasivity index (CAI) and its effects on wear of selected rock cutting tools, Tunnelling and Underground Space Technology, 23 (2008) 351-359.

[15] R. Plinninger, H. Kasling, K. Thuro, Wear prediction in hardrock excavation using the CERCHAR abrassivenes index (CAI), EUROCK & 53rd Geomechanics Colloquim2004.

[16] ASTM, Standard Test Method for Laboratory Determination of Abrasiveness of Rock Using the CERCHAR Method, D7624-10, American Society for Testing and Materials2010.

[17] J. Rostami, L. Ozdemir, A. Bruland, F. Dahl, Review of issues related to Cerchar abrasivity testing and their implications on geotechnical investigations and cutter cost estimates, RETC, Seattle, WA, USA, 2005, pp. 738-751.

[18] W.P. Dong, Y.H.J. Au, A. Mardapittas, Characteristics of acoustic emission in drilling, Tribol Int, 27 (1994) 169-170.

[19] V. Baranov, E. Kudryavstev, G. Sarychev, V. Schavelin, Acoustic emission in friction, Elsevier2007.

[20] G.R. Khanlari, A.A. Momeni, M. Karakus, Assessment of Fatigue Behavior of Alvand Monzogranite, J. Eng. Geol., 8 (2014) 2003-1019.

[21] G.R. Khanlari, M. Heidari, A.A. Momeni, Assessment of weathering processes effect on engineering properties of Alvand granitic rocks (west of Iran), based on weathering indices, Environ Earth Sci, 67 (2012) 713-725.

[22] H.R. Hardy, Application of acoustic emission techniques to rock mechanics research, Acoustic Emission, ASTM STP 5051972, pp. 41-83.

Chapter 7

Conclusions and recommendations

7.1 Conclusions

The main objective of this thesis is to study the applicability of AE technique to ID rock drilling and drilling-related rock properties. Special attention is devoted to the shortcomings mentioned in Section 1.3. The major research outcomes of this thesis are listed as follows:

- AE monitoring is a feasible technique to optimize ID drilling performance since changes in drilling conditions and effects of drilling parameters can be accurately mapped by analysing AE.
- Through 'Step tests', it has been demonstrated that there is a direct link between AE amplitude and drilling parameters. A series of linear relations have concluded that the signal amplitude alone could accurately estimate the current depth of cut, WOB or TOB in real time. Furthermore, it can also be determined that AE amplitude behaves erratically before increasing voltage suddenly at a certain depth of cut, approximately 80μm/rev. A plausible explanation is that there is a change in cutting behaviour of the bit, from a more stable, grinding mechanism, to an aggressive nature.
- Little variation in the peak frequency and frequency range of AE over time was found after performing frequency analysis on the signals of accelerated wear tests. It was also found that fundamental frequencies ranged from 20 to 50 kHz.

- Multiple tool condition monitoring systems are obtained, with AE_{rms} and measuring-while-drilling variables as input parameters of pattern recognition/machine learning techniques, in order to predict the ID drilling tool wear state. All in all, AE_{rms} and TOB are considered the most adequate input variables for a wear monitoring system of ID bits because of the lesser input variables and still accurate classification performance with all the different pattern recognition algorithms. Further, this finding is consistent with what has already been found for wear evaluation in metal drilling as well as with the major contribution in terms of specific energy that TOB provides when compared to WOB in MWD.
- The length of flat wear in a conic steel pin, CAI, was accurately predicted from AE parameters, rock properties and Cerchar testing parameters using the newly proposed approach. The results of Gamma test and V-ratio analyses demonstrate the advantages of including rock properties along with AE features as input variables. They significantly reduce the noise or error variance in the CAI prediction model. It has also been demonstrated that predicting CAI from a tool condition monitoring viewpoint is a feasible approach. Finally, the main sources of AE during CAI abrasivity tests are fracture generation and propagation for crystalline rocks and grain dislocation and appearance of wear debris for sedimentary rocks.
- For granitic rocks, results indicate that there is a correlation between CAI and AE parameters derived from the Gutenberg-Richter law, a-value and b-value. The former, which is related to total number of events, has stronger correlation with CAI and the latter corresponds to event size and therefore is more related to grain size. The main conclusions draw from this research are as follows: A-value is the parameter that is recommended to express CAI of granitic rocks through AE as it best correlates with CAI. SEM analyses point out fractures propagation as the main source generating the AE in granitic rocks during CAI testing.

7.2 Recommendations for further work

As with any research work, there are some limitation in the current work. Future work is recommended as follows:

- In this research, a sudden increase on the AE generated is found at approximately 80µm/rev. The increase is believed to reflect a change in drilling conditions. In this regard, it would be of interest to test different rocks in order to study the effect of rock type in the jump (cutting mechanism) generated on the AE amplitude at about 80 microns/rev. Also, further studies could be undertaken by utilising different bit configurations (size and properties), bit geometries (full face) as well as different rock types.
- Further research is required in terms of tool condition monitoring systems as the current work just sets the basis of the applications of tool condition monitoring to ID rock cutting applications. Mainly two improvements can be done: (i) One research avenue could be focused towards establishing which parameters of the AE, both in time-domain and frequency-domain, are better to classified wear states of the bits. (ii) The other field in which research is still required is in the set-up of ID drilling and the definition of multiple wear states of the tools. Hence, robustness of the models increases and so does its predictability.
- At present, the research is ongoing and more work is required in the field of abrasivity in order to develop the first tool condition monitoring system that may predict CAI from AE features exclusively. Although this methodology is still far from having industry application, it is a promising field of research. Finally, apparatus based monitoring is not feasible in this type of abrasivity tests (CAI) since generated waves are of high frequency, thus they suffer higher attenuation rate

Appendix A

Scripts

Script for TCM system via SVM

```
% Convert input to table
Input Table =  table(trainingData);
Input Table.Properties.VariableNames = % {' column '  ;

% Split matrices in the input table into vectors
inputTable.column_1 = inputTable.column (:,1);
inputTable.column_2 = inputTable.column (:,2);
inputTable.column_3 = inputTable.column (:,3);
inputTable.column_4 = inputTable.column (:,4);
inputTable.column_5 = inputTable.column (:,5);

% Extract predictors and response
% This code processes the data into the right shape for training the classifier.
predictorNames = {'column_1', 'column_2', 'column_3', 'column_4'};
predictors = inputTable(:, predictorNames);
response = inputTable.column_5;

% Train a classifier
% This code specifies all the classifier options and trains the classifier.
classificationSVM = fitcsvm(...
    predictors, ...
    response, ...
```

```
    'KernelFunction', 'linear', ...
    'PolynomialOrder', [], ...
    'KernelScale', 'auto', ...
    'BoxConstraint', 1, ...
    'Standardize', true, ...
    'ClassNames', [0; 1]);

trainedClassifier.ClassificationSVM = classificationSVM;
convertMatrixToTableFcn = @(x) table(x, 'VariableNames', 'column'});
splitMatricesInTableFcn = @(t) [t(:,setdiff(t.Properties.VariableNames,
{'column'})), array2table(table2array(t(:,{'column'})), 'VariableNames',
{'column_1', 'column_2', 'column_3', 'column_4'})];
extractPredictorsFromTableFcn = @(t) t(:, predictorNames);
predictorExtractionFcn = @(x)
extractPredictorsFromTableFcn(splitMatricesInTableFcn(convertMatrixToTableF
cn(x)));
svmPredictFcn = @(x) predict(classificationSVM, x);
trainedClassifier.predictFcn = @(x) svmPredictFcn(predictorExtractionFcn(x));
% Convert input to table
inputTable = table(trainingData);
inputTable.Properties.VariableNames = {'column'};

% Split matrices in the input table into vectors
inputTable.column_1 = inputTable.column(:,1);
inputTable.column_2 = inputTable.column(:,2);
inputTable.column_3 = inputTable.column(:,3);
inputTable.column_4 = inputTable.column(:,4);
inputTable.column_5 = inputTable.column(:,5);

% Extract predictors and response
% This code processes the data into the right shape for training the
```

```
% classifier.
predictorNames = {'column_1', 'column_2', 'column_3', 'column_4'};
predictors = inputTable(:, predictorNames);
response = inputTable.column_5;

% Perform cross-validation
partitionedModel = crossval(trainedClassifier.ClassificationSVM, 'KFold', 5);

% Compute validation accuracy
validationAccuracy = 1 - kfoldLoss(partitionedModel, 'LossFun', 'ClassifError');

% Compute validation predictions and scores
[validationPredictions, validationScores] = kfoldPredict(partitionedModel);
```

Script for Gamma test

```
import sys

import random

import numpy as np

import pandas as pd

from sklearn import cross_validation

import sklearn.preprocessing

import scipy

import argparse

import statistics

import matplotlib.pyplot as plt

import sys

from sklearn.cross_validation import train_test_split

from sklearn.cross_validation import StratifiedKFold

from sklearn.grid_search import GridSearchCV

import sklearn.linear_model


if len(sys.argv) < 2:

    file_name = '/home/esepulveda/Documents/projects/santiago/cai.csv'

else:

    file_name = sys.argv[1]
```

```
database = pd.read_csv(file_name,na_values=[-999,""])
n = len(database)

variables = ["hardness","ucs","quartz","e","rms","a-value","b-value","events"]
outputs = "cai"
target_raw = np.empty(n)
target_raw[:] = database[outputs]
yvariance = np.var(target_raw) #96.4898239744

print yvariance
ninputs = len(variables)
data_raw = np.zeros((n,ninputs))
for k,v in enumerate(variables):
    data_raw[:,k] = database[v]
standardiser_data = sklearn.preprocessing.StandardScaler()
data_raw = standardiser_data.fit_transform(data_raw)

for i in xrange(2,n):
    results = []
    #neighbor
```

```
xdist, ydist = statistics.gamma_test_kdtree(data_raw,target_raw,i)

slope, intercept, r_value, p_value, std_err = statistics.gamma_test(data_raw,target_raw,i,xdist, ydist)

#print slope, intercept, r_value, p_value, std_err

gamma = intercept

vratio = gamma/yvariance

r2 = 1.0 - vratio

#linear model# data_test,data_train,target_test,target_train = train_
#test_split(data_raw,target_raw,test_size=0.3,random_state =123456)

model = sklearn.linear_model.LinearRegression()

model.fit(data_raw,target_raw)

predictions = model.predict(data_raw)

r2_lm = sklearn.metrics.r2_score(target_raw, predictions)

ret = [gamma,vratio,r2,r2_lm]

print i,",",gamma
```

Script for predicting CAI via ANN

```
import sys
import random
import numpy as np
import pandas as pd
from sklearn import cross_validation
import sklearn.preprocessing
import scipy
import argparse
import statistics
import matplotlib.pyplot as plt
import pickle

from pybrain.structure import FeedForwardNetwork
from pybrain.structure import LinearLayer, SigmoidLayer,TanhLayer
from pybrain.structure import FullConnection
from pybrain.supervised.trainers import BackpropTrainer
from pybrain.tools.shortcuts import buildNetwork
from pybrain.datasets import SupervisedDataSet

database = pd.read_csv('/home/Documents/projects/santiago/cai.csv',na_values=[
999,""])
n = len(database)

#variables = ["hardness","ucs","quartz","rms","a-value","e"]
variables = ["hardness","ucs","quartz","e","rms","events"]

m = len(variables)
n = len(database)
data = np.empty((n,m))
```

```
for i,v in enumerate(variables):
        data[:,i] = database[v]

target= np.empty(n)
tname = "cai" #"cu_roug_rec" #"au_roug_rec"
target[:] = database[tname]

standardiser_data = sklearn.preprocessing.StandardScaler()

data = standardiser_data.fit_transform(data)
target_original = target.copy()

seed = 5970777

x_train, x_test, y_train, y_test = sklearn.cross_validation.train_test_split(data,
target, test_size=0.15, random_state=seed)
x_train, x_validation, y_train, y_validation =
sklearn.cross_validation.train_test_split(x_train, y_train, test_size=0.20,
random_state=seed)

print len(y_train), len(y_validation), len(y_test)

print "stats:"
print "all :",np.mean(target),np.var(target)
print "training :",np.mean(y_train),np.var(y_train)
print "validation:",np.mean(y_validation),np.var(y_validation)
print "test :",np.mean(y_test),np.var(y_test)

learning_rate = 0.01
weight = 0.01 #
max_iterations = 10000
```

```
iterations_between_reports = 0

#datasets
ds = SupervisedDataSet(m, 1)
for i in xrange(len(data)):
        ds.addSample(data[i,:], target[i])

ds_train = SupervisedDataSet(m, 1)
for i in xrange(len(x_train)):
        ds_train.addSample(x_train[i,:], y_train[i])

ds_validation = SupervisedDataSet(m, 1)
for i in xrange(len(x_validation)):
        ds_validation.addSample(x_validation[i,:], y_validation[i])

ds_test = SupervisedDataSet(m, 1)
for i in xrange(len(x_test)):
        ds_test.addSample(x_test[i,:], y_test[i])

np.random.seed(seed)
scipy.random.seed(seed)
random.seed(seed)

ffn = buildNetwork(m,24,1,bias=True,hiddenclass=TanhLayer,outclass=
LinearLayer)
trainer = BackpropTrainer(ffn,ds_train,learningrate=learning_rate,verbose=True,
momentum=0.0,weightdecay=weight)

terror, verror = trainer.trainUntilConvergence(maxEpochs= max_iterations,
trainingData=ds_train,validationData=ds_validation,testingData=ds_test,continue
Epochs=10)
```

```
print len(terror),len(verror)

quit()
training_error = 2 * trainer.testOnData(dataset=ds_train) #,
trainer.testOnData(dataset=ds_train)
test_error = 2 * trainer.testOnData(dataset=ds_test) #,
trainer.testOnData(dataset=ds_train)
validation_error = 2 * trainer.testOnData(dataset=ds_validation) #,
trainer.testOnData(dataset=ds_train)
#save fnn
pickle.dump(ffn,open("ffn.dump","w"))

#training
output = np.array([x[0] for x in ffn.activateOnDataset(dataset=ds_train)])
r2_tra = sklearn.metrics.r2_score(y_train, output)
coef_tra = np.corrcoef(y_train, np.array(output))[0,1]

#test
output = np.array([x[0] for x in ffn.activateOnDataset(dataset=ds_test)])
r2_test = sklearn.metrics.r2_score(y_test, output)
coef_test = np.corrcoef(y_test, np.array(output))[0,1]

#validation
output = np.array([x[0] for x in ffn.activateOnDataset(dataset=ds_validation)])
r2_val = sklearn.metrics.r2_score(y_validation, output)
coef_val = np.corrcoef(y_validation, np.array(output))[0,1]

#overall
output = np.array([x[0] for x in ffn.activateOnDataset(dataset=ds)])
r2_all = sklearn.metrics.r2_score(target, output)
```

```
coef_all = np.corrcoef(target, np.array(output))[0,1]

print training_error,validation_error,test_error,r2_tra,r2_test,r2_val,r2_all

#Export
#restore fnn
def dump_conections(n):
        for mod in n.modules:
                for conn in n.connections[mod]:
                        print conn
                        for cc in range(len(conn.params)):
                                print conn.whichBuffers(cc), conn.params[cc]

def get_results(ffn,dataset,target):
        output = np.array([x[0] for x in ffn.activateOnDataset(dataset=dataset)])
        r2 = sklearn.metrics.r2_score(target, output)
        coef = np.corrcoef(target, np.array(output))[0,1]
        results = np.empty((len(output),3))
        results[:,0] = target
        results[:,1] = output
        results[:,2] = target - output
        return r2,coef,results

if __name__ == "__main__":
        database = pd.read_csv('/home /Documents/projects/santiago/cai.csv',
        na_values=[-999,""])

        variables = ["hardness","ucs","quartz","e","rms","events"]
        n = len(database)
        m = len(variables)
        data = np.empty((n,m))
```

```
for i,v in enumerate(variables):
        data[:,i] = database[v]
target= np.empty(n)
tname = "cai"
target[:] = database[tname]

standardiser_data = sklearn.preprocessing.StandardScaler()
data = standardiser_data.fit_transform(data)
target_original = target.copy()

seed = 5970777

x_train, x_test, y_train, y_test = sklearn.cross_validation.train_test_split
(data, target, test_size=0.15, random_state=seed)
x_train, x_validation, y_train, y_validation = sklearn.cross_validation
.train_test_split(x_train, y_train, test_size=0.20, random_state=seed)

#datasets
ds = SupervisedDataSet(m, 1)
for i in xrange(len(data)):
ds.addSample(data[i,:], target[i])

ds_train = SupervisedDataSet(m, 1)
for i in xrange(len(x_train)):
ds_train.addSample(x_train[i,:], y_train[i])

ds_validation = SupervisedDataSet(m, 1)
for i in xrange(len(x_validation)):
ds_validation.addSample(x_validation[i,:], y_validation[i])
```

```
ds_test = SupervisedDataSet(m, 1)
for i in xrange(len(x_test)):
ds_test.addSample(x_test[i,:], y_test[i])

print len(y_train), len(y_validation), len(y_test)
print "stats:"
print "all :",np.mean(target),np.var(target)
print "training :",np.mean(y_train),np.var(y_train)
print "validation:",np.mean(y_validation),np.var(y_validation)
print "test :",np.mean(y_test),np.var(y_test)
ffn = pickle.load(open("ffn.dump"))

header = "True value, Prediction, Error"
delimiter = ","
#training
r2_tra,coef_tra,results = get_results(ffn,ds_train,y_train)
np.savetxt("training_results.csv",results,fmt="%10.4f",header=header,deli
miter=delimiter)

#test
r2_test,coef_test,results = get_results(ffn,ds_test,y_test)
np.savetxt("test_results.csv",results,fmt="%10.4f",header=header,delimite
r=delimiter)

#validation
r2_val,coef_val,results = get_results(ffn,ds_validation,y_validation)
np.savetxt("validation_results.csv",results,fmt="%10.4f",header=header,de
limiter=delimiter)

#overall
r2_all,coef_all,results = get_results(ffn,ds,target)
```

```
        np.savetxt("all_results.csv",results,fmt="%10.4f",header=header,delimiter
        =delimiter)

        print "r2 tra :",r2_tra
        print "r2 val :",r2_val
        print "r2 test:",r2_test
print "r2 all :",r2_all
```